The characterisation of unilateral finline by transverse resonance diffraction

Olley, C. A.

Award date:
1987

Awarding institution:
University of Bath

THE CHARACTERISATION OF UNILATERAL FINLINE BY TRANSVERSE RESONANCE DIFFRACTION.

submitted by C.A.Olley
for the degree of PhD
of the University of Bath
1987

ProQuest LLC
789 East Eisenhower Parkway
P.O. Box 1346
Ann Arbor, MI 48106-1346

To my Parents.

CONTENTS.

SUMMARY

This thesis considers the application of the Transverse Resonance Diffraction Method to Finline, a waveguiding structure commonly employed at millimetric frequencies.

This method operates in the space domain making use of finite transverse circuits and takes into explicit account the fins and their associated edge conditions.

Using the concept of a rotation, field components derivable from electric and magnetic fields normal to the substrate layer are decomposed into fields due to transverse TM and TE parallel plate modes. With the help of the resulting transverse equivalent network and the orthogonality of parallel plate modes, a system of integral equations linking the fields at the slot aperture is formed.

These are solved by making use of a conformal mapping originally introduced by Schwinger for the analysis of irises in waveguides. This gives rise to basis functions which are quasi-static solutions to the wave equation within the fin gap. Modes at cut-off are thus found to possess slot field variations given by distinct Schwinger functions, allowing modes to be catagorised in terms of families sharing a common slot field variation.

With finline field information available, losses and Q-factors are evaluated, and these are compared with experiment in order to assess validity. In addition results on "finline impedance" are presented.

Finally, with detailed knowledge of the finline field configuration and the mode spectrum, the step discontinuity problem is addressed. To avoid excessive computational effort a number of simplifications are employed giving results which agree closely with those observed experimentally.

LIST OF PUBLICATIONS.

"Characterisation of Unilateral Finline Mode Spectrum Including Loss Analysis", Proc. 16'th European Microwave Conference, Dublin, 1986. pp. 551-516.

"Systematic Characterization of the Spectrum of Unilateral Finline", IEEE trans, MTT-34, Nov, 1986.

ACKNOWLEDGEMENTS.

The author would like to thank Professor T.E.Rozzi for his expert supervision and guidance during the course of this work.

Thanks are also due to the Science and Engineering Research Council and The Marconi Research Centre for supporting this work, and the University of Bath for the use of its facilities.

The author would also like to thank F.C. DeRonde for his interest in the experimental work and M.C.Perkins for his interest in the computational aspects.

Finally, thanks are due to numerous colleagues at Bath and Chelmsford for their help and encouragement.

CHAPTER ONE : INTRODUCTION

1.1 General Introduction

The work contained in this thesis is primarily concerned with the theoretical analysis of finline, a waveguiding structure suitable for millimetric circuit integration. But firstly what are millimetre waves and why are they useful ?

Broadly speaking the millimetric region extends from 30Ghz to 300Ghz i.e a free space wavelength between 10mm and 1mm, although a lower limit of 20Ghz is more appropriate from a systems point of view. Over this frequency range atmospheric absorption due to water vapor increases linearly from virtually zero at 20Ghz, to 10dB/Km at 300Ghz. Superimposed onto this are absorptive peaks due to both water and oxygen molecules.

The short wavelength implies that narrow beams can be formed from physically small antennas, useful not only for radar applications but for point to point and satellite communications. The data capacity of millimetric links is inherently greater, and since beamwidths can be made small and atmospheric attenuation relatively high, interference problems can be alleviated. In fact, these absorption characteristics can be exploited to make millimetre waves particularly useful for short range secure communications.

Although millimetric sources have long been available and millimetric systems have been realised using conventional rectangular waveguide, the incurred expense has prohibited the widespread application of millimetre waves to all but a few military requirements. In the early seventies it was realised that the full

potential of the millimetric part of the spectrum would not be fully realised unless cheap and reliable components become available. Besides the need for active devices, this requires new and improved forms for transmission media.

The near optical character of mm-waves led early investigations into open waveguiding structures, such as image-line, ideal for antenna and coupler applications and relatively easy to construct. However the outstanding difficulty with such open structures is the inability to interface with discrete active devices. This later requirement, that of circuit integration, has lead to other forms of transmission media.

At the lower microwave frequencies, circuit integration is usually achieved by employing microstrip techniques. However their extension into the millimetric region is fraught with difficulties of a fundamental nature.

Although the wave-like properties of signal propagation at microwave frequencies must be recognised , the microstrip structure is essentially based on the low frequency voltage-current concept. At millimetric frequencies problems with the electromagnetic nature of signals can become acute. Bends and corners present the problems of radiation and the excitation of surface wave modes. These can lead to various forms of stray coupling within a conventional system. The obvious solution here is to enclose the microstrip lines within guiding channels, i.e boxed microstrip. But this waveguide concession instantly increases the cost of mm wave systems. Furthermore, the concentration of fields within the microstrip substrate leads to increasing dielectric losses with frequency, and an unnecessary miniaturisation due to reduced guided wavelength.

At millimetric frequencies compatibility with conventional

rectangular waveguide is paramount, since it is the only low loss non radiative transmission media commonly available in this region. Transition into microstrip relies upon E-probe coupling, and this complicates the mechanical design of hybrid systems. As such factors compound, a point is eventually reached where less conventional solutions become attractive. This point is generally met at the onset of the millimetric region.

Thus a whole series of E-plane waveguides have emerged, beginning in 1974 when Meier [1] proposed finline as a structure suitable for millimetric circuit integration with diode devices.

Finline, as shown in figure(1.1.1a), can be regarded either as a planar form of ridge waveguide or simply a boxed slotine. It operates by concentrating guided fields into the slot region between the metal fins, thereby allowing:

i) compatibility with diode devices mounted across the fins

ii) ease of transition into rectangular waveguide

iii) a relaxation of the housing's mechanical tolerances .

The circuit definition is essentially provided by the fin metallisation with the substrate serving as mechanical support.

Figures (1.1.1b) and (1.1.1c) show bilateral and antipodal finline , which can also find application in millimetric circuits. Whilst on the more general theme of E-plane circuits, figure (1.1.2a) shows coupled finline (or boxed coplanar waveguide) and figure (1.1.2b) suspended stripline (a form of planar coaxial line). Finally figure(1.1.2c) shows a more practical realisation of unilateral finline for the higher millimetric frequencies. Here the metallisation thickness is significant as are the substrate holding groves. These lead to deviations in performance from that of the

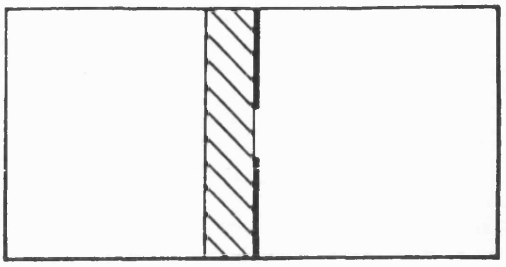

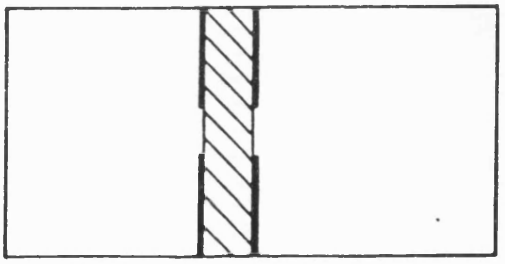

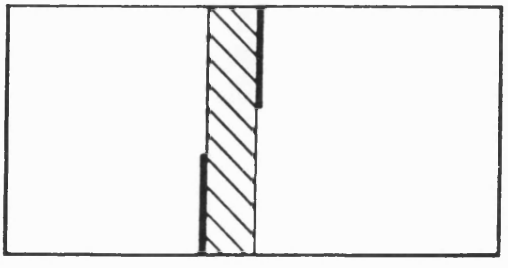

Figures (1.1.1a), (1.1.1b) and (1.1.1c) Unilateral, Bilateral and Antipodal Finline.

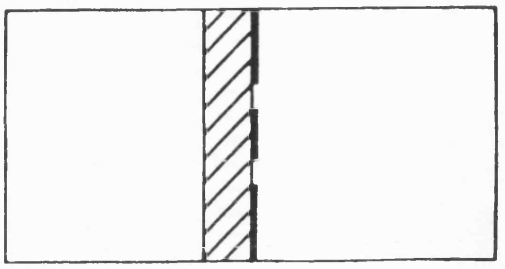

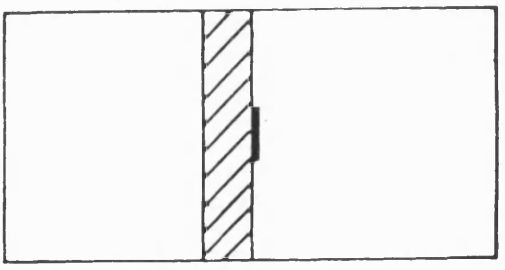

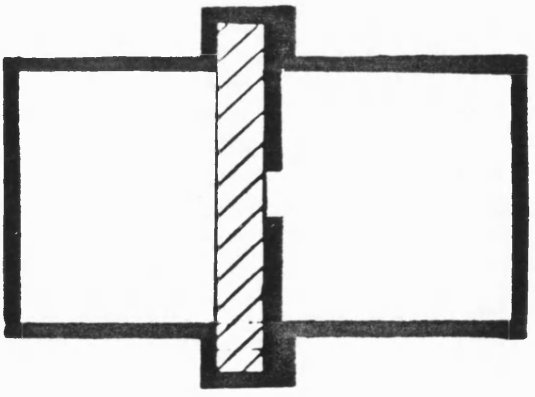

Figures (1.2.1a), (1.2.1b) and (1.2.1c) Boxed Coplanar Waveguide, Suspended Stripline and Practical Finline.

idealised structure which will be discussed later.

To date, the E-plane technology has been used to realise integrated mixers, modulators, phase-shifters and switches, examples of which are given in [2], [3] and [4]. These employ more fundamental passive devices such as magic-T's and rat races etc.

1.2 Review of Past Work - Basic Analyses.

The first fully rigorous theoretical analysis of finline structures was given by Hofmann in 1976 [5]. This author was concerned with the dispersion characteristic and the "impedance" defined from the slot voltage to power flow ratio. The three finline configurations unilateral, bilateral and antipodal as previously illustrated in figures (1.1.1a) to (1.1.1c) were considered. With reference to figure (1.2.1a), the y directed fields in the three subregions (1), (2) and (3) were expanded in terms of functions of x and y so that the Helmholtz equation and the boundary conditions of the dielectrically loaded waveguide are satisfied. The currents on the fin were then used to express the Fourier coefficients of these functions via a linear integral operator. Solution for a finline mode was then obtained by imposing the remaining boundary conditions of the gap and applying Galerkin's method with two sets of orthogonal testing functions to expand the gap field. Because the fin currents and slot field exist in complementary spaces, the current distributions vanished from the resulting system of matrix equations and solution was found by seeking zeros to a determinant.

Hofmann presented useful results for various forms of Q-band finline. However, because the method requires the calculation of a large number of inner products it consumed large amounts of CPU time. Furthermore, the edge condition at the fins was not included in the

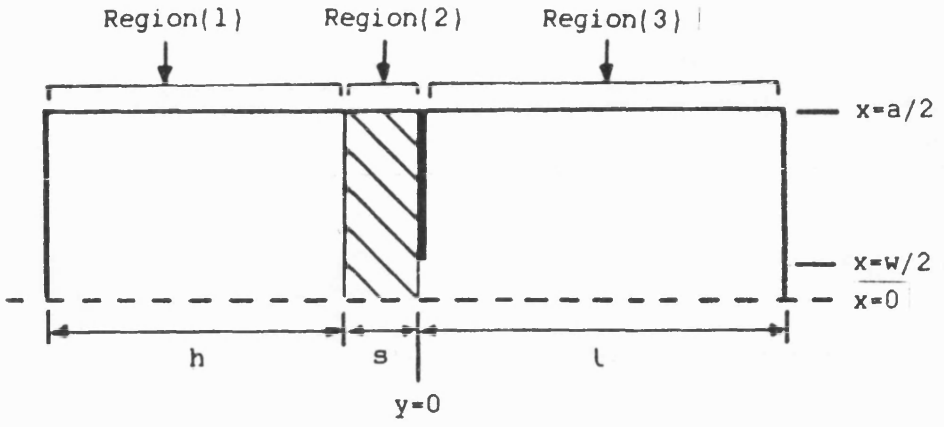

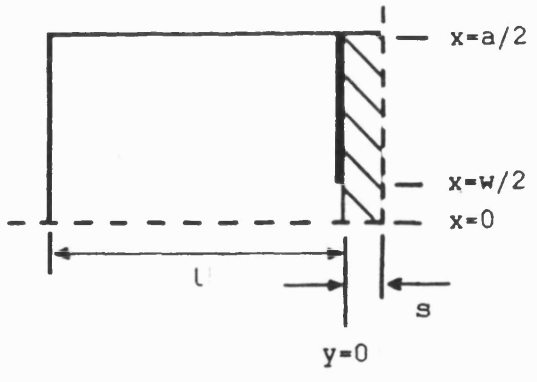

Figures (1.2.1a) and (1.2.1b) Axis Orientation and Dimensional Detials for the Analysis of Unilateral And Bilateral Finline.

basis set which led to relative convergence problems.

With the aim of producing closed form expressions the for characteristics of the fundamental mode in unilateral finline which can be used for the synthesis of the required finline characteristics, Saad and Begemann [6] saw a similarity with ridged waveguide and used the transverse resonance method of Cohn [7] to solve for cut off wavelength and effective dielectric constant. The fins were modelled as a π-network, shunt capacitances and a series inductance, in order to account for the effect of the side walls on the fin gap field using empirical expressions for the component values. By solving for the cut-off wavenumber, with and without the dielectric present, an approximation to the propagation coefficient of the fundamental mode was obtained. The finline impedance was also obtained from an initial calculation of the impedance at infinite frequency modified by the dispersion relation, a technique commonly employed with ridged waveguides.

To facilitate the first order design of finline filter circuits, which require a knowledge of finline fields, Saad and Schunemann [8] 1978, developed an equivalent transmission line representation of the finline structure. However only the bilateral structure with two planes of symmetry as given by figure (1.2.1b) was considered. Using expansions for the fields E_x and H_z in terms of functions of x and y satisfying the Helmholtz equation in the two subregions (1) and (2), solution for modes TE at cut-off is found from a transcendental equation. A similar procedure is employed to solve for modes TM at cut-off. The analysis of the metallic strip in the bilateral finline that followed employed an approximate description of the modes away from cut-off within a mode matching procedure to design simple bandpass filters to within 5% of the desired centre frequency. Whilst

achieving an approximate filter design, the method used to determine finline cut-off's is of particular interest since it is much more rigorous than [6], even though it was only applied to bilateral finline in this case.

It was not until 1979 that a reliable and rigorous technique for the general field solution of finline was published by Itoh [9]. Having developed the spectral domain technique for microstrip problems, Itoh applied it to the solution of finline. The hybrid nature of the finline wave was described in terms of two scalar potentials given by the z-directed fields. These were then taken through a discrete Fourier transform, with respect to the eigenfunctions in the x-domain, which resolved the potentials into infinite sets of coefficients. Using these to express the transformed versions of the fields E_x, E_z, H_z and H_x a relationship between the aperture field and the fin currents was obtained. Galerkin's method was then applied by expanding onto a basis set for the transformed aperture field. Finline eigenvalues were then obtained from the zeros of a determinant equation. From knowledge of the two z-directed fields the complete finline field could be derived, thus allowing the computation of various finline parameters such as "impedance" and loss.

Although Itoh only initially considered symmetrical bilateral finline, the first rigorous results on dispersion and impedance since 1974 were published. In addition solutions for the first higher order mode were given, thus to defining the frequency range of operation.

It also appears that independently of Itoh, Knorr and Shayda [10], applied the spectral domain method to finline, but they included a matrix approach which simplified the formulation stages. These authors then presented an analysis of the unilateral finline

structure including results on fundamental mode dispersion, impedance and comparisons with the limiting cases of finned and dielectrically loaded waveguides to assess validity. Despite employing a simple pulse function as an approximation to the slot field, good agreement was found over the full range of guide parameters .

However, as finline structures were applied to the higher millimetric frequencies discrepancies between existing analyses and practice became apparent. This is because the effects of metallisation thickness and the substrate mounting had been neglected as an idealised structure had only been considered. Beyer [11] published the first results from a rigorous analysis including these effects by dividing the structure into four subregions. For each of these subregions TM-to-z and TE-to-z potentials were defined so that the Helmholtz equation is satisfied. However, the subsequent formulation for the fundamental mode assumed a purely TE expansion. The boundary conditions at all but one of the common interfaces were satisfied and then the Ritz-Galerkin method applied to match fields at the remaining interface. Eigenvalues for the fundamental finline mode were thus found from a zero determinant relation.

Results obtained from expansions of 10 or more at either side of the final interface were seen to give good agreement with experiment. Here metallisation thickness was found to be the most critical parameter, giving variations to the order of 5% in the dispersion of a 75Ghz finline, as it was varied between 0 and 70μm. However, latter workers were to disagree.

Motivated by the emergence of more generalised finline structures, Itoh and Hofmann [12] presented a more general analysis using the spectral-domain technique, employing an improvement to the formulation stages. By noting that without the fins present the

structure will support TE-to-y and TM-to-y modes, the concept of a rotation, [13], was employed to derive an equivalent transmission-line representation. This enabled a relationship between the aperture field and the fin currents to be readily obtained. Results for unilateral and coupled finline were presented. Although the effect of finite metallisation was not included, by introducing a fourth subregion in the slot to take account of this the basic method can be modified to analyse more realistic structures , [14].

As the analysis of finline structures began to reach a state of maturity, Mirshekar-Syahkal and Davies [15] published the first paper giving a theoretical treatment of finline losses at Q-band. Since the spectral-domain technique is able to provide a satisfactory field solution, it was possible to evaluate losses due to a finite metallic conductivity and the dielectric loss tangent. Results for dispersion and impedance are in agreement with previous workers [9], since these results are found to be relatively insensitive to the particular fin gap expansion. However, results for loss were found not to converge since the fin gap expansion was chosen in terms of Legendre polynomials which do not contain the required edge condition. Even though checks were made with the limiting case as the fins vanish into the side walls, there was no experimental comparison to assess the general validity of the loss results.

1.3) Review of Past Work - Higher Order Modes.

With a view to a characterisation of finline discontinuities, Saad and Schunemann [16] developed an analysis leading to closed form approximations to the fundamental and higher order finline modes. By matching fields under the condition $\beta=0$ a series of transcendental

equations leading to solutions for the mode cut-off's were obtained. The concept of a frequency independent effective dielectric constant was also introduced, and together with the cut-off's the dispersion of the fundamental mode was seen to be closely approximated. The cut-off wavenumbers of higher order modes are also seen to be in approximate agreement with exact results, whilst the effect of any dispersion errors on the resulting field distributions were seen to be of the same order of magnitude.

Vahldieck, [17] 1984, produced dispersion results for the fundamental and first few higher order modes in various finline structures including the effects of metallisation thickness and substrate holding grooves. The fields in the various subregions are expressed in terms of z-directed TE and TM potentials each constructed from a suitable set of eigenfunctions. The transverse resonance principle was then used to derive a system of chain matrices linking the amplitude coefficients of the respective eigenfunctions. Solution was obtained by imposing the boundary conditions at the two end walls which resulted in seeking zeros to a determinant. For numerical solution the size of expansion must be limited so that the matrix size does not become prohibitive. However, in order to adequately describe the fin edge condition, a typical matrix size of 30 by 30 was implied. In contrast to Beyer, results show that the effect of substrate mounting grooves is the more significant, particularly for the higher order modes.

In 1984 Omar and Schunemann presented an analysis employing the singular integral equation technique [18]. Operating in the space-domain this method offers a considerable reduction in matrix order and was argued to be superior over the spectral-domain technique when solving for higher order modes. A discussion on the edge effects at

the fin was given which clearly describes how the LSE and LSM modes supported by the dielectrically loaded waveguide must be coupled together in finlines resulting in a hybrid mode. These observations are fully exploited by formulating the problem separately for LSE and LSM waves, leaving the coupling to the later stages of the analysis. Results for the first 20 modes in a bilateral finline were presented , calculated mode coupling ceofficients prove orthogonality and show the existence of inductive and capacitive modes.

A subsequent paper by Omar and Schunemann [19] analysed unilateral finline and examined how under certain circumstances inductive and capacitive modes become coupled to give a mode of complex propagation. This effect, whereby two waves exhibiting complex conjugate phase constants had long been known to occur in waveguides containing a dielectric inserts, and is now believed to be widespread amongst planar transmission lines. Further theoretical results were presented, illustrating the coupling which occurs between complex mode pairs.

However, despite the advent of ever more powerful rigorous analyses, such as [20], the circuit designer's need for a quick an accurate solution is still not being met. For this reason, works such as Pramanick and Bhartia [21], which presented a set of closed form expressions providing reasonably accurate dispersion and impedance results over a range of guide parameters, are frequently encountered. Such results are useful for the computer aided optimisation of finline circuits, but are limited in their scope of application.

1.4 Objectives of thesis.

Even though the Spectral Domain Approach is relatively efficient in comparison with other analyses, there is still a need for more efficiency, coupled to simple closed form expressions with improved accuracy. There is also a need for work on finline discontinuities, although several papers have been published on this subject, details of which are given later in this thesis. Mode matching approaches are frustated by difficulties in obtaining a sufficient number of appropriate higher order modes. There is therefore a great need for a clear understanding of the finline mode spectrum, and work is needed on the efficient determination of higher order modes.

1.5) Outiline of Thesis.

Chapter (2) gives some of the backround theory required for this thesis. Section (2.1) gives a review of the basic equations defining electromagnetic fields in terms of vector potentials. It is then shown in section (2.2) how these may be applied to the analysis of dielectrically loaded waveguide, and how this problem may be solved using transverse resonance. After theory on edge conditions in section (2.3), section (2.4) presents a variational formulation for waveguide discontinuities.

Chapter (3) develops the Transverse Resonance Diffraction method, and it is specifically applied to unilateral finline. Section (3.1) defines the y-directed Hertzian potentials from which the finline fields will be derived. Section (3.2) then introduces the rotation due to Itoh [13] which resolves the LSE and LSM fields into fields due to transverse TM and TE parallel plate modes. This then

enables a relationship between transverse-to-y fields to be readily obtained. Section (3.3) establishes a set of coupled integral equations describing the effects of the fin involving Green's admittances following directly from results of the previous section. Section (3.4) introduces the Schwinger mapping, [22], to solve these equations. Originally introduced for the analysis of infinitely thin irises in waveguide, this mapping gives rise to basis functions which not only satisfy the fin edge condition implicitly, but are in fact quasi-static solutions to the wave equation within the fin gap.

Although a quick solution for the fundamental mode is included in section (3.4), the integral equations defining the effect of the fin are solved by the Ritz-Galerkin method using basis functions derived from the Schwinger mapping in section (3.5). Here dispersion results for the fundamental mode are compared with experiment at X-band. Chapter (3) is completed by developing the dual formulation based upon an expansion for the fin currents in section (3.6). By employing appropriate Gegenbauer polynomials over the fins, this solution is seen to give good agreement with results obtained using Schwinger functions in the gap.

Chapter (4) continues to develop the aperture formulation, and considers the cut-off condition in section (4.1). Here it is seen that LSE and LSM components of the finline field decouple. However, by virtue of the Schwinger mapping, a further decoupling is seen to occur which leads to a convenient categorisation of modal solutions. Modes at cut-off are found to be either purely LSE or LSM and to possess slot field variations given by distinct Schwinger functions. Thus modes may be catagorised in terms of families sharing a common slot field variation. Section (4.2) examines the form of transverse admittances subject to the cut-off condition and introduces a

systematic means of solving for the cut-off frequencies of the various mode families. A discussion of results is given in section (4.3) and the occurrence of complex mode propagation illustrated. The relationship between the limiting case of finline mode families modes in conventional waveguide is also established. Section (4.4) introduces a simple relation which can be employed to describe the dispersion of finline modes, and the approximation to the fundamental mode is employed to describe the phase characteristics of a finline taper.

Chapter (5) considers the evaluation of various finline parameters. Section (5.1) shows how the complete finline field can be obtained from the aperture field expansion. After giving examples of fields over the cross-section, attention turns to a description of the wall currents. Section (5.2) gives the backround theory to conduction and dielectric loss factors, and the Q-factor. Section (5.3) discusses the evaluation of these parameters in finline and section (5.4) presents the results. An investigation into their variation with housing and substrate materials is also included, and a comparison with measured results at X-band given.

Finally, with detailed knowledge of the finline field configuration and the mode spectrum, the step discontinuity problem is addressed in chapter (6). To avoid excessive computational effort a number of simplifications are introduced in section (6.1). Section (6.2) applies these to a variational formulation, the results of which are then compared with experiment. Whilst section (6.3) applies both these results and the simplified dispersion relation to investigate a simple filter structure.

References - Chapter (1)

1) Meier P.J. 'Integrated Fin-Line Millimeter Componenets'; IEEE trans MTT-22, December 1974, pp 1200-1216.

2) Kpodo E, Schunemann K, Begemann G. 'A Quadriphase Fin-Line Modulator.' IEE trans MTT-28, July 1980, pp 747-751.

3) Beyer A, Solbach K, 'A New Fin-Line Ferrite Isolator For Integrated Millimeter-Wave Circuits.' IEEE trans, MTT-29, Dec 1981, pp 1344-1348.

4) Menzel W, Callsen H, '140 GHz Finline Compenents.' IEEE trans, MTT-33, Jan 1985, pp 53-55.

5) Hofmann H. 'Fin-line Dispersion', Electron let, vol 12, Aug 1976 pp 428-429.

6) Saad, A.M.K. and Begemann G.,'Electrical Performance of Finlines of Various Configurations' IEE MOA, Jan 1977, vol 1 pp 81-88.

7) Cohn, S.B.: 'Properties of Ridged Waveguide.' Proc IRE, 1947, pp 783-788.

8) Saad, A.M.K and Schunenmann K. 'A Simple Method for Analyzing Fin-Line Structures.' IEEE trans, MTT-26, Nov 1978, pp 1002-1011.

9) Schmidt L-P and Itoh T. 'Sectral Domain Analysis of Dominant and Higher Order Modes in Fin-Lines' IEEE trans, MT-28, Nov 1980, pp 981-985.

10) Knorr J.B. and Shayda P.M. 'Millimeter-Wave Fin-Line Chracteristics' IEEE trans, MTT-28, July 1980, pp 737-743.

11) Beyer A. 'Analysis of the Characteristics of an Earthed Finline.' IEEE trans, MTT-29, July 1981, pp 676-680.

12) Schmidt L-P, Itoh T. and Hofmann H. 'Characteristics of Unilateral Finline Structures with Arbitrarily Located Slots.' IEEE trans, MTT-29, April 1981, pp 352-355.

13) Itoh, T. , 'Spectral Domain Immitance Approach for Dispersion Characteristics of Generalised Printed Tranmission Lines.' IEEE trans MTT-28, July 1980, pp 733-736.

14) Kitazawa, T., Hayashi, Y. and Suzuki, M. , 'Analysis of the Dispersion Characteristic of Slot Line with Thick Metal Coating.' IEEE trans MTT-28, April 1980, pp 387-392.

15) Mirshekar-Syahkal, D. and Davies J.B. , 'An Accuate, Unified Solution to Various Fin-line Structures of Phase Constant Characteristic Impedance and Attenuation.' IEEE trans MTT-30 Nov 1982 pp 1854-1861.

16) Saad, A.M.K and Schunemann, K. , 'Closed From Approximations for Fin-Line Eigenmodes.' IEE Proc, Vol 129, Pt H, October 1982, pp253-261.

17) Vahldieck, R. , 'Accurate Hybrid-Mode Analysis of Various Finline Configurations Including Multilayered Dielectrics, Finite Metalization Thickness, and Substrate Holding Grooves.' IEEE trans, MTT-32, November 1984, pp 1454-1460.

18) Omar, A.S. and Schunemann, K., 'Formulation of the Singular Integral Equation Technique for Planar Transmission Lines.' IEEE trans MTT-33, December 1985, pp 1313-1321.

19) Omar, A.S. and Schunemann, K. , 'Space-Domain Decoupling of LSE and LSM Fields in Generalized Planar Guiding Structures.' IEEE trans, MTT-32, December 1984, pp 1626-1632.

20) Bornemann, J. , 'Rigorous Field Theory Analysis of Quasiplanar Waveguides.' IEE proc, vol 132, Pt H, February 1985, pp 1-5.

21) Pramanick, P. and Bhaartia, P. , 'Accurate Analysis Equations and Synthesis Technique for Unlateral Finlines.' IEEE trans, MTT-33, January 1985, pp 24-29.

22) Collin, R.E. , 'Field Theory of Guided Waves.' McGraw-Hill, New York, 1960.

CHAPTER TWO: BACKROUND THEORY

Starting from an assumption of Maxwell's equations, the divergence equations, and the constitutive relations, this chapter will firstly introduce Hertzian vector potentials. These are then applied to the problem dielectrically loaded waveguide. It is then shown how the transverse resonance technique arises, with the extension to more complicated uniform structures assumed to follow naturally.

Section three gives a derivation of the metallic edge condition, which will be of fundamental importance to the analysis of finline. Finally, as an illustration of variational techniques, a general formulation for waveguide discontinuities is given, with particular reference to the Ritz-Galerkin method.

2.1) Hertzian Vector Potentials.

It is readily shown how Maxwell's lead to wave equations, but their general solution for electromagnetic waves subject to prescribed boundary conditions can be a complex problem. This, however, can be considerably simplified by employing auxiliary potential functions.

In a source free and homogeneous medium an electromagnetic field can be completely described by a superposition of electric and magnetic Hertzian vector potentials [1] as:

$$\underline{H} = j\omega\varepsilon \nabla \times \underline{\Pi}_e + k^2 \underline{\Pi}_h + \nabla\nabla\cdot\underline{\Pi}_h \qquad (2.1.1a)$$

$$\underline{E} = k^2 \underline{\Pi}_e + \nabla\nabla\cdot\underline{\Pi}_e + j\omega\mu \nabla \times \underline{\Pi}_h \qquad (2.1.1b)$$

where $\underline{\Pi}_e$ and $\underline{\Pi}_h$ are solutions of the Helmholtz equation:

$$\nabla^2\underline{\Pi} + k^2 \underline{\Pi} = 0$$

with $k^2 = \mu\varepsilon\omega^2$

The boundary conditions acting on $\underline{\Pi}_e$ and $\underline{\Pi}_h$ may be determined from those conditions acting on the electromagnetic field by expanding equations (2.1.1) in full. For instance a field representation in terms of z-directed Hertzian potentials, gives:

$$\underline{E} = j\omega\mu \begin{bmatrix} \frac{\partial}{\partial y} \\ -\frac{\partial}{\partial x} \\ 0 \end{bmatrix} \Psi_h(x,y) + \begin{bmatrix} -j\beta & \frac{\partial}{\partial x} \\ -j\beta & \frac{\partial}{\partial y} \\ k^2 - \beta^2 \end{bmatrix} \Psi_e(x,y) \qquad (2.1.3)$$

$$\underline{H} = j\omega\varepsilon \begin{bmatrix} \frac{\partial}{\partial y} \\ -\frac{\partial}{\partial x} \\ 0 \end{bmatrix} \Psi_e(x,y) + \begin{bmatrix} -j\beta & \frac{\partial}{\partial x} \\ -j\beta & \frac{\partial}{\partial y} \\ k^2 - \beta^2 \end{bmatrix} \Psi_h(x,y) \qquad (2.1.4)$$

where a propagating type z-variation of $\exp(-j\beta z)$, has been assumed.

The function $\Psi_e(x,y)$ is thus found from a scalar wave equation subject to the boundary conditions of E_z, and $\Psi_h(x,y)$ is found using the boundary conditions on H_z. If there are no additional conditions imposed on the remaining fields, "transverse electric" (TE) solutions described purely in terms of $\Psi_e(x,y)$ and "transverse magnetic" (TM) solutions described purely in terms of $\Psi_h(x,y)$ can

exist independently. In general these are five field solutions with one of the z-directed field components absent.

However, if the boundary conditions are satisfied by functions which do not vary with, say the y-coordinate, as in the case of parallel plate waveguide, modal fields now only contain three field components:

$$\underline{E} = j\omega\mu \begin{bmatrix} 0 \\ -\frac{\partial}{\partial x} \\ 0 \end{bmatrix} \Psi_h(x) + \begin{bmatrix} -j\beta & \frac{\partial}{\partial x} \\ 0 \\ k^2 - \beta^2 \end{bmatrix} \Psi_e(x) \qquad (2.1.5)$$

$$\underline{H} = j\omega\varepsilon \begin{bmatrix} 0 \\ -\frac{\partial}{\partial x} \\ 0 \end{bmatrix} \Psi_e(x) + \begin{bmatrix} -j\beta & \frac{\partial}{\partial x} \\ 0 \\ k^2 - \beta^2 \end{bmatrix} \Psi_h(x) \qquad (2.1.6)$$

In finline, modes will require at least five field components, six in general. Consequently the problem will have to be formulated in terms of two coupled potentials. The next section will introduce suitable potentials and a further section will introduce the nature of the additional boundary condition which couples them together.

2.2) Dielectrically Loaded Waveguide.

Dielectrically loaded waveguide provides a natural starting point from which to develop solution for a wide range of E-plane structures. It forms the basic waveguide into which the

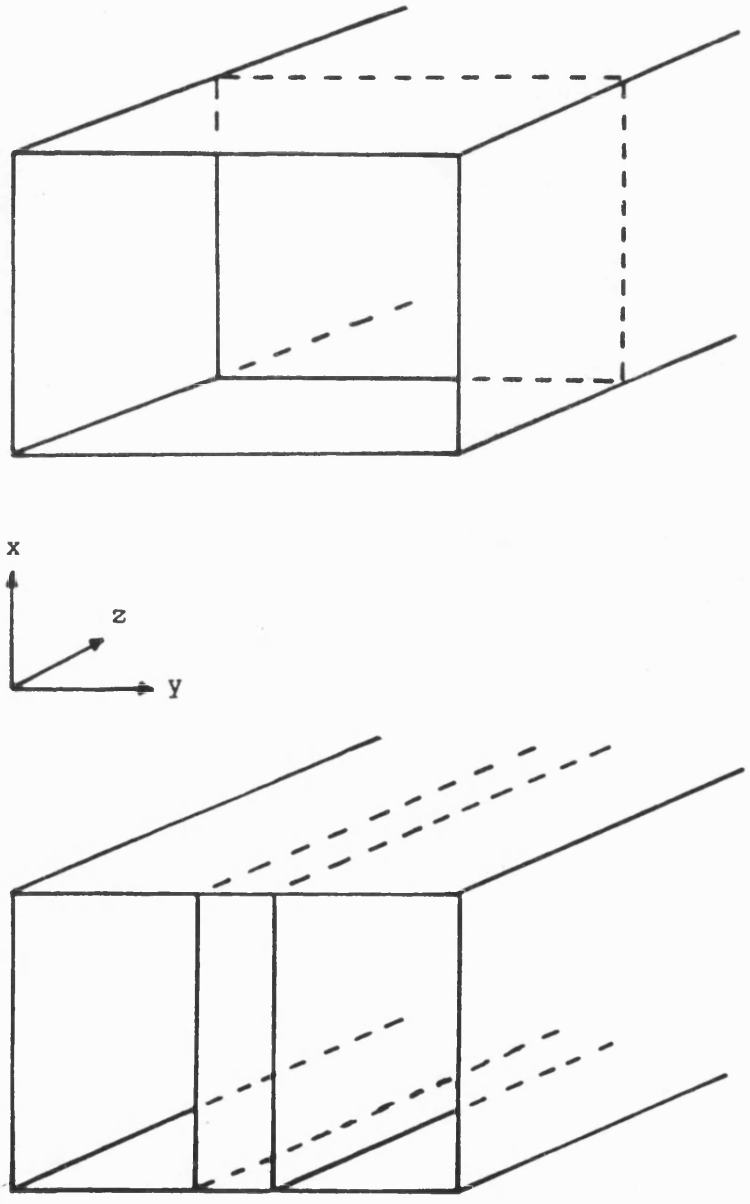

Figures (2.2.1a) and (2.2.1b) Conventional Rectangular Waveguide Containing an Abrupt Change in Internal Medium and Dielectrically Loaded Waveguide.

metallisations defining E-plane circuits are introduced. This section will use Hertzian vector potentials to solve for this basic waveguide, and will introduce the concept of transverse resonance.

Firstly consider a conventional rectangular waveguide which experiences a change in the z-direction, the direction of propagation, and in this particular case a change in the interior medium as illustrated by figure (2.2.1a). It is readily apparent that the boundary conditions at the interface can be satisfied by either TE-to-z or TM-to-z modes alone. Following from this, it is natural to suppose that a waveguide uniformly loaded by a dielectric slab lying in the x-z longitudinal plane, as illustrated by figure (2.2.1b), can be solved in terms of y-directed Hertzian potentials of either the magnetic or electric type. Indeed, as is shown in [2], dielectrically loaded waveguide in general can support modes requiring five field components with either the y-directed electric or magnetic field absent. These two types of mode are classified as "longitudinal section electric", LSE, and "longitudinal section magnetic", LSM, respectively.

For simplicity, consider the symmetrical case as given by figure (2.2.2) . The problem can be simplified by inserting either a magnetic or an electric wall at y=0 to formulate the problem separately for modes exhibiting even or odd symmetry. Since the fundamental mode is even, the formulation employing a magnetic wall at y=0 will be given here.

In terms of a magnetic Hertzian potential, the fields are given as:

$$\underline{E} = -j\omega\mu\nabla \times \underline{\Pi}_h \qquad (2.2.1)$$

$$\underline{H} = k^2 \underline{\Pi}_h + \nabla\nabla\cdot\underline{\Pi}_h \qquad (2.2.2)$$

where: $\underline{\Pi}_h = \hat{y}\, \Psi_h(x,y,z)$, $\hat{y}$ being a unit vector in the y-direction.

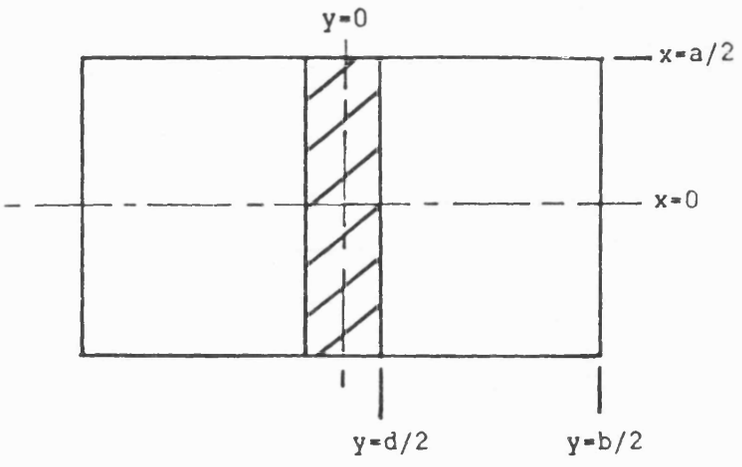

Figure (2.2.2) Axis Orientation and Dimensional Detials for the Analysis of Dielectrically Loaded Waveguide.

Thus from equations (2.2.1) and (2.2.2) the resulting electromagnetic field will not contain a y-directed electric component, E_y. Assuming propagation in the z-direction with phase constant β, the remaining fields will have a common z dependence of $\exp(-j\beta z)$ which can be neglected in the transverse boundary problem. Furthermore, the x-variation of the fields E_x, H_y and H_z can be assumed of the form $\cos(n\pi x/a)$, and that of the fields E_z and H_x as $\sin(n\pi x/a)$, in accordance with boundary conditions in x. Solution for Ψ_h may be obtained by using the remaining boundary conditions with y, including those of the air-dielectric interface. Thus:

i) For $0 < y < d/2$,

$$\Psi_h(x,y) = A \cos k_d y \cos \frac{n\pi x}{a} \qquad (2.2.3a)$$

ii) For $d/2 < y < b/2$,

$$\Psi_h(x,y) = B \sin k_a(b/2 - y) \cos \frac{n\pi x}{a} \qquad (2.2.3b)$$

Where k_d and k_a are the y-directed wavenumbers in the dielectric and air filled regions of relative permittivities ε_r and 1.0 respectively. Solution of the wave equation, therefore, requires that:

$$\beta^2 = k_d^2 + \left(\frac{n\pi}{a}\right)^2 - \varepsilon_r k_o^2 = k_a^2 + \left(\frac{n\pi}{a}\right)^2 - k_o^2$$

whilst the constants A and B must be determined so as to satisfy the boundary conditions at the interface.

Firstly, continuity of the longitudinal field at y=d/2 involves the field E_z. Now:

$$E_z = j\omega\mu \frac{\partial \Psi_h}{\partial y}$$

Thus taking the y-derivatives of equations (2.2.3a) and (2.2.3b), and applying the above boundary condition gives a relation linking the coefficients A and B as:

$$- A\, k_d \sin k_d\, d/2 = - B\, k_a \cos k_a(b/2-d/2) \qquad (2.2.4)$$

To eliminate the coefficients A and B so that solution for β, the propagation coefficient of a mode in the waveguide, can be determined a second boundary condition is imposed. For continuity of flux normal to the interface consider the field H_y :

$$H_y = \Psi_h \left[\left(\frac{n\pi}{a}\right)^2 + \beta^2 \right]$$

giving a second relation:

$$A \cos k_d\, d/2 = B \sin k_a(b/2-d/2) \qquad (2.2.5)$$

Dividing equation (2.2.4) by equation (2.2.5) gives a transcendental equation from which a solution for β, and hence the function Ψ_h, can be determined:

$$k_d \tan k_d d/2 = k_a \cot k_a(b/2-d/2) \qquad (2.2.6)$$

This equation leads directly to the concept of a transverse resonance by noting that the TE wave admittance taken in the y-direction is given by:

$$Y = - \frac{H_x}{E_z} = \frac{H_z}{E_x} = - \frac{\partial \Psi_h / \partial y}{j\omega\mu\, \Psi_h} \qquad (2.2.7)$$

Equation (2.2.6) may thus be written as:

$$-j\, Y_d \tan k_d d/2 + j\, Y_a \cot k_a(b/2-d/2) = 0 \qquad (2.2.8)$$

Where the term, $- j\, Y_d \tan k_d d/2$, is the admittance seen looking

along a TE waveguide within the dielectric medium a distance d/2 away from an open circuit. Similarly, $j\,Y_a \cot k_a\,(b/2-d/2)$, is the admittance seen looking onto a short circuit.

Equation (2.2.8) gives solution for the even symmetric modes in dielectrically loaded waveguide, and an interpretation in terms of the resonance a transverse equivalent network as given by figure (2.2.3a).

Modes exhibiting odd symmetry about y=0 are similarly obtained from the solution of:

$$j\,Y_d \cot k_d d/2 \;+\; j\,Y_a \cot k_a(b/2-d/2) \;=\; 0 \qquad (2.2.9)$$

corresponding to the equivalent network of figure (2.2.3b)

This concept can be applied to solve for uniform multilayer structures directly from a transverse equivalent network with relative ease. However, E-plane structures such as finline are non-uniform with x and cannot be solved using transverse resonance alone. The technique has been applied to determine the cut-off frequencies of ridged waveguide, [3], and finline, [4], by introducing approximate lumped reactive elements where transverse discontinuities occur. These examples, however, cannot describe the general case. The next chapter will develop the transverse resonance diffraction method as an extension of the basic concept by including the effects of discontinuities in the transverse plane in a rigorous formulation. But firstly these effects must be defined.

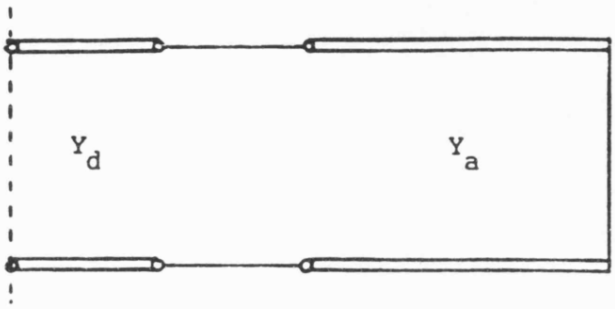

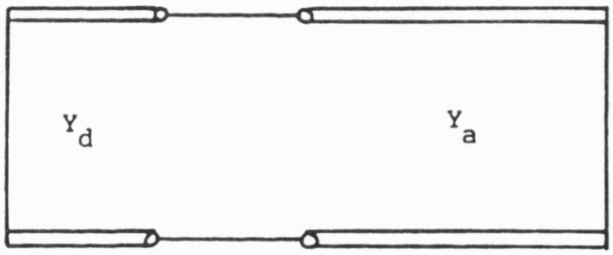

Figures (2.2.3a) and (2.2.3b) Equivalent Transverse Networks for Asymmetric and Symmetric Modes in Dielectrically Loaded Waveguide.

2.3) Edge conditions.

The previous section has already assumed the boundary conditions at an interface between media, but for the purposes of this section it is instructive to state them in full, as:

i) Continuity of tangential fields $\underline{E}$ and $\underline{H}$.

ii) Continuity of normal fields $\underline{D}$ and $\underline{B}$.

Then at the boundary between free space and a perfect conductor, it is readily shown that:

i) The tangential electric field vanishes.

ii) The normal magnetic field vanishes.

For the analysis of E-plane structures such as finline, there is a further boundary condition caused by metallic edges which must be satisfied. Here, it is found that certain field components become infinite as the edges are approached but in a manner such that the total energy remains finite.

To analyse the general behaviour of fields in the vicinity of metallic edges, consider the general case of the conducting wedge as shown in figure (2.3.1). The following analysis in taken from chapter (1) of Collin [5].

Writing out explicitly the two Maxwell curl equations in cylindrical coordinates r, z, θ and assuming harmonic fields, one obtains:

$$\frac{1}{r}\frac{\partial}{\partial r} rE_\theta - \frac{1}{r}\frac{\partial}{\partial \theta} E_r = -j\omega\mu H_z \qquad (2.3.1a)$$

$$\frac{\partial}{\partial z} E_r - \frac{\partial}{\partial z} E_z = -j\omega\mu H_\theta \qquad (2.3.1b)$$

$$\frac{1}{r}\frac{\partial}{\partial \theta} E_z - \frac{\partial}{\partial z} E_\theta = -j\omega\mu H_r \qquad (2.3.1c)$$

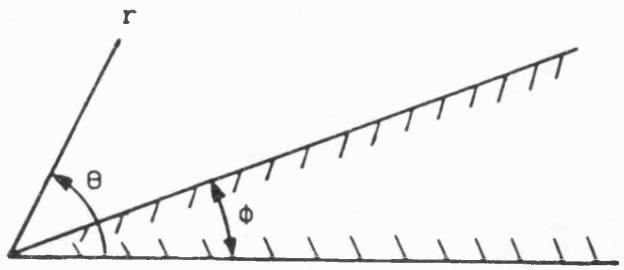

Figure (2.3.1) Metallic Wedge in Cylindrical Polar Coordinates.

and,

$$\frac{1}{r}\frac{\partial}{\partial r}rH_\theta - \frac{1}{r}\frac{\partial}{\partial \theta}H_r = -j\omega\mu E_r \qquad (2.3.2a)$$

$$\frac{\partial}{\partial z}H_r - \frac{\partial}{\partial z}H_z = -j\omega\mu E_\theta \qquad (2.3.2b)$$

$$\frac{1}{r}\frac{\partial}{\partial \theta}H_z - \frac{\partial}{\partial z}H_\theta = -j\omega\mu E_r \qquad (2.3.2c)$$

In the vicinity of $r \longrightarrow 0$ the fields may be expressed as a power series in r with coefficients functions of θ and z.

$$H_z = r^\alpha (a_0 + a_1 r + \cdots\cdot) \qquad (2.3.3a)$$

$$H_\theta = r^\alpha (b_0 + b_1 r + \cdots\cdot) \qquad (2.3.3b)$$

$$H_r = r^\alpha (c_0 + c_1 r + \cdots\cdot) \qquad (2.3.3c)$$

$$E_z = r^\alpha (A_0 + A_1 r + \cdots\cdot) \qquad (2.3.4a)$$

$$E_\theta = r^\alpha (B_0 + B_1 r + \cdots\cdot) \qquad (2.3.4b)$$

$$E_r = r^\alpha (C_0 + C_1 r + \cdots\cdot) \qquad (2.3.4c)$$

By substituting equations (2.3.3) and (2.3.4) into (2.3.1) and (2.3.2), and equating for powers of r, it is immediately found that $A_0 = 0$ and $a_0 = 0$. This implies that the tangential fields E_z and H_z are in fact finite on the edge. To solve for the exponent, α, giving the singularity in the remaining fields, the relations obtained between coefficients may be manipulated to form a straightforward differential equation. For instance an equation involving the coefficient C_0, the exponent α and ordinate θ is obtained as:

$$\frac{\partial^2}{\partial \theta^2}C_0 + (1+\alpha)^2 C_0 = 0 \qquad (2.3.5)$$

Since the boundary conditions on C_0 with θ must be consistent with the radial field, E_r, α can be determined. Solutions to equation (2.3.5) are of the form:

$$C_0 = X \sin(\alpha+1)\theta + Y \cos(\alpha+1)\theta \qquad (2.3.6)$$

where X and Y are arbitrary constants.

Now E_r and hence C_0 must vanish for $\theta = \phi$ and $\theta = 2\pi$ irrespective of r. Thus,

$$X \sin(\alpha+1)\phi + Y \cos(\alpha+1)\phi = 0 \qquad (2.3.7a)$$

$$X \sin(\alpha+1)2\pi + Y \cos(\alpha+1)2\pi = 0 \qquad (2.3.7b)$$

The above equations are then manipulated to eliminate X and Y, giving:

$$\tan(\alpha+1)\phi = \tan(\alpha+1)2\pi \qquad (2.3.8)$$

This has solutions of the form:

$$(\alpha+1)\phi = (\alpha+1)2\pi + n\pi$$

where n is any integer. Re-arranging for α gives the result:

$$\alpha = \frac{n\pi}{2\pi - \phi} - 1 \qquad (2.3.9)$$

The arctan function has brought ambiguity into the solution over the choice of n. But imposing the condition that the energy density $|E|^2$ is finite in the cylindrical element $2\pi r\, dr$ leads to a minimum value for α of -1, corresponding to an integrable singularity of E on the edge. The trivial solution with n = 0 is therefore not allowed. Thus for a 180° edge occurring in planar metallic structures, the choice of n = 1 with $\phi = \pi$ gives $\alpha = -0.5$.

With the edge located along the line pointing in the z-direction and passing through the point $(x_0, y_0, 0)$ in cartesian coordinates as illustrated by figure (2.3.2), the variation of radial fields in the vicinity of the edge must be of the form:

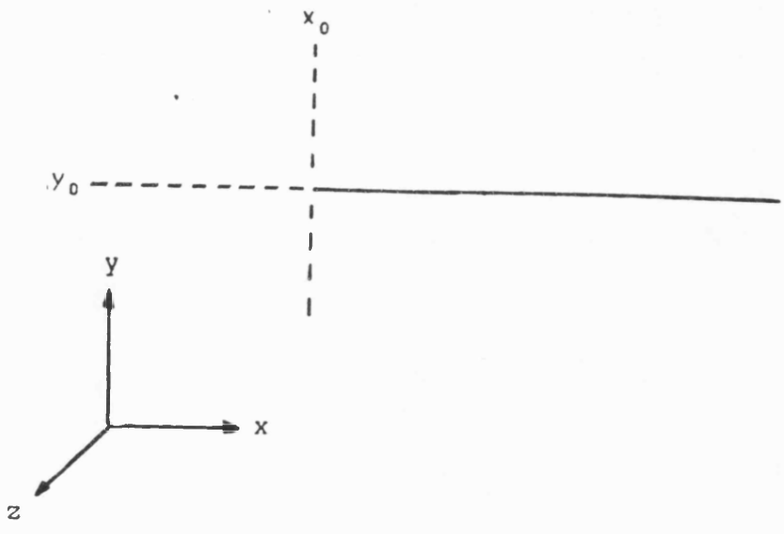

Figure (2.3.2) 180° Metallic Edge in Rectangular Cartesian Coordinates

$$f(x,y) = \frac{1}{\sqrt{(x - x_0)^2 + (y - y_0)^2}} \qquad (2.3.10)$$

For $y = y_0$ and in the vicinity of $x \longrightarrow x_0$, this variation may be written:

$$f(x) = \frac{1}{\sqrt{1 - \left[\frac{x}{x_0}\right]^2}} \qquad (2.3.11)$$

It is this this particular form which will be required when considering fields in the fin-gap.

2.4i) Variational Formulation for Waveguide Discontinuities.

Before solving for finline, this section has been included to introduce a formulation for discontinuity problems as generalised two port networks which can be found in chapter (8) of [5]. Besides being required latter when considering finline discontinuities, the following derivation serves to illustrate variational principles which are employed in the general formulation.

Consider the waveguide discontinuity structure as given by figure (2.4.1). Orthogonal scalar mode solutions to the transverse field in waveguide(1) will be denoted by ψ_n, and solutions in waveguide(2) by ϕ_n. If fundamental mode of amplitude b_1 is incident from the region $z > 0$ and that of the region $z < 0$ is incident with amplitude a_1, then continuity of transverse electric field at $z=0$ implies:

$$[(1 + R_1)a_1 + T_{21}b_1]\,\psi_1 + \sum_{n=2}^{\infty} a_n \psi_n =$$

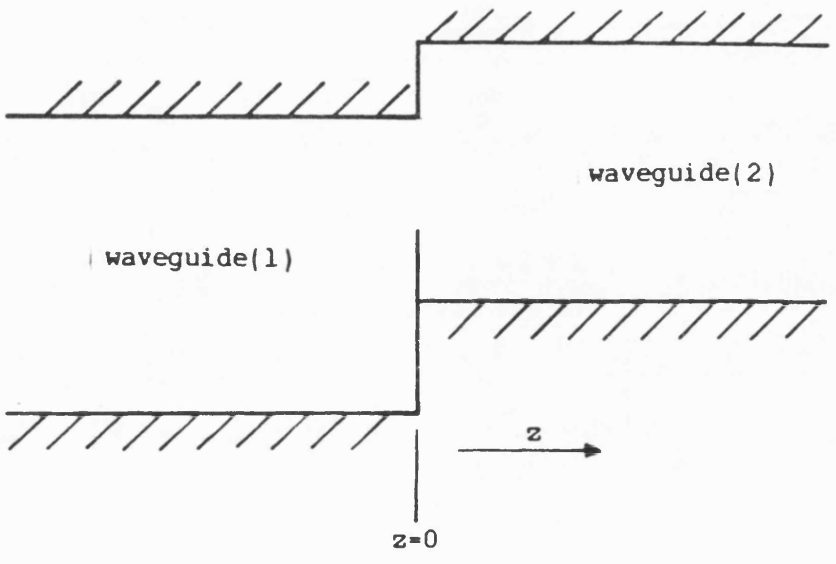

Figure (2.4.1) Typical Waveguide Discontinuity.

$$[(1 + R_2)b_1 + T_{12}b_1]\,\Phi_1 + \sum_{n=2}^{\infty} b_n \Phi_n \qquad (2.4.1)$$

Where;

R_1 = reflection coefficient of the discontinuity as seen by the fundamental mode in waveguide(1).

R_2 = reflection coefficient of the discontinuity as seen by the fundamental mode in waveguide(2).

T_{12} = transmission coefficient of the fundamental mode from waveguide(1) into waveguide(2).

T_{21} = transmission coefficient of the fundamental mode from waveguide(2) into waveguide(1).

(N.B. $T_{12} = S_{21}$, $T_{21} = S_{12}$.)

If the transverse magnetic fields are simply related to the transverse electric fields through scalar admittances g_n and h_n in the two waveguides, continuity of transverse magnetic field implies:

$$[(1 - R_1)a_1 - T_{21}b_1]g_1\,\Psi_1 - \sum_{n=2}^{\infty} a_n g_n \Psi_n =$$

$$[(1 - R_1)a_1 - T_{21}b_1]h_1\,\Phi_1 + \sum_{n=2}^{\infty} a_n h_n \Phi_n \qquad (2.4.2)$$

The following equivalent transmission line quantities are now introduced:

$$V_1 = (1 + R_1)a_1 + T_{21}b_1 \qquad (2.4.3a)$$

$$V_2 = (1 + R_2)b_1 + T_{12}a_1 \qquad (2.4.3b)$$

$$I_1 = (1 - R_1)g_1 a_1 - T_{21}b_1 g_1 \qquad (2.4.3c)$$

$$I_2 = -(1 - R_1)h_1 b_1 - T_{12}a_1 h_1 \qquad (2.4.3d)$$

The amplitudes a_1 and b_1 may be arbitrarily chosen so that $I_2=0$ or $I_1=0$. The aperture electric field, F, is thus a linear superposition of fields proportional to I_1 and I_2.

$$F = I_1 F_1 - I_2 F_2 \qquad (2.4.4)$$

Thus by orthogonality :

$$V_1 = \int (I_1 F_1 - I_2 F_2)\, \psi_1 \, dx \qquad (2.4.5a)$$

$$V_2 = \int (I_1 F_1 - I_2 F_2)\, \phi_1 \, dx \qquad (2.4.5b)$$

$$a_n = \int (I_1 F_1 - I_2 F_2)\, \psi_n \, dx \qquad (2.4.5c)$$

$$b_n = \int (I_1 F_1 - I_2 F_2)\, \phi_n \, dx \qquad (2.4.5d)$$

The first two of the above show that the discontinuity may be represented as an equivalent T-network given by a Z-matrix as shown in figure (2.4.2) so that:

$$V_1 = Z_{11} I_1 - Z_{12} I_2$$
$$V_2 = Z_{21} I_1 - Z_{22} I_2$$

where:

$$Z_{11} = \int F_1 \psi_1 \, dx$$

$$Z_{12} = \int F_2 \psi_1 \, dx$$

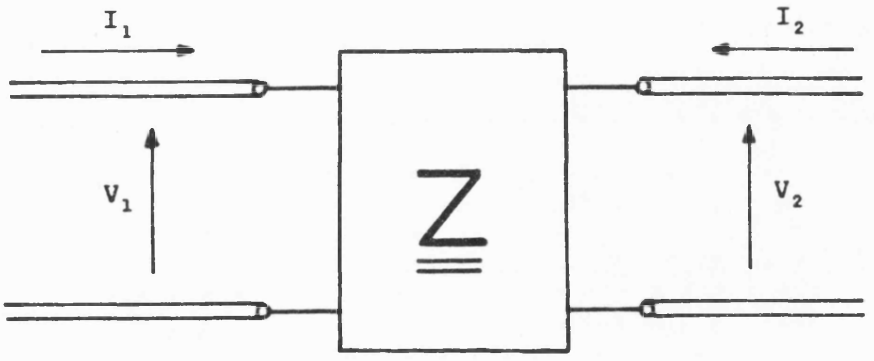

Figure (2.4.2) Equivalent Circuit of Waveguide Discontinuity.

$$Z_{21} = \int F_1 \, \phi_1 \, dx$$

$$Z_{22} = \int F_2 \, \phi_1 \, dx$$

Substituting for a_n and b_m into equation (2.4.1) and using expressions for I_1 and I_2 as defined previously gives:

$$I_1 \, \psi_1 - \sum_{n=2}^{\infty} g_n \, \psi_n \int (I_1 \, F_1 - I_2 \, F_2) \, \psi_n \, dx$$

$$= I_2 \, \phi_1 + \sum_{n=2}^{\infty} h_n \, \phi_n \int (I_1 \, F_1 - I_2 \, F_2) \, dx$$

or

$$I_1 \, \psi_1 - I_2 \, \phi_1 =$$

$$\int (I_1 \, F_1 - I_2 \, F_2) \left[\sum_{n=2}^{\infty} g_n \, \psi_n(x) \, \psi_n(x') + h_n \, \phi_n(x) \, \phi_n(x') \right] dx'$$

$$= -j \int (I_1 \, F_1 - I_2 \, F_2) \, G(x|x') \, dx' \qquad (2.4.7)$$

where

$$-j \, G(x|x') = \sum_{n=2}^{\infty} g_n \, \psi_n(x) \, \psi_n(x') + h_n \, \phi_n(x) \, \phi_n(x')$$

If the higher order modes corresponding to $n > 1$ are below cut-off, then:

$$g_n = -j|g_n| \quad ; \quad h_n = -j|h_n|$$

and G is a real function providing some computational advantage.

Since I_1 and I_2 are chosen as linearly independent variables, equation (2.4.7) is equivalent to two separate equations:

$$\psi_1 = -j \int F_1 \, G \quad dx \tag{2.4.8}$$

$$\phi_1 = -j \int F_2 \, G \quad dx \tag{2.4.9}$$

Multiplying equation (2.4.8) by F_1, integrating and dividing by $\left[\int F_1 \, \psi_1 dx \right]^2$ gives:

$$\frac{1}{\int F_1 \, \psi_1 \, dx} = \frac{1}{Z_{11}} \quad \frac{-j \iint G(x|x') \;\; F_1(x) \; F_1(x') \; dx \; dx'}{\left[\int F_1 \, \psi_1 \;\; dx \right]^2} \tag{2.4.10}$$

and similarly for the remaining elements of the Z-matrix of the equivalent circuit, namely:

$$\frac{1}{Z_{22}} = \frac{-j \iint G(x|x') \;\; F_2(x) \; F_2(x') \; dx \; dx'}{\left[\int F_2 \, \phi_1 \;\; dx \right]^2} \tag{2.4.11}$$

$$\frac{1}{Z_{21}} = \frac{-j \iint G(x|x') \;\; F_2(x) \; F_1(x') \; dx \; dx'}{\iint F_1 \, F_2 \, \psi_1 \, \phi_1 \; dx \; dx'} \tag{2.4.12}$$

$$\frac{1}{Z_{12}} = \frac{-j \iint G(x|x')\ F_1(x)\ F_2(x')\ dx\ dx'}{\iint F_2\ F_1\ \phi_1\ \psi_1\ dx\ dx'} = \frac{1}{Z_{21}} \qquad (2.4.13)$$

These are all found to exhibit variational properties with respect to arbitrary first order variations in the trial field functions F. For example consider equation (2.4.11) and vary F_2 from is true value. Expanding for $F_2 + \delta F_2$ gives:

$$\left[\int F_2\ \phi_1 dx\right]^2 \delta\frac{1}{Z_{22}} + \frac{2}{Z_{22}} \iint F_1(x')\ \delta F_2(x)\ \phi_2(x)\ \phi_1(x')\ dx\ dx'$$

$$= -\ j2 \iint G(x|x')\ F_2(x')\ \delta F_2(x)\ dx\ dx'$$

or

$$\left[\int F_2\psi_1 dx\right]^2 \delta\frac{1}{Z_{22}} = 2\int \delta F_2(x')\left[-j\int G(x|x')\ F_2(x)\ dx - \phi_1(x')\right]dx$$

By virtue of equation(2.4.9) the integrand to the right is identically zero, as are changes in Z_{22} due to ∂F_2.

2.4ii) Ritz-Galerkin Formulation.

By adopting new notation, equations (2.4.10) to (2.4.13) defining the Z-matrix elements may be condensed into:

$$x_{ij} = \frac{<F_j\ \theta_j><F_i\ \theta_i>}{<F_i\ G\ F_j>} \qquad (2.4.14)$$

where $\theta_i = \psi_i$, $\theta_j = \phi_j$

and since the elements of the Z-matrix are purely imaginary:

$$x_{ij} = Im\,(Z_{ij}) \quad , \quad i=1,2 \quad j=1,2$$

Then by expanding the fields F_1 and F_2 in terms of the function set $\{ U_k \}$:

$$F_i = \sum_{k=1}^{N} \lambda_{ik} \; U_k$$

$$F_j = \sum_{k=1}^{N} \lambda_{jk} \; U_k$$

equation (2.4.14) may be written in terms of matrix notation as:

$$x_{ij} = \frac{\underline{\lambda}_j^T \; \underline{P}_i \; \underline{P}_j^T \; \underline{\lambda}_i}{\underline{\lambda}_j \; \underline{\underline{B}}^T \; \underline{\lambda}_i} \qquad (2.4.15)$$

where:

$\underline{\lambda}_j^T$ is a row vector of elements $(\lambda_j)_k$.

$\underline{\lambda}_i$ is a column vector of elements $(\lambda_i)_k$

$\underline{P}_j^T$ is a row vector of elements $\langle \theta_j \; U_k \rangle$

$\underline{P}_i$ is a column vector of elements $\langle \theta_i \; U_k \rangle$

and $\underline{\underline{B}}$ a matrix of elements $\langle U_k \; G \; U_l \rangle$

The stationary properties of equation (2.4.15) are characterised by:

$$\nabla \; (\underline{\lambda}_j \; \underline{P}_i^T \; \underline{P}_j \; \underline{\lambda}_i^T - x_{ij} \; \underline{\lambda}^T{}_j \; \underline{\underline{B}} \; \underline{\lambda}_i \;) = 0$$

with $\nabla \; x_{ij} = 0$ w.r.t $\underline{\lambda}_i$ or $\underline{\lambda}_j$

carrying out the differentiation with respect to $\underline{\lambda}_j$ gives:

$$\underline{P}_i \; \underline{P}_j^T \; \underline{\lambda}_i - x_{ij} \; \underline{\underline{B}} \; \underline{\lambda}_i = 0$$

which for a non singular matrix $\underline{\underline{B}}$ gives an eigenvalue equation:

$$\underline{\underline{B}}^{-1}\ \underline{P}_i\ \underline{P}_j^T\ \underline{\lambda}_i\ =\ x_{ij}\ \underline{\lambda}_i$$

from which it may be deduced:

$$x_{ij} = \underline{P}_j^T\ \underline{\underline{B}}^{-1}\ \underline{P}_i$$

This general result allows the extension to a multiport description of the discontinuity which can include the effects of higher order mode interaction. Moreover, provided the function set $\{ U_k \}$ can adequately describe the fields across the discontinuity, the Ritz-Galerkin method will converge to an exact field solution ,[6].

References - Chapter (2)

1) Stratton J. A. 'Electromagnetic Theory.' McGraw-Hill, New York, 1941

2) Harrington R. 'Time Harmonic Electromagnetic Fields.' McGraw-Hill, New York, 1961.

3) Cohn, S.B.: 'Properties of ridged waveguide.' Proc IRE, 1947, pp 783-788.

4) Saad, A.M.K. and Begenmann G.,'Electrical performance of finlines of various configurations' IEE MOA, Jan 1977, vol 1 pp 81-88.

5) Collin, R.E , 'Field Theory of Guided Waves.' McGraw-Hill, New York, 1960.

6) Harrington, R. , "Matrix Methods for Field Problems.", Proc IEEE Vol 55, No 2, Feb, 1967.

CHAPTER THREE: DEVELOPMENT OF THE TRANSVERSE RESONANCE DIFFRACTION METHOD

In this chapter the TRD method is developed specifically for the finline case. To avoid additional complexity the analysis will consider the idealised unilateral Finline structure with fins symmetrical about the x-axis as given by figure (3.1.1).

Some insight into the nature of the field configuration in finline may be seen by first considering the structure without fins. The resulting dielectrically loaded waveguide is known to possess two orthogonal sets of field solution: TE to y and TM to y. The presence of the fins now impose additional boundary conditions. These excite higher order members of the aformentioned mode sets, whilst the field twisting associated with the edge causes a coupling between the two sets resulting in a hybrid six field finline mode.

3.1) Choice of Field Representation.

Since the dielectrically loaded waveguide formed by the substrate and housing supports only TE to y and TM to y modes respectively it is convenient to describe the finline fields in terms of y-directed electric and magnetic Hertzian vector potentials:

$$\underline{\Pi}_h = \hat{y}\ \Psi_h(x,y)\ e^{-j\beta z} \qquad (3.1.1)$$

$$\underline{\Pi}_e = \hat{y}\ \Psi_e(x,y)\ e^{-j\beta z} \qquad (3.1.2)$$

where propagation is assumed in the z direction with the as yet unkown phase constant β. $\hat{y}$ is the unit vector in the y-direction. Ψ_h and Ψ_e are general scalar functions of x and y.

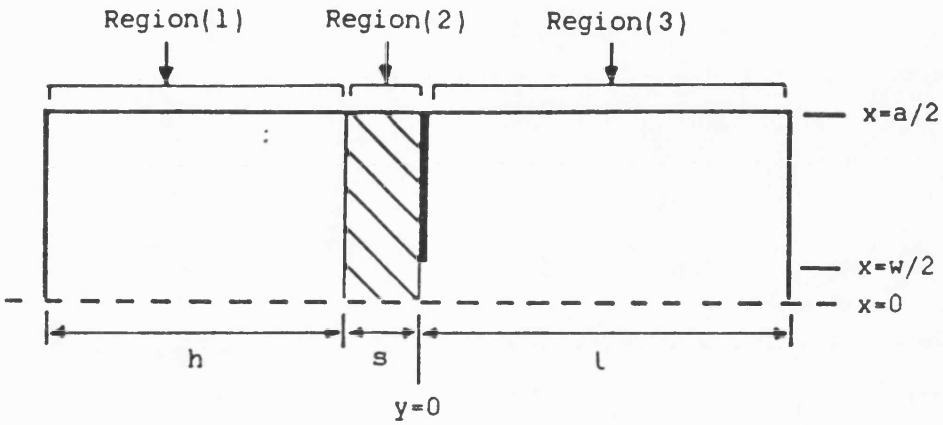

Figure (3.1.1) Idealised Unilateral Finline - axis positioning and dimension details.

The resulting electric and magnetic fields are given by:

$$\underline{E} = -j\omega\mu\nabla\times\underline{\Pi}_h + k^2\underline{\Pi}_e + \nabla\nabla\cdot\underline{\Pi}_e \qquad (3.1.3)$$

$$\underline{H} = k^2\underline{\Pi}_h + \nabla\nabla\cdot\underline{\Pi}_h + j\omega\varepsilon\,\nabla\times\underline{\Pi}_e \qquad (3.1.4)$$

Or more explicitly,

$$\underline{E} = \begin{bmatrix} \frac{\partial}{\partial x}\frac{\partial}{\partial y} \\ k^2 + \frac{\partial^2}{\partial y^2} \\ -j\beta\frac{\partial}{\partial y} \end{bmatrix} \Psi_e(x,y) + \begin{bmatrix} \omega\mu\beta \\ 0 \\ -j\omega\mu\frac{\partial}{\partial x} \end{bmatrix} \Psi_h(x,y)$$

$$\underline{H} = \begin{bmatrix} \frac{\partial}{\partial x}\frac{\partial}{\partial y} \\ k^2 + \frac{\partial^2}{\partial y^2} \\ -j\beta\frac{\partial}{\partial y} \end{bmatrix} \Psi_h(x,y) + \begin{bmatrix} -\omega\varepsilon\beta \\ 0 \\ j\omega\varepsilon\frac{\partial}{\partial x} \end{bmatrix} \Psi_e(x,y)$$

For the analysis the functions $\Psi_e(x,y)$ and $\Psi_h(x,y)$ are expanded in terms of the appropriate eigenfunctions of the dielectrically loaded waveguide :

$$\Psi_h(x,y) = \sum_n^{\infty} U_{hn}\,\Psi_{hn}(x,y) = \sum_n^{\infty} U_{hn}\,\phi_{hn}(x)\,\psi_{hn}(y) \qquad (3.1.5)$$

$$\Psi_e(x,y) = \sum_n^{\infty} U_{en}\,\Psi_{en}(x,y) = \sum_n^{\infty} U_{en}\,\phi_{en}(x)\,\psi_{en}(y) \qquad (3.1.6)$$

Where U_{en} and U_{hn} are the respective modal amplitudes. In view of the boundary conditions at the side walls, the functions ϕ are chosen to be the eigenfunctions of parallel plate waveguide:

$$\phi_{hn} = \sqrt{\frac{\delta n}{a}} \cos \frac{n\pi}{a} x \qquad (3.1.7)$$

$$\phi_{en} = \sqrt{\frac{\delta n}{a}} \sin \frac{n\pi}{a} x \qquad (3.1.8)$$

Where the Neuman delta, $\delta_n = 2$ for $n > 0$, $= 1$ for $n=0$, so that:

$$\int_{-a/2}^{a/2} \phi_{hm}\, \phi_{hn}\, dx = \int_{-a/2}^{a/2} \phi_{em}\, \phi_{en}\, dx = \delta_{mn}$$

The location of fins is symmetrical about x=0 so that the analysis need only involve even values of n (i.e. to ignore odd symmetric modes).

The functions ψ_{en} and ψ_{hn} describing the y variation must be specically defined in the three regions (1), (2) and (3) so that the respective boundary conditions to electric and magnetic fields are satisfied. It is also convenient that the boundary conditions at the interface between regions (1) and (2) be satisfied irrespective of the transverse wavenumber. Those between regions (2) and (3) are fulfilled upon solution of the finline mode. For this later reason the functions are chosen to be normalised such that $\psi_{en}(y) = \psi_{hn}(y) = 1.0$ for y=0.

Since the vector potentials $\underline{\Pi}_e$ and $\underline{\Pi}_h$ are purely y-directed, the Helmholtz vector wave equations reduce to the scalar form. For these to be satisfied for arbritrary expansion coefficients U_{en} and U_{hn}, each of the functions Ψ_{en} and Ψ_{hn} must itself satisfy the scalar wave equation. Thus the y-directed wavenumbers for the free space (air) regions (1) and (3) are given as:

$$k_n^a = \sqrt{\left[\frac{n\pi}{a}\right]^2 + \beta^2 - k_o^2} \qquad (3.1.9)$$

and for the substrate region (2) as:

$$k_n^s = \sqrt{\left(\frac{n\pi}{a}\right)^2 + \beta^2 - \varepsilon_r k_o^2} \qquad (3.1.10)$$

From the explicit forms of (3.2.3) and (3.2.4) boundary conditions at the perfecly conducting metallic end walls y=-(h+s) and y=l give:

i) Zero derivative of ψ_{en} at end walls.

ii) $\psi_{hn} = 0$ at end walls.

Whilst at the interface between regions (1) and (2) four further conditions are imposed:

iii) Continuous derivative of ψ_{en} at interface since $\psi_{en} \sim E_t$.

iv) ψ_{en} discontinuous by ε_r at interface since $\psi_{en} \sim E_n$.

v) Continuous derivative of ψ_{hn} at interface since $\psi_{hn} \sim H_t$.

vi) ψ_{hn} continuous at interface.

Thus in region (2):

$$\psi_{en} = \frac{\cosh\left[k_n^s(s+y) + \theta_{en}\right]}{\cosh(k_n^s s + \theta_{en})} \qquad (3.1.11)$$

$$\psi_{hn} = \frac{\sinh\left[k_n^s(s+y) + \theta_{hn}\right]}{\sinh(k_n^s s + \theta_{hn})} \qquad (3.1.12)$$

and in region (1):

$$\psi_{en} = A_{en} \frac{\cosh k_n^a(h+s+y)}{\cosh k_n^a h} \qquad (3.1.13)$$

$$\psi_{hn} = A_{hn} \frac{\sinh k_n^a(h+s+y)}{\sinh k_n^a h} \qquad (3.1.14)$$

Where, by imposing conditions (iii) to (vi) gives:

$$\theta_{en} = \text{arc tanh } \varepsilon_r \frac{k_n^a}{k_n^s} \tanh k_n^a h$$

$$\theta_{hn} = \text{arc coth } \frac{k_n^a}{k_n^s} \coth k_n^a h$$

$$A_{en} = \frac{\varepsilon_r \cosh \theta_{en}}{\cosh(k_n^s s + \theta_{en})}$$

$$A_{hn} = \frac{\sinh \theta_{hn}}{\sinh(k_n^s s + \theta_{hn})}$$

Finally, the potentials in region (3) are chosen as:

$$\psi_{en} = \frac{\cosh k_n^a(l-y)}{\cosh k_n^a l} \qquad (3.1.15)$$

$$\psi_{hn} = \frac{\sinh k_n^a(l-y)}{\sinh k_n^a l} \qquad (3.1.16)$$

Figures (3.1.2a) and (3.1.2b) show plots of these potentials for various values of k_n.

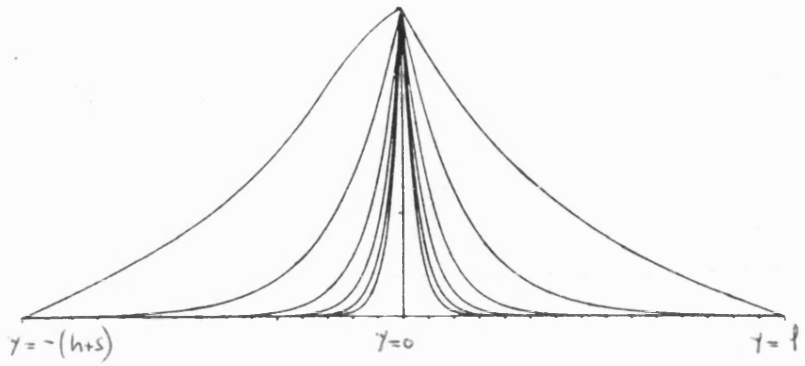

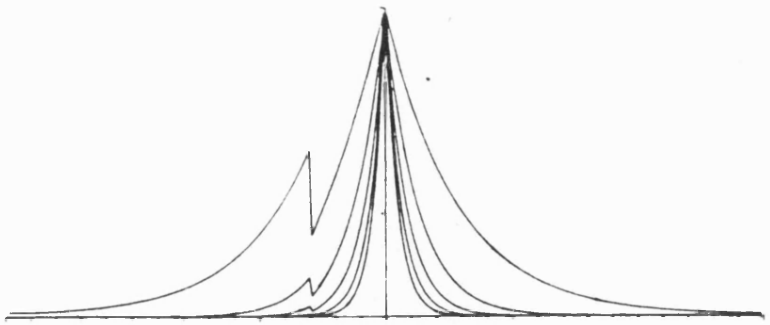

Figures (3.1.2a) and (3.1.2b) Magnetic and Electric Potentials.

3.2) Decomposition into Transverse TE and TM Components.

It is clear that in deriving the functions ψ describing the y variation of fields the boundary conditions for transverse propagating TE and TM waves have been implicitly satisfied. It is the purpose of this section to show how these lead to give a convenient equivalent transverse network representation to the field problem. To this end the fields E_x , E_z , H_x and H_z are of particular interest.

With the z-variation assumed, it is only the x-variation which distinguish fields for a given y. Consider fields infinitesimally to the left of y=0.

Substituting (3.1.11) and (3.1.12) into (3.1.3) through (3.1.5) and (3.1.6) , the electric fields may be expanded as:

$$E_x = \sum_n^{\infty} E_{xn}\, \Phi_{hn}(x) \qquad (3.2.1)$$

and

$$E_z = \sum_n^{\infty} E_{zn}\, \Phi_{en}(x) \qquad (3.2.2)$$

Where

$$E_{xn} = U_{en}^{L} \left[\frac{n\pi}{a}\right] \; k_n^s \tanh(k_n s + \theta_{en}) + \omega\mu\beta\, U_{hn}^{L} \qquad (3.2.3)$$

and

$$E_{zn} = U_{en}^{L}(-j\beta) \; k_n^s \tanh(k_n s + \theta_{en}) + j\omega\mu \left[\frac{n\pi}{a}\right] U_{hn}^{L} \qquad (3.2.4)$$

At this stage it is useful to introduce a new notation such that the modal amplitudes U_{en} and U_{hn} are represented by voltages and currents on TM and TE transmission lines. Let,

$$U_{en} = \frac{I_{nL}^{TM}}{j\omega\varepsilon \sqrt{\left[\frac{n\pi}{a}\right]^2 + \beta^2}} \qquad (3.2.5)$$

$$U_{hn} = \frac{V_{nL}^{TE}}{j\omega\mu \sqrt{\left[\frac{n\pi}{a}\right]^2 + \beta^2}} \qquad (3.2.6)$$

and define the ratio's

$$\frac{\frac{n\pi}{a}}{\sqrt{\left[\frac{n\pi}{a}\right]^2 + \beta^2}} = \cos \tau_n \qquad (3.2.7)$$

$$\frac{\beta}{\sqrt{\left[\frac{n\pi}{a}\right]^2 + \beta^2}} = \sin \tau_n \qquad (3.2.8)$$

Making use of the above reduces (3.2.3) and (3.2.4) to:

$$E_{xn} = I_{nL}^{TM}(\cos \tau_n) \; Z_{nL}^{TM} + (-j \sin \tau_n) \; V_{nL}^{TE} \qquad (3.2.9)$$

and

$$E_{zn} = I_{nL}^{TM} (-j \sin \tau_n) \; Z_{nL}^{TM} + (\cos \tau_n) \; V_{nL}^{TE} \qquad (3.2.10)$$

where the quantity

$$Z_{nL}^{TM} = \frac{k_n^s}{j\omega\varepsilon} \tanh(k_n^s s + \theta_{en}) \qquad (3.2.11)$$

is recognised as the impedance seen by a TM mode looking left from y=0.

Substituting (3.1.11) and (3.1.12) into (3.1.4) through (3.1.5) and (3.1.6) , the magnetic fields may be expanded as:

$$H_z = \sum_n^{\infty} H_{zn}\, \phi_{hn}(x) \qquad (3.2.12)$$

and

$$H_x = \sum_n^{\infty} H_{xn}\, \phi_{en}(x) \qquad (3.2.13)$$

Where

$$H_{zn} = U^L_{en}\ (-j\omega\varepsilon)\left[\frac{n\pi}{a}\right] + U^L_{hn}\ j\beta\ k^s_n \coth(k^s_n s + \theta_{hn}) \qquad (3.2.14)$$

and

$$H_{xn} = U^L_{en}\ (-\omega\varepsilon\beta) - U^L_{hn}\left[\frac{n\pi}{a}\right] k^s_n \coth(k_n s + \theta_{hn}) \qquad (3.2.15)$$

Upon introduction of (3.2.5) and (3.2.6) the above reduce to:

$$H_{zn} = I^{TM}_{nL} \cos\tau_n + (-j \sin\tau_n)\ V^{TE}_{nL}\ Y^{TE}_{nL} \qquad (3.2.16)$$

and

$$-H_{xn} = I^{TM}_{nL}\ (-j \sin\tau_n) + \cos\tau_n\ V^{TE}_{nL}\ Y^{TE}_{nL} \qquad (3.2.17)$$

where the quantity

$$Y^{TE}_{nL} = \frac{k^s_n}{j\omega\varepsilon} \coth(k^s_n s + \theta_{hn}) \qquad (3.2.18)$$

is recognised as the admittance seen by a TE mode looking left from y=0.

It is now convenient to write the relations (3.2.9), (3.2.10), (3.2.16) and (3.2.17) in matrix form:

$$\begin{bmatrix} E^L_{xn} \\ E^L_{zn} \end{bmatrix} = \underline{\underline{T}}_n \begin{bmatrix} Z^{TM}_{nL} & 0 \\ 0 & 1 \end{bmatrix} \begin{bmatrix} I^{TM}_{nL} \\ V^{TE}_{nL} \end{bmatrix} \qquad (3.2.19)$$

$$\begin{bmatrix} H^L_{zn} \\ -H^L_{xn} \end{bmatrix} = \underline{\underline{T}}_n \begin{bmatrix} 1 & 0 \\ 0 & Y^{TE}_{nL} \end{bmatrix} \begin{bmatrix} I^{TM}_{nL} \\ V^{TE}_{nL} \end{bmatrix} \qquad (3.2.20)$$

Where the matrix $\underline{\underline{T}}_n$ is given by:

$$\underline{\underline{T}}_n = \begin{bmatrix} \cos\tau_n & -j\sin\tau_n \\ -j\sin\tau_n & \cos\tau_n \end{bmatrix}$$

Carrying out a similar procedure for fields infinitesimally to the right of y=0 leads to:

$$\begin{bmatrix} E^R_{xn} \\ E^R_{zn} \end{bmatrix} = \underline{\underline{T}}_n^{-1} \begin{bmatrix} Z^{TM}_{nR} & 0 \\ 0 & 1 \end{bmatrix} \begin{bmatrix} I^{TM}_{nR} \\ V^{TM}_{nR} \end{bmatrix} \qquad (3.2.21)$$

$$\begin{bmatrix} -H^R_{zn} \\ H^R_{xn} \end{bmatrix} = \underline{\underline{T}}_n^{-1} \begin{bmatrix} 1 & 0 \\ 0 & Y^{TE}_{nR} \end{bmatrix} \begin{bmatrix} I^{TM}_{nR} \\ V^{TE}_{nR} \end{bmatrix} \qquad (3.2.22)$$

Where Z^{TM}_n and Y^{TE}_{nR} are TM impedances and TE admittances seen looking right of y=0.

The physical interpretation of equations (3.2.19)-(3.2.22) is that the matrix $\underline{\underline{T}}_n$ represents a rotation in complex space from the axes (x,jz) onto (u,v) as illustrated by figure (3.2.1). Thus the fields in finline may be decomposed into TM-to-y (E_y,E_v,H_u) and TE-to-y (H_y,E_u,H_v) waves propagating at an angle τ_n to the z-axis, analogous to the way in which TE and TM fields of the parallel plate waveguide itself may be described by a plane wave travelling at an angle to the z-axis. This valuable concept, introduced by Itoh [1] in the formulation stages of spectral domain analysis, has been shown here to originate directly from the choice of potentials and is quite general.

Notice also, that due to the choice of the transverse wavenumber, the rotation for fields to the right of y=0 is reversed.

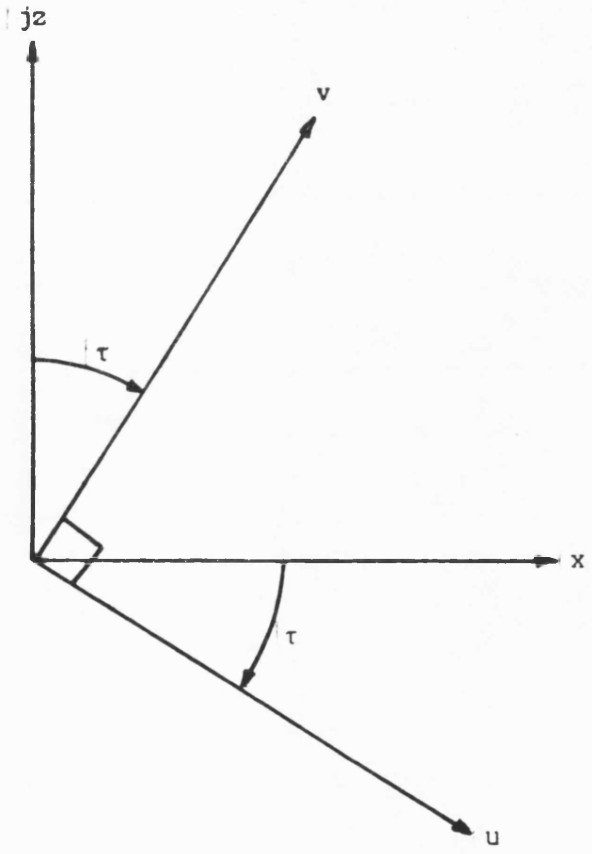

Figure (3.2.1) Rotation of axes in Complex Plane.

Combining equations (3.2.19) and (3.2.20) so as to eliminate voltage and current gives rise to a matrix equation linking the transverse-to-y field coefficients:

$$\begin{bmatrix} H_{zn}^{L} \\ -H_{xn}^{L} \end{bmatrix} = \underline{\underline{T}}_n \begin{bmatrix} Y_{nL}^{TM} & 0 \\ 0 & Y_{nL}^{TE} \end{bmatrix} \underline{\underline{T}}_n^{-1} \begin{bmatrix} E_{xn}^{L} \\ E_{zn}^{L} \end{bmatrix} \qquad (3.2.23)$$

whilst equations (3.2.37) and (3.2.38) produce:

$$\begin{bmatrix} -H_{zn}^{R} \\ H_{xn}^{R} \end{bmatrix} = \underline{\underline{T}}_n^{-1} \begin{bmatrix} Y_{nR}^{TM} & 0 \\ 0 & Y_{nR}^{TE} \end{bmatrix} \underline{\underline{T}}_n \begin{bmatrix} E_{xn}^{R} \\ E_{zn}^{R} \end{bmatrix} \qquad (3.2.24)$$

3.3) Green's Admittances

The formulation is completed by defining the integral relationships linking the fields at the fin aperture. A system of integral equations describing the coupling effects of the fin is readily obtained, which can then be interpreted in terms of an equivalent transverse circuit.

For fields infinitesimally right of y=0:

$$\begin{bmatrix} -H_z \\ H_x \end{bmatrix} = \begin{bmatrix} \hat{Y}_{11}^{R} & \hat{Y}_{12}^{R} \\ \hat{Y}_{21}^{R} & \hat{Y}_{22}^{R} \end{bmatrix} \begin{bmatrix} E_x \\ E_z \end{bmatrix} \qquad (3.3.1)$$

and for fields to the left:

$$\begin{bmatrix} H_z \\ -H_x \end{bmatrix} = \begin{bmatrix} \hat{Y}_{11}^{L} & \hat{Y}_{12}^{L} \\ \hat{Y}_{21}^{L} & \hat{Y}_{22}^{L} \end{bmatrix} \begin{bmatrix} E_x \\ E_z \end{bmatrix} \qquad (3.3.2)$$

Where $\hat{Y}^{L,R}$ are the integral admittance operators of the cross-

section, for example:

$$H_z(x) = \int_{-a/2}^{a/2} Y_{11}^{L}(x,x')\ E_x(x')\ dx' \Big|_{E_z = 0} \qquad (3.3.3)$$

$Y_{11}^{L}(x,x')$ is obtained from (3.2.19) and (3.2.20) in conjunction with the expansions (3.2.1), (3.2.12) and the orthonormal properties of the functions ϕ as follows:

Recalling equation (3.2.24):

$$\begin{bmatrix} H_{zn}^{L} \\ -H_{xn}^{L} \end{bmatrix} = \underline{\underline{T}}_n \begin{bmatrix} Y_{nL}^{TM} & 0 \\ 0 & Y_{nL}^{TE} \end{bmatrix} \underline{\underline{T}}_n^{-1} \begin{bmatrix} E_{xn} \\ E_{zn} \end{bmatrix} \qquad (3.3.4)$$

Expanding for the admitance linking H_{zn}^{L} and E_{xn}^{L} gives

$$Y_{11n}^{L} = Y_{nL}^{TM} \cos^2 \tau_n + Y_{nL}^{TE} \sin^2 \tau_n \qquad (3.3.5)$$

thus (3.2.28) may be writen:

$$H_z^{L}(x) = \sum_{n}^{\infty} E_{xn}\ Y_{11n}^{L}\ \phi_{hn}(x) \qquad (3.3.6)$$

Now by orthogonality

$$E_{xn} = \int_{-a/2}^{a/2} E_x(x')\ \phi_{hn}(x')\ dx' \qquad (3.3.7)$$

So by inserting (3.3.7) into (3.3.6), an integral relationship between the fields H_z and E_x is established:

$$H_z(x) = \sum_{n}^{\infty} Y_{11n}^{L}\ \phi_{hn}(x) \int_{-a/2}^{a/2} E_x(x')\ \phi_{hn}(x')\ dx' \cdot \qquad (3.3.8)$$

The order of integration and summation may be interchanged to put

equation (3.3.8) in the form of equation (3.3.3) from which the kernel $Y^L_{11}(x,x')$ is obtained as;

$$Y^L_{11}(x,x') = \sum_n^{\infty} \left(Y^{TM}_{nL}\cos^2\tau_n + Y^{TE}_{nL}\sin^2\tau_n \right) \phi_{hn}(x)\, \phi_{hn}(x') \qquad (3.3.9)$$

Appling the same proceedure to the other field components gives:

$$Y^L_{22}(x,x') = \sum_n^{\infty} \left(Y^{TE}_{nL}\cos^2\tau_n + Y^{TM}_{nL}\sin^2\tau_n \right) \phi_{en}(x)\, \phi_{en}(x') \qquad (3.3.10)$$

and the cross-coupling kernels

$$Y^L_{12}(x,x') = j \sum_n^{\infty} \cos\tau_n \sin\tau_n (Y^{TE}_{nL} - Y^{TM}_{nL})\, \phi_{en}(x)\, \phi_{hn}(x') \qquad (3.3.11)$$

$$Y^L_{21}(x,x') = j \sum_n^{\infty} \cos\tau_n \sin\tau_n (Y^{TM}_{nL} - Y^{TE}_{nL})\, \phi_{hn}(x)\, \phi_{en}(x') \qquad (3.3.12)$$

Similar results may be obtained for fields to the right of $y = 0$.

However, examination of the convergence properties of these Green's admittances with increasing n reveals that at present only Y_{11n} will converge. This problem is overcome by employing integration by parts as in the case of the inductive diaphragm problem [2]. Thus equations (3.3.1) and (3.3.2) are re-defined as follows:

$$\begin{bmatrix} -H_z(x) \\ \frac{\pi}{a}\int H_x(x)\,dx \end{bmatrix} = \begin{bmatrix} \hat{Y}^R_{11}(x,x') & \hat{Y}^R_{12}(x,x') \\ \hat{Y}^R_{21}(x,x') & \hat{Y}^R_{22}(x,x') \end{bmatrix} \cdot \begin{bmatrix} E_x(x') \\ \frac{a}{\pi}\frac{\partial}{\partial x} E_z(x') \end{bmatrix} \qquad (3.3.13)$$

and for fields to the left:

$$\begin{bmatrix} H_z(x) \\ -\frac{\pi}{a}\int H_x(x)\,dx \end{bmatrix} = \begin{bmatrix} \hat{Y}^L_{11}(x,x') & \hat{Y}^L_{12}(x,x') \\ \hat{Y}^L_{21}(x,x') & \hat{Y}^L_{22}(x,x') \end{bmatrix} \cdot \begin{bmatrix} E_x(x') \\ \frac{a}{\pi}\frac{\partial}{\partial x} E_z(x') \end{bmatrix} \qquad (3.3.14)$$

It is therefore convenient if the field expansion coefficients

are similarly redefined as:

$$E_x(x) = \sum_{n=0}^{\infty} E_{xn}\,\phi_{hn}(x) \tag{3.3.15}$$

$$\frac{a}{\pi}\frac{\partial}{\partial x}\,E_z(x) = \sum_{n=1}^{\infty} E_{zn}\phi_{hn}(x) \tag{3.3.16}$$

$$\frac{\pi}{a}\int H_x(x)\,dx = \sum_{n=1}^{\infty} H_{xn}\phi_{hn}(x) \tag{3.3.17}$$

$$H_z(x) = \sum_{n=0}^{\infty} H_{zn}\,\phi_{hn}(x) \tag{3.3.18}$$

It is noted that the coefficients E_{xn} and H_{zn} are in fact defined as previously, while E_{zn} and H_{xn} have been modified.

All the above field quantities can now be described in terms of the eigenfunction set $\{\phi_{hn}(x)\}$, and furthermore, all are uniform in their boundary conditions with x even at the fin edges. This uniformity is particulary useful in simplifying the solution.

Equations (3.2.23) and (3.2.24), which give the matrix relationship between the field coefficients and are intrinsic components of the Greens admittance, must now be modified to:

$$\begin{bmatrix} -H^R_{zn} \\ H^R_{xn} \end{bmatrix} = \underline{\underline{N}}\;\underline{\underline{T}}_n^{-1} \begin{bmatrix} Y^{TM}_{nR} & 0 \\ 0 & Y^{TE}_{nR} \end{bmatrix} \underline{\underline{T}}_n\;\underline{\underline{N}} \begin{bmatrix} E^R_{xn} \\ E^R_{zn} \end{bmatrix} \tag{3.3.19}$$

and,

$$\begin{bmatrix} H^L_{zn} \\ -H^L_{xn} \end{bmatrix} = \underline{\underline{N}}\;\underline{\underline{T}}_n \begin{bmatrix} Y^{TM}_{nL} & 0 \\ 0 & Y^{TE}_{nL} \end{bmatrix} \underline{\underline{T}}_n^{-1}\;\underline{\underline{N}} \begin{bmatrix} E^L_{xn} \\ E^L_{zn} \end{bmatrix} \tag{3.3.20}$$

where the matrix $\underline{\underline{N}}$ is simply given by:

$$\underline{\underline{N}} = \begin{bmatrix} 1 & 0 \\ 0 & \frac{1}{n} \end{bmatrix}$$

The resulting Green's admittance operators now contain kernels convergent with n, and only involve the function $\phi_{hn}(x)$.

The solution for a finline mode may be now obtained by imposing the continuity of fields over the fin gap. Since continuity of the electric fields is assumed in equations (3.3.13) and (3.3.14),ie no distinction is made between electric field left or right of the slot, continuity of magnetic fields implies that the sum of equations (3.3.13) and (3.3.14) may be equated to zero, resulting in a set of two coupled integral equations:

$$\begin{bmatrix} \hat{Y}_{11} & \hat{Y}_{12} \\ \hat{Y}_{21} & \hat{Y}_{22} \end{bmatrix} \cdot \begin{bmatrix} E_x \\ \frac{a}{\pi} \frac{\partial}{\partial x} E_z \end{bmatrix} = 0.0 \qquad (3.3.21)$$

Where the kernels of the combined operators are given as:

$$Y_{ij}(x,x') = \sum_n Y_{ijn}\, \phi_{hn}(x)\, \phi_{hn}(x') \qquad (3.3.22)$$

$i=1,2 \; ; \; j=1,2$

with

$$Y_{11n} = (Y_{nR}^{TM} + Y_{nL}^{TM}) \cos^2\tau_n + (Y_{nR}^{TE} + Y_{nL}^{TE}) \sin^2\tau_n$$

$$Y_{22n} = \frac{1}{n^2} (Y_{nR}^{TE} + Y_{nL}^{TE}) \cos^2\tau_n + \frac{1}{n^2} (Y_{nR}^{TM} + Y_{nL}^{TM}) \sin^2\tau_n$$

and for the cross-coupling kernels

$$Y_{12n} = j \frac{1}{n} \sin\tau_n \cos\tau_n (Y_{nL}^{TM} - Y_{nR}^{TM} + Y_{nR}^{TE} - Y_{nL}^{TE})$$

$$Y_{21n} = - Y_{12n}$$

It is noted that only the operator $\hat{Y}_{11}(x,x')$ contains any contribution from the fundamental n=0 field variations. This is because n=0 variations are absent from TM to y fields from physical

considerations. Thus the fundamental TE transverse mode may be completely removed from the system of integral equations since it only involves the fields E_{xO} , E_{yO} and H_{zO} , giving:

$$\hat{\underline{\underline{Y}}} \cdot \begin{bmatrix} E_x \\ \frac{a}{\pi}\frac{\partial}{\partial x} E_z \end{bmatrix} + Y_0 \begin{bmatrix} E_{xo} \\ 0 \end{bmatrix} = 0 \qquad (3.3.23)$$

Where $Y_0 = Y_{0L}^{TE} + Y_{0R}^{TE}$, $\hat{\underline{\underline{Y}}}$ is the matrix of integral operators as in equation (3.3.21) except that now all summations within the kernels start from n=1.

Thus if the fins are assumed not to cause any coupling to higher order dielectrically loaded waveguide modes, i.e the fins are absent, the first resonance of Y_0 defines solution for the fundamental TE_{01} mode (perturbed by the dielectric). The introduction of fins introduces a susceptance, describing the localised energy storage of higher order transverse modes about the fins. Introducing this susceptance in the transverse equivalent circuit, of figure(3.3.1), enables the dispersion relation for the fundamental finline mode to be recovered. The next section will develop the accurate determination of this susceptance, and a further section will seek to understand its frequency dependence.

3.4) Solution of Integral Equation.

Before proceeding with a general solution to the integral equations (3.3.21), it is noted that provided certain assumptions are made, the coupled integral equations may be reduced to a single integral. Then recognising similarity with the capacitive, a variational expression for the fin admittance within the transverse network recovered. Although this form of solution is not strictly

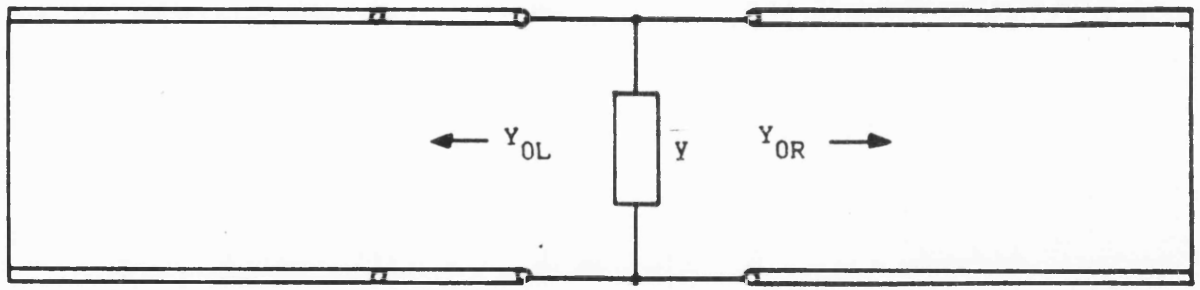

Figure (3.3.1) Simplified Transverse Equivalent Circuit.

valid for the general case , this approach does produce fairly accurate results for the fundamental finline mode with minimal computational effort.

3.4i) Simple variational formulation.

Assuming that E_x dominates the electric field within the fin gap, then equation (3.3.21) may be written as:

$$Yo \int_{-a/2}^{a/2} E_x(x)\phi_{ho}(x)\,\phi_{ho}(x')\,dx + \int_{-a/2}^{a/2} \sum_{n=1}^{\infty} Y_{11n}\,\phi_{hn}(x)\,E_x(x)\,\phi_{hn}(x')\,dx = 0$$

Multiplying by $E_x(x')$, performing a second integration and re-arranging gives a variational expression for the fin susceptance appearing in the dispersion equation:

$$Yo + \frac{\displaystyle\int_{-a/2}^{a/2}\int \sum_{n=1}^{\infty} Y_{11n}\,\phi_{hn}(x)\,E_x(x)\phi_{hn}(x')\,E_x(x')\,dx\,dx'}{\left[\displaystyle\int_{-a/2}^{a/2} E_x(x)\,\phi_{ho}(x)\,dx\right]^2} = 0 \qquad (3.4.1)$$

The variational nature of the term denoting the fin susceptance implies that a first order approximation to the aperture field E_x will yield a second order result, providing that the trial field sufficiently resembles the actual field. This is accurate for small fin gaps, whilst for larger gaps where the susceptance term is small, errors in the approximation will have even less effect on solutions for finline dispersion.

Since the integrals are to be evaluated across the the guide at

y=0 and the electric field E_x vanishes on the fins, the range of integration need only cover the fin gap. Furthermore, if only symmetrical placing of fins is considered, this range may be restricted to the half gap by placing an electric wall at y=0 as in figure( ) . Thus the limits,

$$\int_{-a/2}^{a/2} \quad \text{are replaced by} \quad \int_{0}^{w/2}$$

In order to obtain analytical integration across the half fin gap, whilst adequately incorporating the singularity at y=d/2 into an approximation for $E_x(x)$, the mapping originally introduced by Schwinger [3] for the analysis of infinitely thin irises is now utilised. This mapping, which will now be derived, is in fact the conformal mapping between a parallel plate waveguide and a waveguide containing an iris.

3.4ii) The Schwinger Mapping.

Consider the parallel plate system in the θ plane as shown in figure (3.4.1a). Fields at ρ=0 may be mapped into the region between the two lines in the T plane, figure (3.4.1b), by :

$$T = \cosh \theta \qquad (3.4.2)$$

Fields within the iris region given in figure (3.4.2a) in the Z plane are mapped into the region between another two lines in the T plane, figure (3.4.2b), by :

$$T = \cosh Z \qquad (3.4.3)$$

In order to make points P_1' correspond with B_2' and P_2' with C_2', two scalar coefficients are introduced into equation (3.4.2), giving a mapping between the structures of figures (3.4.1a) and (3.4.2a) via

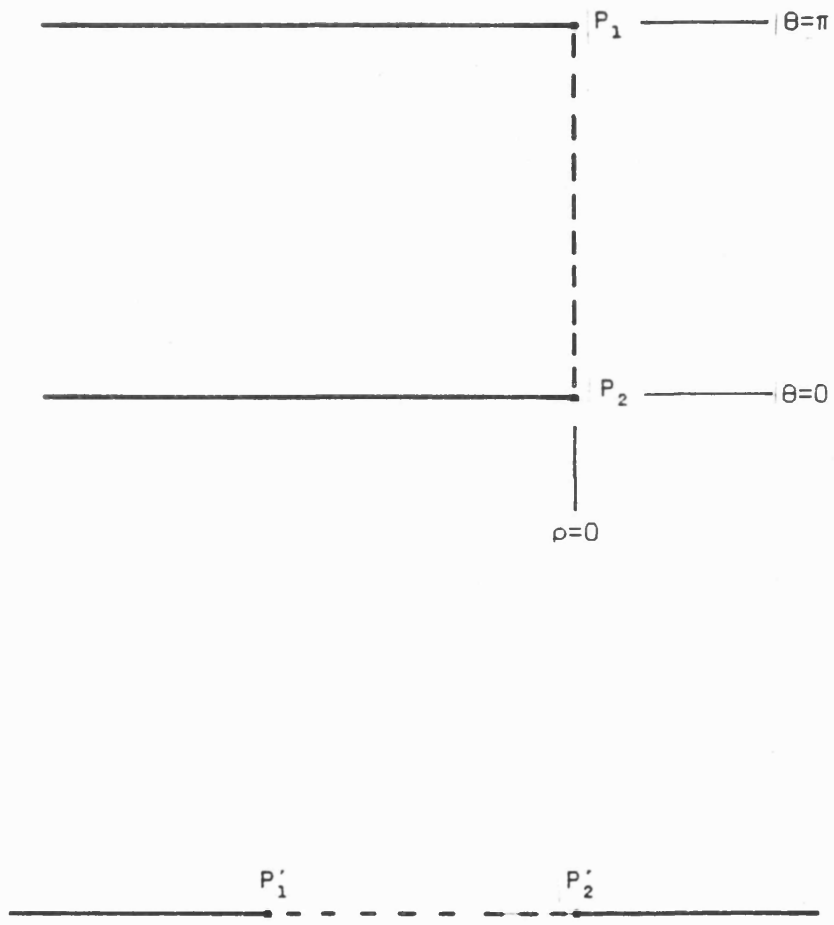

Figures (3.4.1a) and (3.4.1b) Illustration of Conformal Mapping from θ plane into T plane

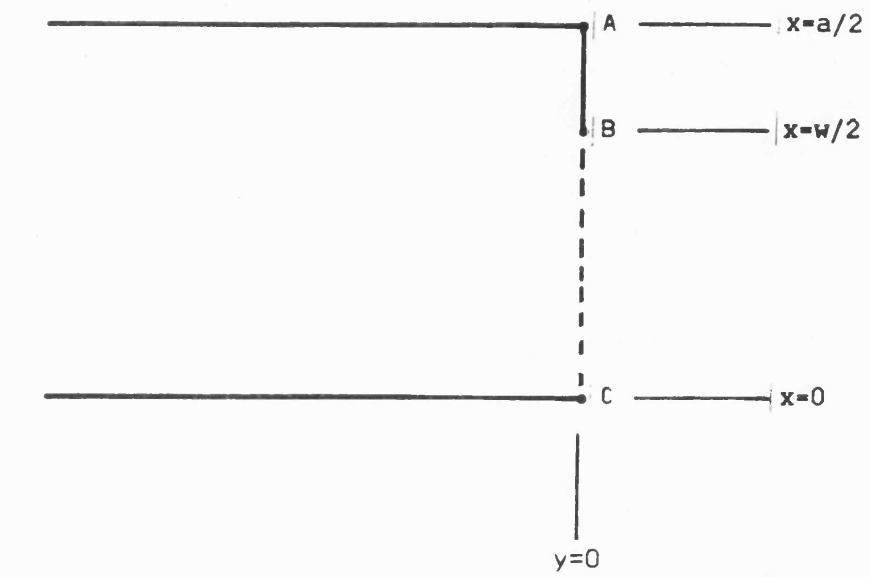

Figures (3.4.2a) and (3.4.2b) Illustration of Conformal Mapping from Z plane into t plane

an intermediate two line structure as defined by:

$$\cosh Z = \alpha_1 + \alpha_2 \cosh \theta \qquad (3.4.4)$$

The nature of a conformal mapping implies that solutions of the two dimensional Laplace equation are invariant. This, therefore, also applies to the two dimensional wave equation,

$$\nabla_t^2 \phi + (k^2 - \beta^2) \phi = 0$$

if the derivative term ∇_t^2 dominates, as is the case in finline in the vicinity of the fin edges. Thus the mapping of the eigenmodes of the parallel plate structure gives a very close approximation to the eigenmodes of the iris aperture region in finline. Although the mapping will not produce an exact solution directly, even at cut-off, because the end walls must perturb the field to some extent.

Since the structure of figure (3.1.1) is being considered, the particular mapping onto an asymmetrical iris is required. The coefficients α_1 and α_2 are obtained from the requirements that:

i) The point $x = 0$ corresponds to $\theta = 0$

ii) The point $x = w/2$ corresponds to $\theta = \pi$

Giving:

$$\alpha_1 = \cos^2 \frac{\pi w}{2a} \qquad (3.4.5)$$

$$\alpha_2 = \sin^2 \frac{\pi w}{2a} \qquad (3.4.6)$$

The required singularity is implicitly satisfied by the mapping, since from the change of variable:

$$\int_0^{\pi} F(\theta)\, d\theta = \int_0^{w/2} F(\theta(x)) \frac{\partial \theta}{\partial x}\, dx \qquad (3.4.7)$$

The general function F(θ) is conveniently expanded in terms of the eigenfunctions of the parallel plate system:

$$F(\theta) = \sum_m a_m f_m(\theta) \qquad (3.4.8)$$

Where a_m are arbritary expansion coefficients and the functions f_m are given as: $f_m(\theta) = \sqrt{\frac{\delta m}{\pi}} \cos \theta$

with δm the Neuman delta. The derivative term is found to be:

$$\frac{\partial \theta}{\partial x} = \frac{\sqrt{\frac{2\pi}{a}} \sin \frac{2\pi}{a} x}{\sqrt{1 - \left[\frac{\cos \frac{2\pi}{a} - \alpha_1}{\alpha_2}\right]^2}} \qquad (3.4.9)$$

As $x \longrightarrow w/2$ and with reference to equations (3.4.5) and (3.4.6) it is seen that the denominator term to in the above equation (3.4.9) becomes:

$$\sqrt{1 - \delta^2}$$

where $\delta \longrightarrow 1$ at the same rate at which $x \longrightarrow w/2$, thus providing the required singularity as shown by figure (3.4.3).

The task of mapping respective eigenfunctions between structures of the x and θ domains is greatly eased by defining a linear relationship between the sets $\{\phi_{hn}(x)\}$ and $\{f_m(\theta)\}$ as follows:

$$\phi_{hn}(x) = \sum_{m=0}^{n} P_{nm} f_m(\theta) \qquad (3.4.10)$$

The coefficients P_{nm} may be obtained analytically in terms of α_1 and α_2 using properties of the Chebyshev polymonials.

Since $\cos nx = T_n(\cos x)$ one may write:

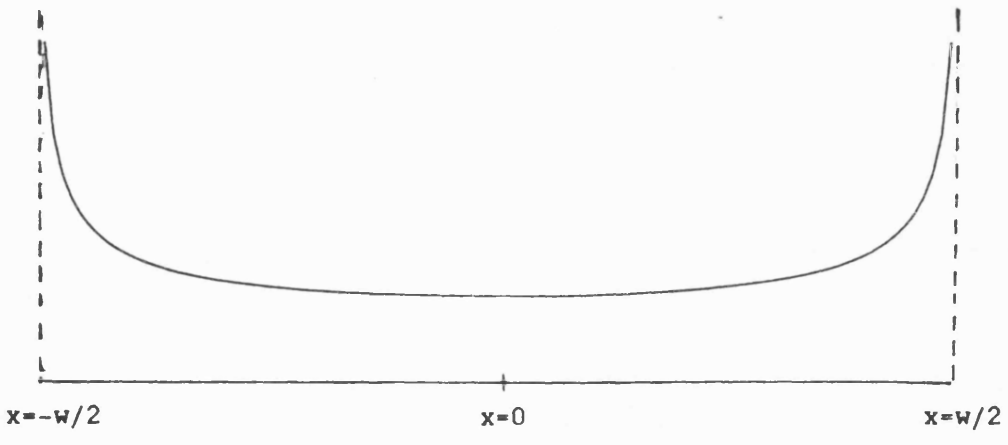

Figure (3.4.3) Plot of Derivative Term $d\theta/dx$

$$\cos \frac{2n\pi}{a} = T_n(\alpha_1 + \alpha_2 \cos\theta) = \sum_{m=0}^{n} P'_{nm} \cos m\theta \qquad (3.4.11)$$

Using the recursive formula for Chebyshev polynomials:

$$T_n(x) = 2x\, T_{n-1}(x) - T_{n-2}(x)$$

in (3.4.11) gives,

$$\sum_{m=0}^{n} P'_{nm} \cos m\theta = 2(\alpha_1 + \alpha_2 \cos\theta) \sum_{m=0}^{n-1} P'_{n-1,m} \cos m\theta - \sum_{m=0}^{n-2} P'_{n-2,m} \cos m\theta \qquad (3.4.12)$$

Taking the term $2\alpha_2 \cos m\theta$ into the summations, using the trigonometric double angle formulae, and noting the special case m=1 gives the left hand side of (3.4.12) as:

$$2\alpha_1 \sum_{m=0}^{n} P'_{n-1,m} \cos m\theta + \alpha_2 \sum_{m=0}^{n-1} P'_{n-1,m} \cos(m+1)\theta + \alpha_2 \sum_{m=0}^{n-1} P'_{n-1,m} \cos(m-1)\theta + \alpha_2 \delta_{1m} P'_{n-1,0} \cos\theta - \sum_{m=0}^{n-2} P'_{n-2,m} \cos m\theta$$

which may be re-written as:

$$2\alpha_1 \sum_{m=0}^{n} P'_{n-1,m} \cos m\theta + \alpha_2 \sum_{m=1}^{n} P'_{n-1,m-1} \cos m\theta + \alpha_2 \sum_{m=-1}^{n-2} P'_{n-1,m+1} \cos m\theta + \alpha_2 \delta_{1m} P'_{n-1,0} \cos\theta - \sum_{m=0}^{n-2} P'_{n-2,m} \cos m\theta$$

Upon substitution into the L.H.S of equation (3.4.12) and equating the common factor of cos mθ, one obtains the sought

recursive relationship between the coefficients:

$$P'_{nm} = 2\alpha_1 P'_{n-1,m} + \alpha_2 P'_{n-1,m-1} + \alpha_2 P'_{n-1,m+1} + \alpha_2 \delta_{1m} P'_{n-1,0} - P'_{n-2,m} \qquad (3.4.13)$$

Thus, given the initial definition,

$$P'_{00} = 1 \ , \quad P'_{10} = \alpha_1 \ , \quad P'_{11} = \alpha_2$$

the array P'_{nm} may be generated as required.

$$\begin{bmatrix} P'_{00} & 0 & . & . & . & . & 0 \\ P'_{10} & P'_{11} & 0 & . & . & . & . \\ P'_{20} & P'_{21} & P'_{22} & 0 & . & . & . \\ . & & & & & . & . \\ . & & & & & & . \\ . & & & & & & 0 \\ P'_{N0} & . & . & . & . & . & P'_{NN} \end{bmatrix}$$

Finally, the coefficients P_{nm} of equation (3.4.10) linking the two orthonormal sets $\{\phi_{hn}(x)\}$ and $\{f_m(\theta)\}$ are obtained from P'_{nm} by applying the normalisation:

$$P_{nm} = \sqrt{\frac{\delta n}{\delta m}} \sqrt{\frac{\pi}{2a}} \ P'_{nm} \qquad (3.4.14)$$

3.4iii) Transverse Resonance Diffraction Solution for the Fundamental Mode

Having now established much of the background to the Schwinger mapping, the latter is now applied to the variational expression (3.4.1). Thus obtaining:

$$Y_0 + \frac{\int_0^{\pi}\int_0^{\pi} \sum_n Y_{11n}\, \phi_{hn}(x(\theta))\, F(\theta)\, \phi_{hn}(x(\theta'))\, F(\theta')\, d\theta\, d\theta'}{\left[\int_0^{\pi} F(\theta)\, \phi_{ho}(x(\theta))\, d\theta\right]^2} = 0 \qquad (3.4.15)$$

where $F(\theta)$ is the trial field in the θ domain.

For this, the simple variational formulation, the trial field $F(\theta)$ = constant = $f_m(\theta)$; m = 0, is chosen. Utilising (3.4.10) and by orthogonality of the functions f_m, the above is reduced to a summation involving only admittances and the coefficients P_{nm}:

$$Y_0\, P_{00}^2 + \sum_{n=1}^{\infty} Y_{11n}\, P_{n0}^2 = 0 \qquad (3.4.16)$$

The above transcendental equation (through the tangent functions) contains only the one unknown, β, the phase constant of a finline mode which can be solved for using an iterative procedure.

However, by applying the results of appendix AI the quasi-static component can be extracted from the infinite sum in the dispersion equation to give:

$$y_0 + \sum_{n=1}^{nd} \left(y_{11n} - \frac{y_{s11}}{n}\right) P_{n0}^2 + y_{s11} A_{00} = 0 \qquad (3.4.17)$$

Although the convergence properties of the remaining summation in equation (3.4.17) above are much better than those of equation (3.4.16), they can be improved further by removing an additional quasi-static component resulting from the effect of a thin substrate on the TM admittance term to give:

$$y_0 + \sum_{n=1}^{nd} \left[y_{11n} - \frac{1}{n} \left(y_{s11} + \frac{k^2}{jun} S_n\right)\right] P^2_{n0}$$

$$+ \frac{k^2}{ju} \sum_{n=1}^{ns} \frac{S_n}{n} P^2_{n0} + y_{s11} A_{00} = 0 \qquad (3.4.18)$$

The first term appearing in the above expression, y_0, is the (normalised) admittance of the fundamental TE transverse mode, which has a very strong frequency variation. The second term, the first summation, converges very quickly with n , but is dynamic i.e it exhibits a latent frequency variation and the sum must be calculated separately at any particular frequency. The remaining summation need only be evaluated once for any particular fin gap and converges quickly once the exponential term begins to dominate S_n (see equation AI.10), since the sum itself exhibits no frequency variation. Whilst in the final term A is known analytically and the frequency variation of the asymptotic quasi-static admittance has already been determined. Implementation of (3.4.18) in a simple computer program yielded a very efficient solution for finline dispersion with good accurracy.

3.5) General Ritz-Galerkin Formulation

The simple variational formulation was derived through several sections in order to introduce fully the Schwinger mapping and various numerical aspects which enable an efficient solution to be succesfully implemented. Here the general solution is developed as a Galerkin formulation leading to an exact solution of the aperture fields.

Firstly the Schwinger mapping is applied to the general integral

equation (3.3.21), and then the fields $F_x(\theta)$ and $F_z(\theta)$ are expressed as a finite expansion in terms of the functions $f_m(\theta')$. Equation (3.3.21) thus becomes:

$$Y_0 \; E_{x0} \; \Phi_{h0}(x(\theta)) \; + \; \sum_{m=0}^{\infty} \; \hat{\underline{Y}} \; \cdot \; \begin{bmatrix} X_m \\ Z_m \end{bmatrix} f_m(\theta') \; = \; 0 \qquad (3.5.1)$$

where X_m and Z_m are expansion coeficients to the unkown fields as given by:

$$X_m \; = \; \int_0^{\pi} F_x(\theta) \; f_m(\theta) \; d\theta$$

$$Z_m \; = \; \int_0^{\pi} F_z(\theta)) \; f_m(\theta) \; d\theta$$

These lead to expansions in E_x and E_z as given by figures (3.5.1a) and (3.5.1b).

Writing the admittance operator out more explicitly and utilising the integration over the aperture gives:

$$Y_0 \; E_{x0} \; \Phi_{h0}(x(\theta)) \; + \; \sum_{m=0}^{M} \; \sum_{n=1}^{\infty} \begin{bmatrix} Y_{11n} & Y_{12n} \\ Y_{21n} & Y_{22n} \end{bmatrix} \Phi_{hn}(x(\theta) \; P_{nm} \begin{bmatrix} X_m \\ Z_m \end{bmatrix} = 0 \qquad (3.5.2)$$

Multiplying by $f_m(\theta)$ and integrating, gives rise to:

$$\sum_{k=0}^{M} \; E_{x0} \; Y_0 \begin{bmatrix} P_{0k} \\ 0 \end{bmatrix} + \sum_{m=0}^{M} \; \sum_{n=1}^{\infty} \begin{bmatrix} Y_{11n} & Y_{12n} \\ Y_{21n} & Y_{22n} \end{bmatrix} P_{nk} \; P_{nm} \begin{bmatrix} X_m \\ Z_m \end{bmatrix} = 0 \qquad (3.5.3)$$

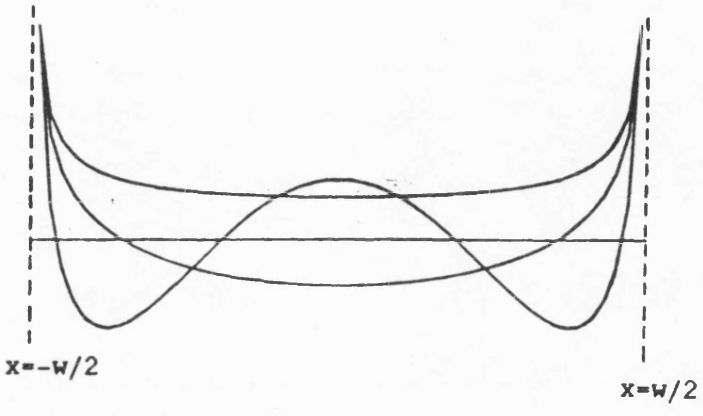

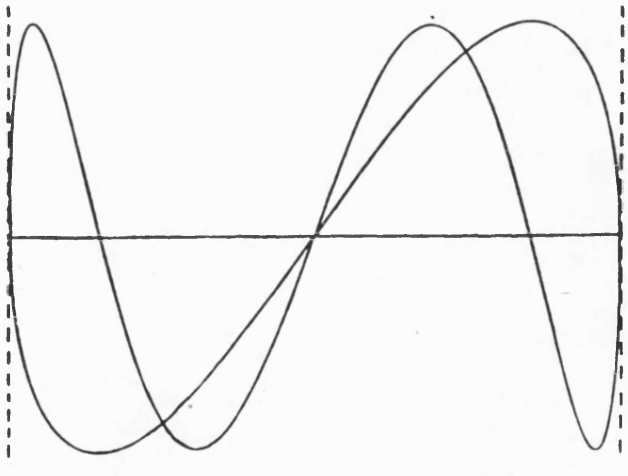

Figures (3.5.1a) and (3.5.1b) Field Expansions for Ex and Ez.

Which may be conveniently expressed in matrix form as:

$$E_{x0}\, Y_0 \begin{bmatrix} \underline{P}_0 \\ 0 \end{bmatrix} + \begin{bmatrix} \underline{\underline{Y}}_{11} & \underline{\underline{Y}}_{12} \\ \underline{\underline{Y}}_{21} & \underline{\underline{Y}}_{22} \end{bmatrix} \cdot \begin{bmatrix} \underline{X} \\ \underline{Z} \end{bmatrix} = 0 \qquad (3.5.4)$$

where $\underline{P}_0$, $\underline{X}$ and $\underline{Z}$ are column vectors of elements P_{0k} , X_m , and Z_m respectively. Elements of the submatrices $\underline{\underline{Y}}_{11}$, $\underline{\underline{Y}}_{12}$ etc, are given by:

$$Y_{ij} = \sum_{n=1}^{\infty} Y_{ijn}\, \underline{P}_n \cdot \underline{P}_n^T$$

$$i = 1,2 \; ; \; j = 1,2$$

with vectors $\underline{P}_n$ of elements P_{nm}.

To complete the Galerkin formulation, the quantity E_{x0} must be expressed in terms of the field expansion. Due to the orthogonality of the functions $\phi_{hn}(x)$ the coefficients E_{xn} are obtained as:

$$E_{xn} = \int_{-a/2}^{a/2} \phi_{hn}(x)\, F_x(x)\, dx \qquad (3.5.5)$$

Applying the Schwinger mapping to the above , expanding $\phi_{hn}(x(\theta))$ and $F_x(\theta)$ in terms of $f_m(\theta)$, and utilising the integration gives rise to an expression for E_{xn} in terms of the slot field expansion:

$$E_{xn} = \sum_{m=0}^{M} P_{nm}\, X_m \qquad (3.5.6)$$

Similarly an expression for E_{zn} is obtained as:

$$E_{zn} = \sum_{m=0}^{M} P_{nm}\, Z_m \qquad (3.5.7)$$

(Note that from physical considerations the field E_{z0} cannot exist

and that therefore variations corresponding to m=0 have no physical meaning for E_z. The expansion set for the field E_z is therefore chosen to be as that for E_x except that n=0 components are absent. This requires that the coefficients P_{00} must be set to zero in the E_z expansion. However, this has no effect whatsoever on the discretisation of the admittance operator since n=0 is absent in any case.)

Using compact vector notation, E_{x0} can be written as:

$$E_{x0} = \begin{bmatrix} \underline{P}_0^T & 0 \end{bmatrix} \cdot \begin{bmatrix} \underline{X} \\ \underline{Z} \end{bmatrix} \qquad (3.5.8)$$

Expanding (3.6.4) gives two simultaneous matrix equations:

$$- Y_0 E_{x0} \underline{P}_0 = \underline{\underline{Y}}_{11} \cdot \underline{X} + \underline{\underline{Y}}_{12} \cdot \underline{Z} \qquad (3.5.9a)$$

$$0 = \underline{\underline{Y}}_{21} \cdot \underline{X} + \underline{\underline{Y}}_{22} \cdot \underline{Z} \qquad (3.5.9b)$$

Solving for $\underline{X}$ gives:

$$\underline{X} = - Y_0 E_{x0} \left[\underline{\underline{Y}}_{11} - \underline{\underline{Y}}_{12} \underline{\underline{Y}}_{22}^{-1} \underline{\underline{Y}}_{21} \right]^{-1} \cdot \underline{P}_0 \qquad (3.5.10)$$

Whilst using (3.5.8) to substitute for E_{x0}, and by virtue of the common factor $\underline{X}$, the resonance equation for the general case is finally obtained as:

$$Y_0 + \left(\underline{P}_0^T \cdot \left[\underline{\underline{Y}}_{11} - \underline{\underline{Y}}_{12} \underline{\underline{Y}}_{22}^{-1} \underline{\underline{Y}}_{21} \right]^{-1} \cdot \underline{P}_0 \right)^{-1} = 0 \qquad (3.5.11)$$

If one term expansion is employed and the coupling operators Y_{12} and Y_{21} assumed to be negligble, then the result (3.4.16) of the simple variational formulation is obtained, implying that the Galerkin method has built in variational properties. When these terms

are included, equation (3.5.11) includes an expression for the fin admittance, including all hybrid effects, which becomes increasingly accurate with expansion (matrix order). The solution of (3.5.11) for general finline modes thus proceeds using an iterative proceedure as before.

3.5i) Theoretical and Experimental Results.

Table (3.1) shows a comparison of the calculated dispersion between:-

(0) Simple variational

(1) 1st order Ritz-Galerkin (R.G.)

(2) 2nd order R.G.

(3) 3rd order R.G.

These results show that convergence is very fast. Table (3.2a) gives the values of the expansion coefficients X_m and Z_m obtained at the solution point in a 4th order solution for a moderate fin gap. These show that E_x does indeed dominate the gap field for the fundamental mode, and the rapid convergence of X_m show how well the Schwinger mapping approximates the field in finline.

Results for the fundamental mode with a large fin gap show that convergence of the Schwinger function expansion for the gap field is weaker as the field obtained by the mapping is perturbed by the presence for the end walls. However, table (3.2b) shows that even for the extreme cases a 3rd order expansion is sufficient. In general the 2nd order solution is acceptable, whilst for extremly narrow fin-gaps, table (3.2c), convergence in expansion is very fast. In fact, since the E_z field is small, the simple variational solution with

Table (3.1) Comparison of Dispersion Results for Various Expansion Orders in X-Band Finline, Normalised fin-gap = 0.2 , guide dimensions as figure (3.5.2).

	b/k			
Frequency/GHz	0	1	2	3
8.0	0.850961	0.849011	0.849001	0.849001
9.0	0.896874	0.894764	0.894754	0.894753
10.0	0.928497	0.926166	0.926158	0.926158
11.0	0.951156	0.948801	0.948794	0.948794
12.0	0.968224	0.965711	0.965703	0.965702

scalar equations gives very good results.

Figure (3.5.2) shows a selection of dispersion curves for various fin-gaps and substrate permittivities, the dashed curve is for the waveguide formed by the housing alone. It can be seen that whilst the effect a reducing fin-gap reduces the cut-off frequency, increasing the substrate permittivity will reduce both the cut-off frequency and the guided wavelength ($\beta/k \sim 1/(\lambda_g/\lambda_o)$).

In order to assess validity an experiment was devised to measure the guided wavelength in finline.

A finline section was shorted at both ends, including a direct short on the metalisation. Then by introducing small coupling probes into the cavity, the resonant frequencies were observed on a network analyiser giving a display as shown in figure (3.5.3). Since each resonance corresponds to an integral number of half wavelengths along the section, knowledge of the actual resonant frequency, length, and the integral number, enables the dispersion characteristic to be experimentally determined.

The results obtained for two finlines are shown in tables (3.3) and (3.4). Figures (3.5.4a) and (3.5.4b) give the experimental points with the theoretical dispersion curve. For the narrower fin-gap (2.31mm in 10.16mm housing) the agreement is very good. However, the wider fin- gap (5.15mm) shows a small dispcrepancy. This is possibly due to the slightly asymmetric placing of the finline slot in the housing and the excitation of anti-symmetric modes.

Tables (3.2a), (3.2b) and (3.2c) Aperture Field Expansion Coefficients X_m and Z_m for Various Normalised Fin-gaps at X-Band.

X-band finline, F=10.0 Ghz, w/a = 0.200.		
	X_m	Z_m
1	1.000000	-0.003049
2	0.187141	-0.000852
3	-0.014328	0.000042
4	-0.002371	0.000016

X-band finline, F=10.0 Ghz, w/a = 0.800.		
	X_m	Z_m
1	1.000000	-0.015096
2	0.045087	-0.000418
3	-0.043687	0.000200
4	-0.031065	-0.000107

X-band finline, F=10.0 Ghz, w/a = 0.050.		
	X_m	Z_m
1	1.000000	-0.002178
2	0.079288	-0.000214
3	-0.002318	0.000005
4	-0.000014	-0.000000

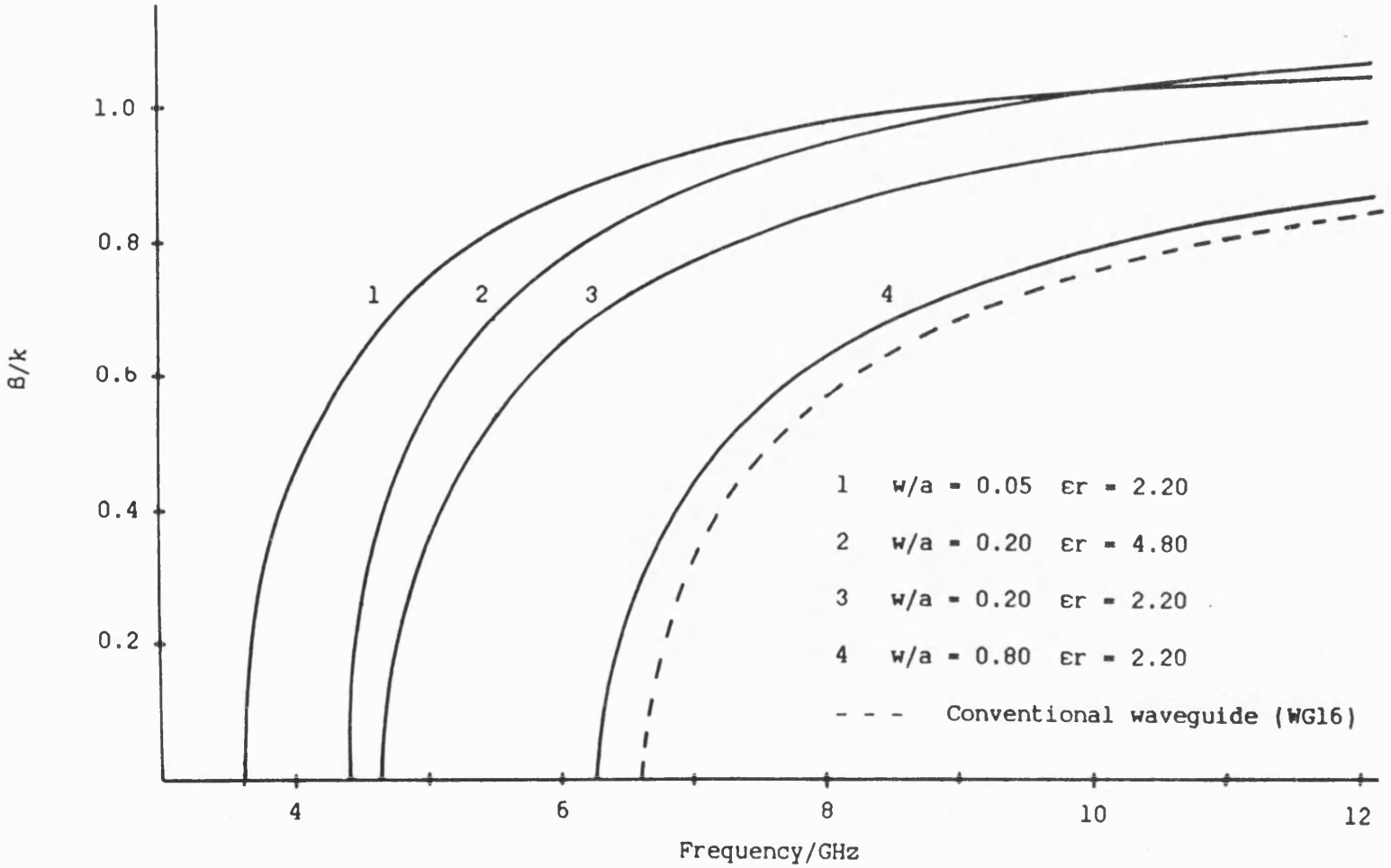

Figure (3.5.2) Dispersion Curves for the Fundamental Finline Mode at X-Band (a = 10.16mm, l = (h+s) = 11.43mm, s = 0.254mm)

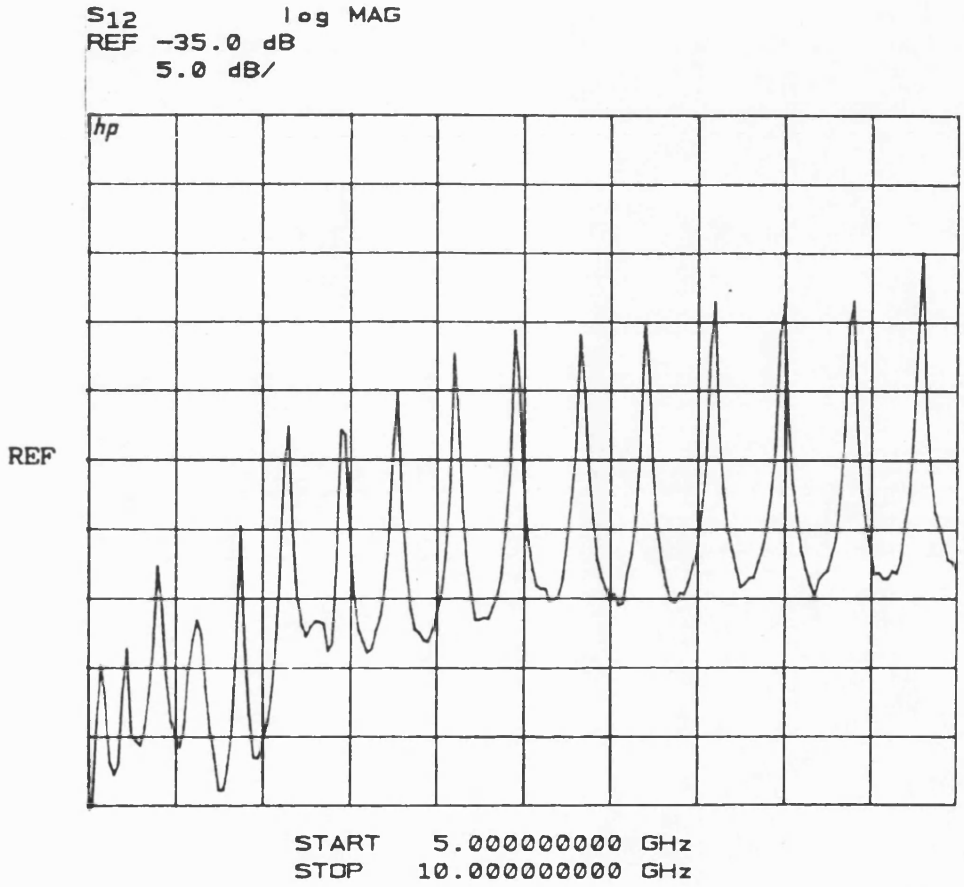

Figure (3.5.3) Frequency Response of Finline Resonator.

Table (3.3) Comparison of Theoretical and Experimental Dispersion.

X-band finline, fin gap = 2.31mm		
Frequency/GHz	Guided wavelength/mm	
	Measured	Calculated
4.920	300.000	299.820
5.020	200.000	207.590
5.200	150.000	148.150
5.390	120.000	119.510
5.610	100.000	100.290
5.857	85.700	86.440
6.141	75.000	75.540
6.447	66.666	67.110
6.772	60.000	60.380
7.113	54.540	54.900
7.472	50.000	50.290
7.843	46.150	46.400
8.223	42.850	43.080
8.612	40.000	40.220
9.010	37.500	37.700
9.414	35.290	35.490
9.825	33.333	33.520
10.241	31.580	31.757
10.663	30.000	30.167
11.091	28.570	28.722
11.516	27.270	27.429
11.946	26.080	26.243
12.388	25.000	25.146

Table (3.4) Comparison of Theoretical and Experimental Dispersion.

X-band finline, fin gap = 5.15mm		
Frequency/GHz	Guided wavelength/mm	
	Measured	Calculated
5.889	600.000	252.300
5.947	300.000	205.100
6.047	200.000	159.720
6.182	150.000	130.680
6.354	120.000	109.190
6.555	100.000	93.520
6.785	85.700	81.560
7.041	75.000	72.190
7.320	66.666	64.700
7.622	60.000	58.540
7.941	54.540	54.450
8.278	50.000	49.380
8.628	46.150	45.480
8.991	42.850	42.310
9.362	40.000	39.580
9.744	37.500	37.160
10.135	35.290	35.023
10.535	33.333	33.109
10.942	31.580	31.391
10.663	30.000	29.842
11.772	28.570	28.444
12.195	27.270	27.166

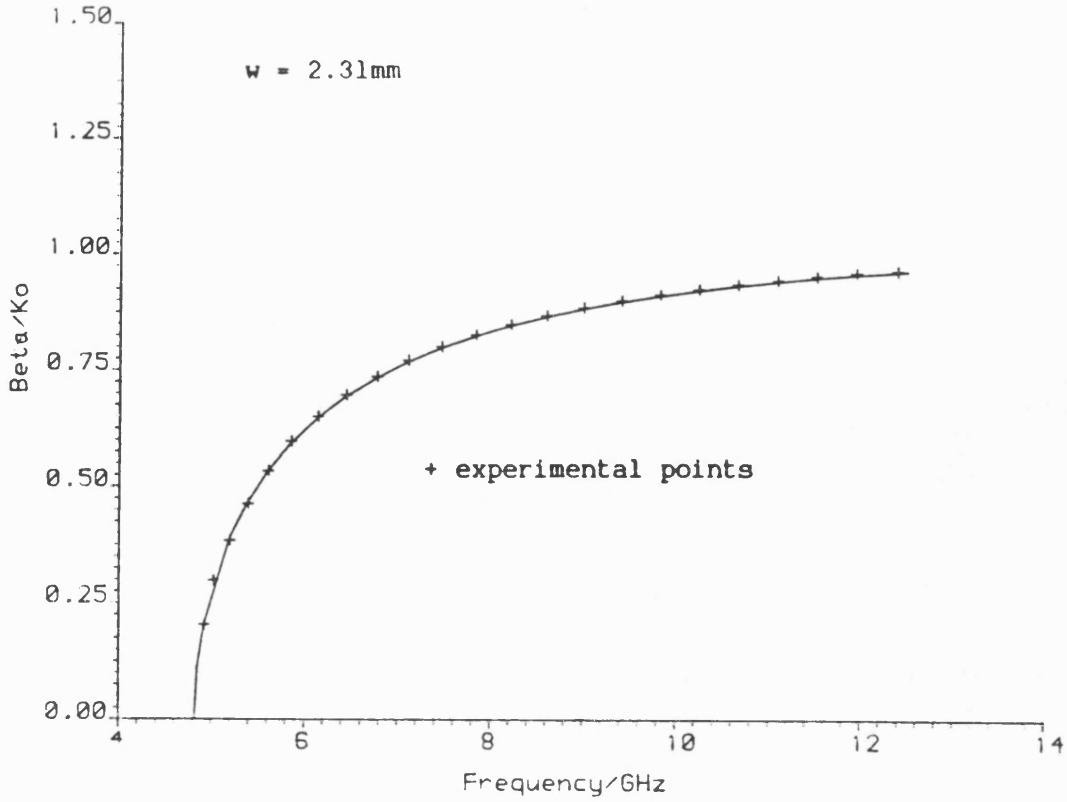

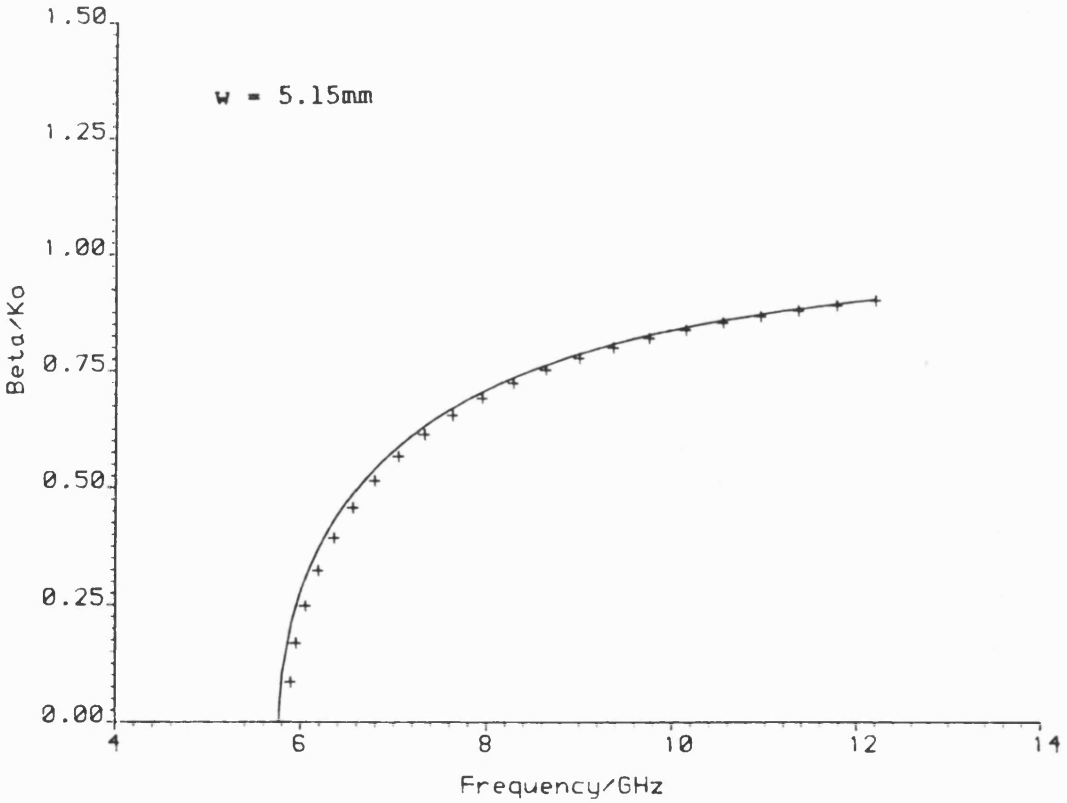

Figures (3.5.4a) and (3.5.4b) Finline Dispersion. (εr = 2.20, guide dimensions as figure (3.5.2))

3.6) Obstacle Formulation

This chapter has concentrated on the aperture formulation, i.e based on an expansion in the slot. But here, for completeness, a comparison will be made with a solution based upon an expansion for the fin currents.

Using the concept of a transverse equivalent network a set of integral equations defining a relationship between electric fields and the fin currents can be readily obtained:

$$\begin{bmatrix} E_x^L \\ \frac{a}{\pi}\frac{\partial}{\partial x} E_z^L \end{bmatrix} = \begin{bmatrix} \hat{Z}_{11}^L & \hat{Z}_{12}^L \\ \hat{Z}_{21}^L & \hat{Z}_{22}^L \end{bmatrix} \cdot \begin{bmatrix} J_x \\ -\frac{\pi}{a}\int J_z \, dx \end{bmatrix} \qquad (3.6.1)$$

for fields infinitesimally left of y=0, whilst for fields to the right:

$$-\begin{bmatrix} E_x^R \\ \frac{a}{\pi}\frac{\partial}{\partial x} E_z^R \end{bmatrix} = \begin{bmatrix} \hat{Z}_{11}^R & \hat{Z}_{12}^R \\ \hat{Z}_{21}^R & \hat{Z}_{22}^R \end{bmatrix} \cdot \begin{bmatrix} J_x \\ -\frac{\pi}{a}\int J_z \, dx \end{bmatrix} \qquad (3.6.2)$$

In order to employ an appropriate set of basis functions, it is convenient to slightly re-define the axis positioning to that of figure (3.6.1). The Greens impedance operators may be obtained from equations (3.2.28) to (3.2.24) using orthogolality as before. Whilst symmetry about x = a/2 implies that only the functions $\phi_{hn}(x)$ corresponding to n even are involved in these operators.

In applying the Galerkin method to achieve solution, equations (3.6.1) and (3.6.2) are expanded directly onto a set of functions over the fin and including the appropriate edge condition. Such an expansion is possible in terms of Gegenbauer polynomials chosen to be orthogonal under the weight function:

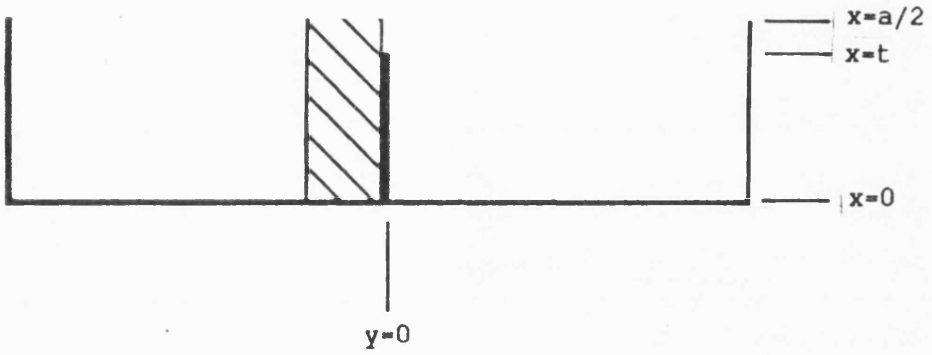

Figure (3.6.1) Axis Orientation for Obstacle Formulation.

$$W(x) = \sqrt{1 - \left(\frac{x}{t}\right)^2}$$

which introduces the required edge condition.

The current expansions may therefore be defined as:

$$J_x(x) = \sum_{m=0}^{M} JX_m \sqrt{1 - u^2} \; C_m^1(u) \qquad (3.6.3)$$

$$\frac{\pi}{a} J_z(x) = \sum_{m=0}^{M} JZ_m \sqrt{1 - u^2} \; C_m^1(u) \qquad (3.6.4)$$

where $u = x/t$ and $C^1(u)$ are Gegenbauer polynomials of order m, with an upper index of unity, given by the weighting function requirement. These are only defined over the region $0 < x < t$ since the current densities $J_x(x)$ and $J_z(x)$ illustrated by figure (3.6.2) cannot exist in the aperture region. Thus the range of integration within the impedance operators is also restricted to this range. To illustrate how the integral equations (3.6.1) and (3.6.2) are converted into matrix equations, consider the relation:

$$E_x^L(x) = \hat{Z}_{11}^L \cdot J_x(x) = \int_0^t Z_{11}(x,x') \, J_x(x') \, dx' \Big|_{J_z = 0} \qquad (3.6.5)$$

expanding the impedance kernel more explicitly:

$$E_x^L(x) = \int_0^t \sum_{n=0}^{\infty} Z_{11n}^L \, \Phi_{hn}(x) \, \Phi_{hn}(x') \, J_x(x') \, dx' \qquad (3.6.6)$$

and inserting the expansion for $J_x(x')$ with a simple change of

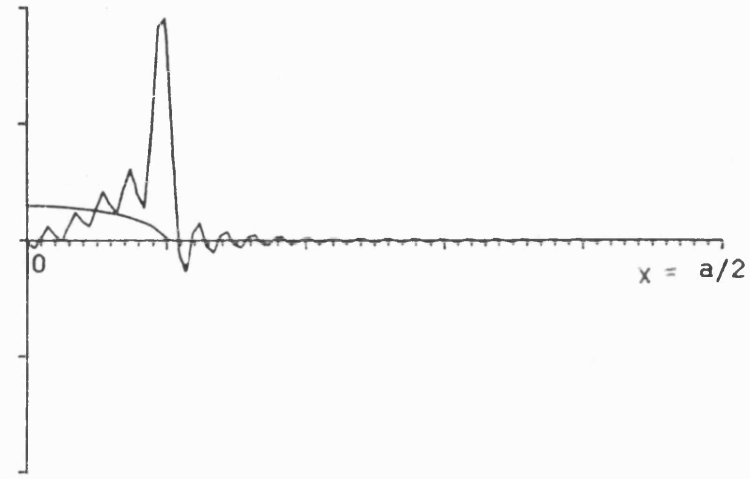

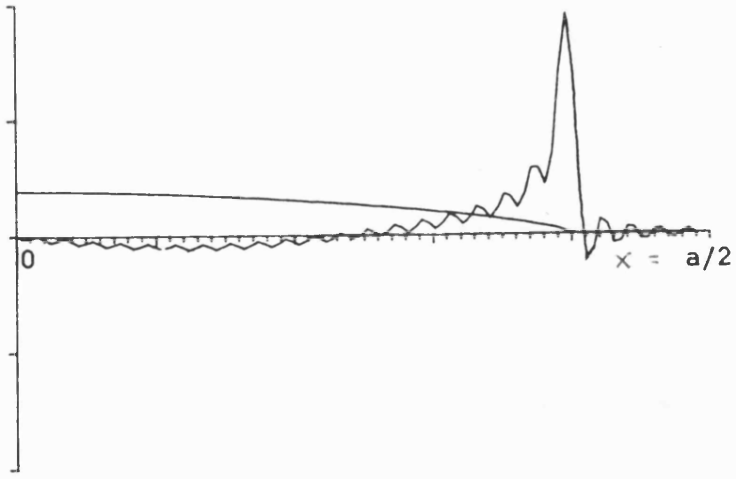

Figures (3.6.2a) and (3.6.2b) Fin Current Distributions of Fundamental Mode for Two Particular Fin Gaps.

variable gives:

$$E_x^L(u) = \int_0^1 \sum_{n=0}^{\infty} Z_{11n}^L \, \phi_{hn}(tu) \, \phi_{hn}(tu') \sum_{m=0}^{M} JX_m \sqrt{1 - u^2} \; C_m^1(u') \, du' \tag{3.6.7}$$

Carrying out the integration above gives:

$$E_x^L(x) = \sum_{m=0}^{M} JX_m \sum_{n=0}^{\infty} Z_{11n}^L \, \phi_{hn}(x) \, Q_{nm} \tag{3.6.8}$$

where the coefficients Q_{nm} are defined as:

$$Q_{nm} = \int_0^t \sqrt{1 - u^2} \; C_m^1(u) \, \phi_{hn}(tu) \, du$$

The above coefficients are obtained analytically from the result given in [4] so that,

$$Q_{nm} = \frac{(-1)^m \; \pi \; \Gamma(2m+2)}{2m!} \; \frac{J_{2m+1}(n\alpha)}{2n\alpha} \; \sqrt{\frac{\delta n}{a}} \tag{3.6.9}$$

where $\alpha = \frac{2\pi t}{a}$.

The relationship between the factorial and the gamma function of integer arguments allows further simplification, but firstly the small argument limit of the Bessel functions must be examined so as to determine the coefficients for the n=0 case.

Consider the Bessel function term appearing in equation (3.6.9):

$$\frac{J_{2m+1}(n\alpha)}{2n\alpha}$$

Employing the small argument limit for the Bessel function gives:

$$\frac{\left(\frac{n\alpha}{2}\right)^{2m+1}}{2n\alpha} \quad \frac{1}{\Gamma(m+1)} \quad = \quad \frac{\left(\frac{n\alpha}{2}\right)^{2m}}{4\,\Gamma(m+1)}$$

from which it can be seen that for n=0 , $Q_{nm} = 0$, unless m=0, in which case

$$Q_{00} = \sqrt{\frac{1}{a}} \quad \frac{\pi}{4} \qquad (3.6.10)$$

For n > 0 equation (3.6.9) simplifies to,

$$Q_{nm} = (-1)^m \pi\,(2m+2) \quad \frac{J_{2m+1}(n\alpha)}{2n\alpha} \quad \sqrt{\frac{2}{a}} \qquad (3.6.11)$$

Whilst for n ---> ∞ the asymptotic form is,

$$Q_{nm} = (-1)^m \pi\,(2m+2) \quad \frac{4}{an\pi\alpha} \quad \frac{\cos\left[n\alpha - \frac{1-2m}{8m+4}\pi\right]}{2n\alpha} \qquad (3.6.12)$$

From the above it can be seen that convergence of the coefficients Q_{nm} is very fast, this feature in fact enables a convergent Green's function to be constructed from the divergent impedances of equations (3.6.1) and (3.6.2).

With the coefficients Q_{nm} known analytically the integral equations may be readily converted into matrix form.

In applying the Galerkin method to the integral equations (3.6.1) and (3.6.2) the aformentioned procedure is carried out and then the electric fields are also expanded in terms of the basis set. The coefficients to this expansion in the illustrated case may be obtained by multiplying equation (3.6.8) by each of the basis functions in turn and integrating. But since tangental electric fields cannot exist on the fins, these coefficients are incidentally zero. Thus equation (3.6.8) becomes:

$$EX^L = \sum_{m=0}^{M} JX_m \sum_{n=0}^{\infty} Z^L_{11n}\, Q_{nm}\, Q_{nk} = 0$$

which is written more conveniently using matrix notation as:

$$\underline{\underline{Z}}^L_{11}\ \underline{JX} = 0 \qquad (3.6.13)$$

Where $\underline{JX}$ a column vector of the coefficients JX_m ,and,

$$\underline{\underline{Z}}^L_{11} = \sum_{n=0}^{\infty} Z^L_{11n}\ \underline{Q}_n \cdot \underline{Q}^T_n$$

Applying the expansion throughout to equations (3.6.1) and (3.6.2) gives:

$$\begin{bmatrix} \underline{EX}^L \\ \underline{EZ}^L \end{bmatrix} = \begin{bmatrix} \underline{\underline{Z}}^L_{11} & \underline{\underline{Z}}^L_{12} \\ \underline{\underline{Z}}^L_{21} & \underline{\underline{Z}}^L_{22} \end{bmatrix} \begin{bmatrix} \underline{JX} \\ -\underline{JZ} \end{bmatrix} = 0 \qquad (3.6.14)$$

and

$$\begin{bmatrix} \underline{EX}^R \\ \underline{EZ}^R \end{bmatrix} = \begin{bmatrix} \underline{\underline{Z}}^R_{11} & \underline{\underline{Z}}^R_{12} \\ \underline{\underline{Z}}^R_{21} & \underline{\underline{Z}}^R_{22} \end{bmatrix} \begin{bmatrix} \underline{JX} \\ -\underline{JZ} \end{bmatrix} = 0 \qquad (3.6.15)$$

where the matrces $\underline{\underline{Z}}_{ij}$ i,j=1,2 are defined in a similar way to $\underline{\underline{Z}}^L_{11}$

The formulation is completed by imposing that the tangental electric fields vanish simultaneously at the surface of the fins giving:

$$\begin{bmatrix} \underline{\underline{Z}}_{11} & \underline{\underline{Z}}_{12} \\ \underline{\underline{Z}}_{21} & \underline{\underline{Z}}_{22} \end{bmatrix} \begin{bmatrix} \underline{JX} \\ -\underline{JZ} \end{bmatrix} = 0 \qquad (3.6.16)$$

where , $Z_{11} = \underline{\underline{Z}}^L_{11} - \underline{\underline{Z}}^R_{11}$ etc.

It is found that n=0 components appear only in the term $\underline{\underline{Z}}_{11}$, and as with the aperture formulation, this component, Z_0, may be taken

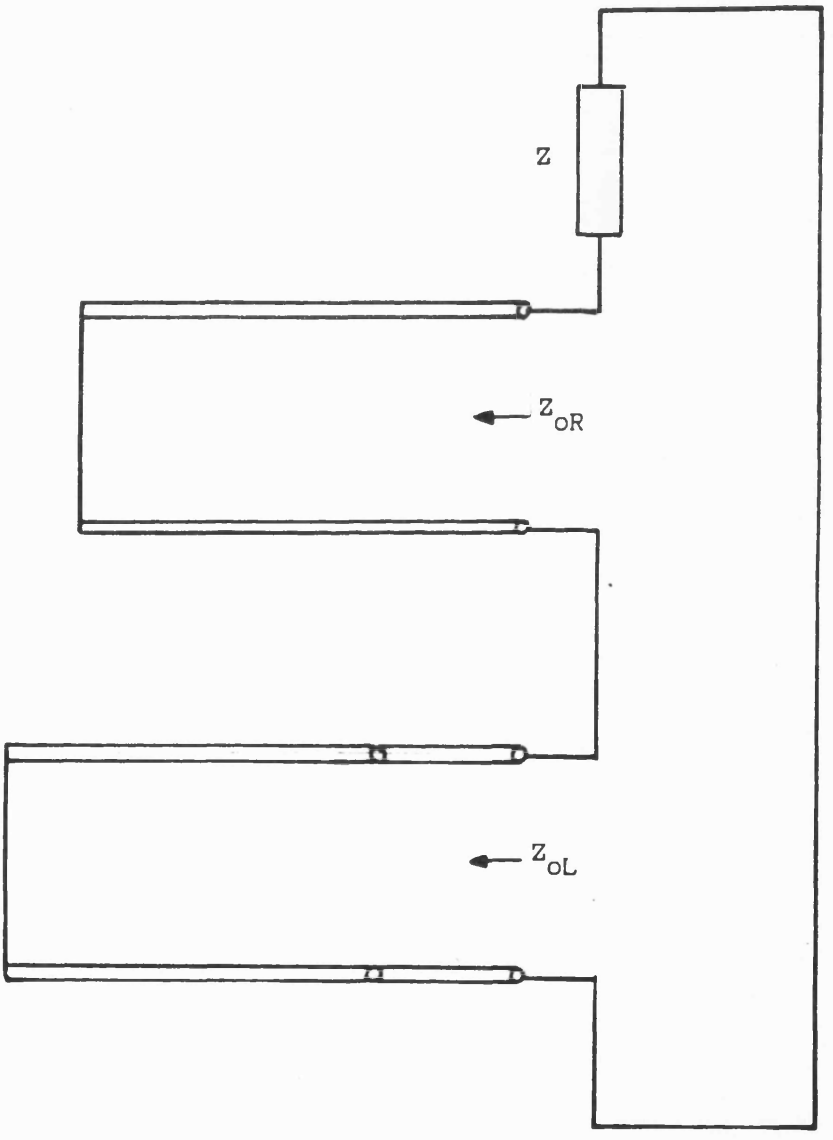

Figure (3.6.3) Series Equivalent Circuit.

out of the matrix system, and equation (3.6.16) becomes:

$$Z_0 + z = 0 \qquad (3.6.17)$$

where the impedance z is given by:

$$\frac{1}{z} = \underline{Q}_0^T \left[\underline{\underline{Z}}_{11} - \underline{\underline{Z}}_{12}\, \underline{\underline{Z}}_{22}^{-1}\, \underline{\underline{Z}}_{21}\right]^{-1} \underline{Q}_0$$

and $$Z_0 = Z_{0L} + Z_{0R}$$

Solutions to equation (3.6.17) may therefore be interpreted as the resonance of the series equivalent circuit as in figure(3.6.3). It is then found that for wide gaps, as fins vanish into the side walls, the fin impedance z becomes large and the solution point reverts to the impedance pole in Z_0 which defines modes in the resulting dielectrically loaded waveguide (identical to the condition $Y_0 = 0$ in equation (3.5.11)).

Numerical implementation of equation (3.6.17) was improved by making use of the quasi static components to form impedance sums from which the frequency variation had been removed. These have to be evaluated numerically for a particular fin gap (whilst the Schwinger approach can evaluate such infinite sums analytically).

3.6i) Comparison of Numerical Results

Dispersion results for the fundamental mode over a range of fin gaps were found to be in close agreement with the aperture formulation, proving the validity of the obstacle approach. Figure (3.6.4) shows dispersion curves obtained from the accurate aperture formulation, compared with points calculated using the obstacle approach employing various order of expansion. Figure (3.6.5) shows

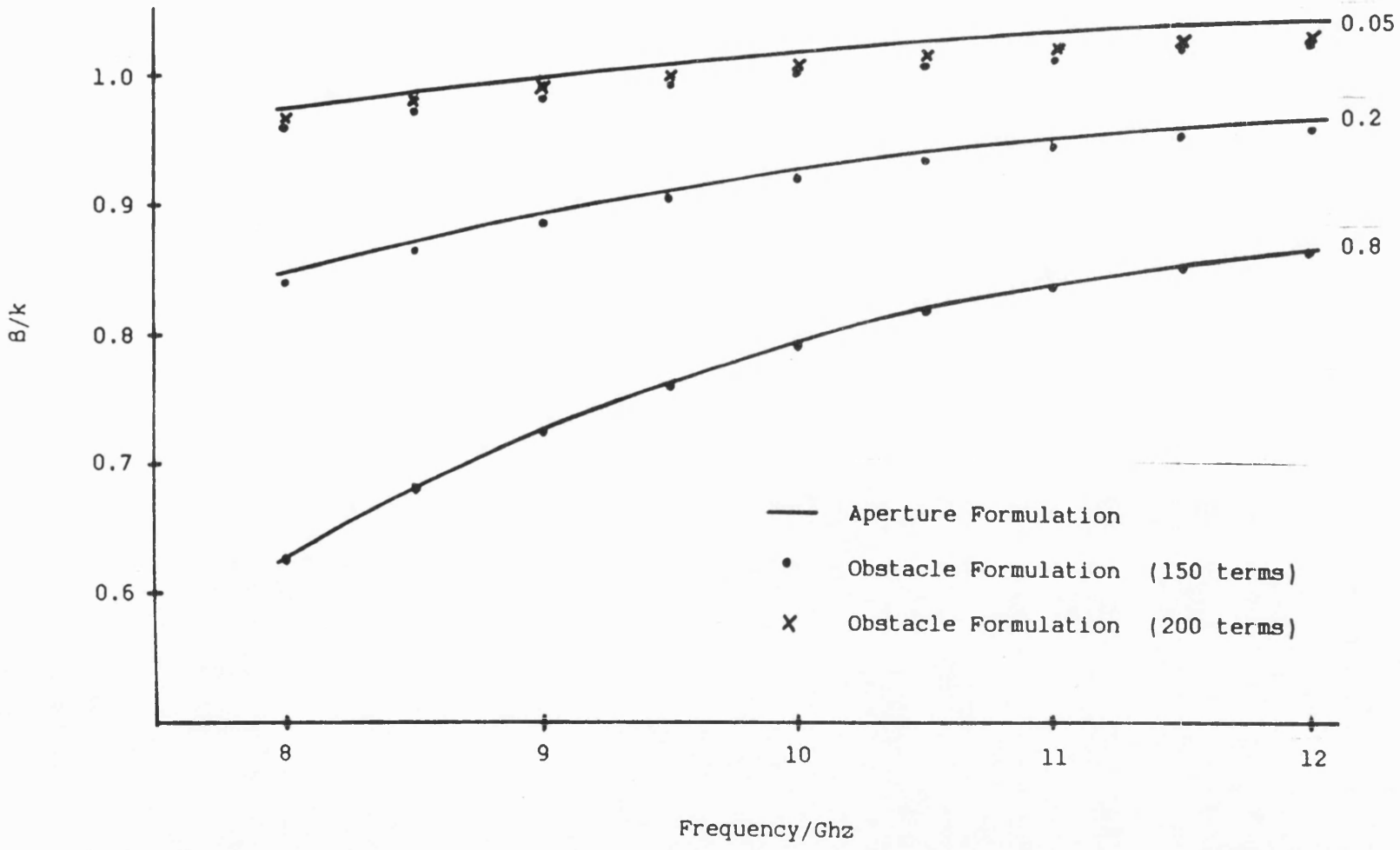

Figure (3.6.4) Comparison of Finline Dispersion Curves.

the convergence properties of both approaches. It can be seen that the two methods approach the true value from either side. The remaining discrepancy arises in the obstacle formulation as it cannot include the analytic result of infinite sums. However a more detailed examination of the convergence properties of the Gegenbauer polynomial expansion for the fin currents reveals further advantages in favour of the aperture (Schwinger) approach.

It was found in general that matrix orders of at least 3 by 3 were required in order to achieve convergence in the x-directed fin current expansion, although the longitudinal current was essentially given by one term. This is shown in Tables (3.5a) to (3.5c) which give the expansion coefficients obtained at 10 Ghz for three different fin gaps. These may be compared with Tables (3.2a) to (3.2b) which give the expansion coefficients of aperture field.

Whilst the results of the two formulations are in close agreement, the aperture formulation is clearly superior by virtue of the fast convergence of the Schwinger expansion for the gap field necessitating, matrices of very low order. Successful use of the Gegenbauer polynomials has been demonstrated and a satisfactory formulation established. Current expansions may in fact be preferable in other E-plane structures such as suspended stripline. However, for the particular case of finline, this thesis will continue to pursue the aperture formulation and investigate higher order modes.

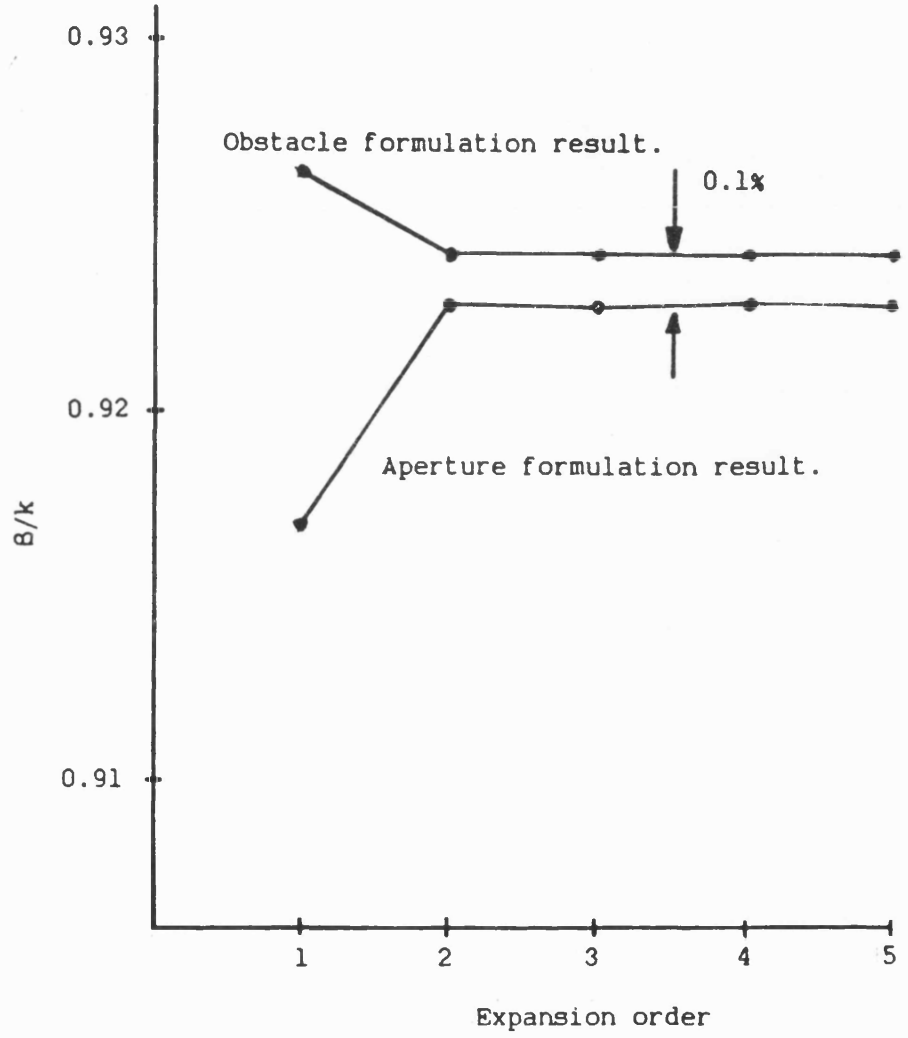

Figure (3.6.5) Convergence of Finline Dispersion Results versus Expansion Order. (X-band finline, frequency = 10GHz, w/a = 0.1)

Tables (3.5a), (3.5b) and (3.5c) Fin Currents Expansion Coefficients JX_m and JZ_m for Various Normalised Fin-gaps at X-Band.

X-band finline, F=10.0 Ghz, w/a = 0.050.		
	JX_m	JZ_m
1	-0.145653	1.000000
2	-0.037377	0.115555
3	-0.010047	0.007631
4	-0.004687	0.014367

X-band finline, F=10.0 Ghz, w/a = 0.200.		
	JX_m	JZ_m
1	-0.055179	1.000000
2	-0.054885	0.143113
3	-0.003898	-0.015850
4	-0.005063	0.012464

X-band finline, F=10.0 Ghz, w/a = 0.800.		
	JX_m	JZ_m
1	-0.520287	1.000000
2	-0.311005	0.496639
3	-0.194383	0.309794
4	-0.133317	0.215881

References - Chapter (3)

1) Itoh, T. , 'Specral Domian Immitance Approach for Dispersion Characteristics of Generalized Printed Transmission Lines.' IEEE trans MTT-26, July 1980, pp 733-736.

2) Collin R.E. 'Field Theory of Guided Waves.' McGraw-Hill, New York, 1960, ch8.

3) Schwinger J. and Saxon D., 'Discontinuities in Waveguides.' Gordon and Breach, New York, 1968.

4) Gradshteyn and Ryzhik, 'Table of Integrals, Series, and Products.' Academic Press, New York, 1965.

CHAPTER FOUR : FINLINE MODE SPECTRUM

For the analysis for finline discontinuities knowledge of higher order finline modes is essential. Although the general solution will find these modes by employing a search for roots at higher effective frequencies, the search routines themselves have to become highly sophisticated as the roots become increasingly difficult to locate.

This chapter considers particular simplifications which may be made to the theory developed so far, which allow the cut-off frequencies to be found in a systematic and reliable manner. In addition, these simplifications allow the finline mode spectrum to be characterised in terms of the slot field at cut-off.

The cut-off theory is taken a stage further to develop a simple means of describing finline dispersion. This can either be used directly for approximate broad band modelling or in conjunction with the general solution as pointers to root positions when searching for exact field solutions.

4.1) Cut-off poperties.

By imposing that $\beta=0$ the system of integral equations describing the effects of the fin is decoupled to give two distinct sets of solutions for the cut-off points of finline modes. This decoupling is seen by explicitly writing out the field components in terms of the LSE and LSM potentials to give:

$$\underline{E} = \begin{bmatrix} \frac{\partial}{\partial x}\frac{\partial}{\partial y} \\ k^2 + \frac{\partial^2}{\partial y^2} \\ 0 \end{bmatrix} \Psi_e(x,y) + \begin{bmatrix} 0 \\ 0 \\ -j\omega\mu \frac{\partial}{\partial x} \end{bmatrix} \Psi_h(x,y) \qquad (4.1.1)$$

$$\underline{H} = \begin{bmatrix} \frac{\partial}{\partial x}\frac{\partial}{\partial y} \\ k^2 + \frac{\partial^2}{\partial y^2} \\ 0 \end{bmatrix} \Psi_h(x,y) + \begin{bmatrix} 0 \\ 0 \\ j\omega\varepsilon \frac{\partial}{\partial x} \end{bmatrix} \Psi_e(x,y) \qquad (4.1.2)$$

Here the LSE and LSM potentials become decoupled such that a particular field component is given only in terms of one potential. This implies that the general complexity of the resulting system of equations will be greatly reduced.

In the T.R.D. formulation this decoupling primarily manifests itself in the terms $\sin\tau_n$ and $\cos\tau_n$ defining the resolution into TE-to-y and TM-to-y parts of the transverse equivalent circuit, since for $\beta=0$:

$$\sin\tau_n = 0 \qquad (4.1.3a)$$

and

$$\cos\tau_n = 1 \qquad (4.1.3b)$$

i.e. the axis rotation angle τ_n, introduced in chapter three, reduces to zero.

Thus the operators $\hat{\underline{Y}}_{12}$ and $\hat{\underline{Y}}_{21}$ appearing in equation (3.3.21) vanish to give two decoupled equations describing the effects of the fin:

$$\hat{Y}_{11}(x,x')\ E_x(x') = 0 \qquad (4.1.4a)$$

and

$$\hat{Y}_{22}(x,x')\ \frac{a}{\pi}\frac{\partial}{\partial x}\ E_z(x') = 0 \qquad (4.1.4b)$$

where the kernels of the operators $\hat{\underline{\underline{Y}}}_{11}(x,x')$ and $\hat{\underline{\underline{Y}}}_{22}(x,x')$ are as follows:

$$Y_{11}(x,x') = \sum_{n=0}^{\infty} \left(Y_{nL}^{TM} + Y_{nR}^{TM} \right) \phi_{hn}(x)\ \phi_{hn}(x')$$

and

$$Y_{22}(x,x') = \sum_{n=1}^{\infty} \frac{1}{n} \left(Y_{nL}^{TE} + Y_{nR}^{TE} \right) \phi_{hn}(x)\ \phi_{hn}(x')$$

Furthermore from equation (4.1.1) it is seen that a mode purely LSE at cut-off is distinguished by the absence of the z-directed electric field component, whilst a mode LSM at cut-off does not contain an x-directed electric field component. Thus modes which are LSE at cut-off may be obtained from equation (4.1.4a), and modes LSM at cut-off from equation (4.1.4b). Numerical solution of these integral equations is obtained by mapping onto the Schwinger basis to form matrix equations:

$$\underline{\underline{Y}}_{11}\ \underline{X} = 0 \qquad (4.1.5a)$$

$$\underline{\underline{Y}}_{22}\ \underline{Z} = 0 \qquad (4.1.5b)$$

where,

$$\underline{\underline{Y}}_{11} = \sum_{n=0}^{\infty} \left(Y_{nL}^{TM} + Y_{nR}^{TM} \right) \underline{P}_n \cdot \underline{P}_n^T$$

$$\underline{\underline{Y}}_{22} = \sum_{n=0}^{\infty} \left(Y_{nL}^{TE} + Y_{nR}^{TE} \right) \underline{P}_n \cdot \underline{P}_n^T$$

and $\underline{X}$ and $\underline{Z}$ are vectors representing the slot field as defined previously in equation (3.5.1).

Solution for the cut-off frequencies could now be obtained by searching for zeros in the determinants $|\underline{\underline{Y}}_{11}|$ and $|\underline{\underline{Y}}_{22}|$.

Although the LSE/LSM decoupling has produced a slightly less complicated system, the search for roots is still not straightforward. However, a further simplification is seen to originate from the Schwinger mapping. Since $\beta = 0$, the wave equation for a system uniform in z is reduced to its two dimensional form:

$$\frac{\partial^2}{\partial x^2} + \frac{\partial^2}{\partial y^2} + k^2 = 0 \qquad (4.1.6)$$

Under these quasi-static conditions, techniques such as two dimensional conformal mapping, giving exact solutions to the Laplace equation, provide near exact solutions to the wave equation , especially where the derivative terms dominate i.e. in the vicinity of the fin edges where the spatial variation of fields is rapid. The Schwinger mapping can therefore be employed to great effect.

The Schwinger mapping provides an orthogonal set of gap field variations which closely approximate solutions to the wave equation at cut-off. Solutions for modes exhibiting a cut-off gap field given by the m`th Schwinger function are found to occur when the m'th diagonal element in the matrices $\underline{\underline{Y}}_{11}$ and $\underline{\underline{Y}}_{22}$ are zero. The system of equations for cut-off may therefore be further decoupled into sets defining families of mode exhibiting a common slot field variation.

The cut-off frequencies of modes which exhibit the m'th order field variation in the slot and which are LSE at cut-off, i.e. the LSE(m) mode families, are given by the solution of the linear transcendental equation:

$$\sum_{n=0}^{\infty} \left(Y_{nL}^{TM} + Y_{nR}^{TM} \right) P_{nm}^{2} = 0 \qquad (4.1.7)$$

Solutions to this equation correspond to the resonance of a transverse equivalent network containing only TM-to-y modes. When only one transverse variation is of the propagating type, the higher order variations may be regarded as localised about the fin, and the simplified equivalent circuit of figure (3.3.1) need only be considered. The method of Cohn [1] for obtaining the cut-off's to the fundamental mode in ridged waveguide and adapted by Saad and Begenmann [2] for finline is seen to correspond to this special case. However, the present method incorporates an exact description of the resulting fin admittance which enables higher order finline modes to be accurately solved. Furthermore, the identification of orthogonal field variations in the slot satisfying the wave equation at cut-off allows further sets of modes to be obtained, and categorised in terms of mode families.

The modes LSE at cut-off may be described as capacitive [3] from the form of the fin admittance. Whilst inductive LSM modes, are obtained at cut-off from:

$$\sum_{n=0}^{\infty} \left(Y_{nL}^{TE} + Y_{nR}^{TE} \right) P_{nm}^{2} = 0 \qquad (4.1.8)$$

As noted in chapter three, m=0 variations in the z-directed electric field are not valid and consequently the LSM(0) family cannot exist.

4.2) Numerical Aspects of Solution for Cut-Off.

At this stage it is instructive to examine the particular case of the transverse admittances for $\beta = 0$. Some consideation here not only leads to a numerically efficient solution, but also, from an understanding of the underlying mathematics the cut-off's can be obtained in a systematic and reliable manner.

At cut-off the effective frequencies defined in appendix AI, and used in the calculation of the transverse admittances, become:

$$w = k_c \qquad (4.2.1a)$$

$$u = \sqrt{\varepsilon_r}\, k_c \qquad (4.2.1b)$$

where k_c is the normalised cut-off wavenumber given by $\frac{a}{\pi} k_o$.

The admittances involved in equations (4.1.7) and (4.1.8) may be written only as functions of n and k_c. Solution for cut-off frequencies is obtained by iteratively seeking roots in k_c. This, however, necessitates repeated calculation of infinite sums and it is therefore useful to extract the quasi-static admittance so that only a dynamic correction series needs to be evaluated at each iteration.

By substitution for u and w in equations (AI.9) and (AI.10) the limits for large n are obtained as:

$$Y_{nR}^{TE} \longrightarrow \frac{n}{j\sqrt{\varepsilon_r}\, k_c} \quad ; \quad Y_{nL}^{TE} \longrightarrow \frac{n}{j\sqrt{\varepsilon_r}\, k_c}$$

$$Y_{nR}^{TM} \longrightarrow j\,\frac{k_c}{\sqrt{\varepsilon_r}\, n} \quad ; \quad Y_{nL}^{TM} \longrightarrow \frac{\sqrt{\varepsilon_r}\, k_c}{n} \qquad (4.2.2)$$

Removing the quasi-static components from (4.1.8) gives:

$$\sum_{n=0}^{nd} Y_{nL}^{TM} + Y_{nR}^{TM} - j \frac{k_c\sqrt{\varepsilon_r'}(1 + 1/\varepsilon_r)}{n} P_{nm}^2$$

$$+ A_{mm} \; j \; k_c \sqrt{\varepsilon_r'} (1 + 1/\varepsilon_r) = 0 \qquad (4.2.3)$$

where the elements A_{mm} have been defined previously in equation (AI.20).

Similarly (4.1.10) becomes:

$$\sum_{n=1}^{nd} \frac{Y_{nR}^{TE} + Y_{nL}^{TE}}{n^2} - j \frac{2}{\sqrt{\varepsilon_r'} k_c n} P_{nm}^2$$

$$+ A_{mm} \; j \; \frac{2}{\sqrt{\varepsilon_r'} k_c} = 0 \qquad (4.2.4)$$

The summations may now be successfully truncated at n=nd. For the fundamental finline mode this truncation typically occurs at n=20. However in calculations for higher order modes this value must be progressively increased. In fcat, in accordance with the transverse variation of field, an increasing number of propagating transverse admittances must be included in the analysis. Because equations (4.1.7) and (4.1.8) which definine the cut-off are simply constructed from sums of admittances, poles that are introduced by the tangent type variations become interlaced with zeros. Figure (4.2.1) illustrates the occurrence of poles and zeros in the formulation for LSE(0) mode cut-off's. Since the zeros correspond to roots of the cut-off equation, knowledge of poles will enable cut-off's to be found in a systematic manner.

The poles may be found from an examination of the the transverse admittances. Consider the transverse admittance seen by TM modes looking right of the fin:

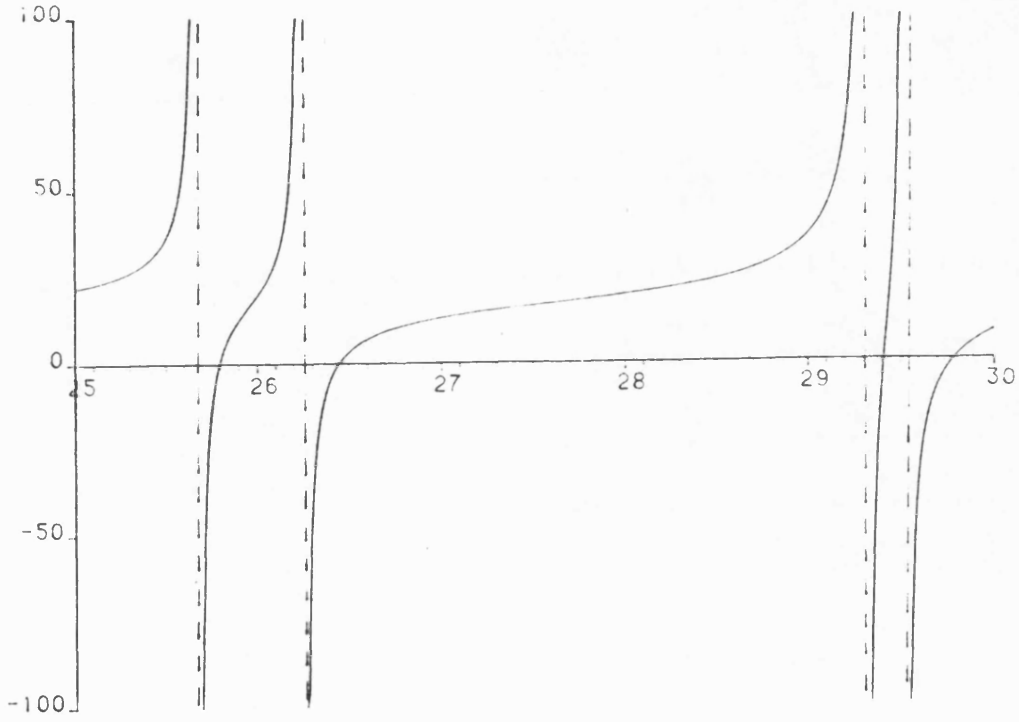

Figure (4.2.1) Typical Occurrence of Roots to the Cut-Off Equation.

$$Y_{nR}^{TM} = j \frac{\sqrt{\varepsilon_r k_c^2 - n^2}}{\sqrt{n^2 - k_c^2}} \coth \sqrt{n^2 - k_c^2} \frac{\pi}{a} l \qquad (4.2.5)$$

It is readily seen that poles occur when,

$$\sqrt{k_c^2 - n^2} \frac{\pi}{a} l = N\pi \quad ; \quad N = 0,1,2,3,...$$

(the pole generated by the modal admittance term outside the cotangent is duly accounted for by the N=0 case).

The TE poles seen to the right are, in fact, identical. However, The determination of admittance poles seen to the left in the mixed dielectric region is not as straightforward and is given in appendix AII.

The poles thus obtained from the regions left and right of the fins now enable cut-off's frequencies for modes in the LSE(m) and LSM(m) mode families to be obtained in a systematic and reliable manner.

Finally, it is worthwhile to note that when the structure exhibits a high degree of symmetry about y = 0, poles from the left and right occur very closely spaced in the cut-off equation. These pole positions do not vary with fin gap, and under these circumstances the cut-off frequencies of certain finline modes will not vary appreciably with fin gap.

4.3) Cut-off Results

Figure (4.3.1) shows the variation in calculated cut-off frequencies versus fin gap for the LSE(0) mode family in X-band finline ($\varepsilon_r = 2.2$). Since the fins are located very closely to the halfway point between the end walls , there is a clear distinction

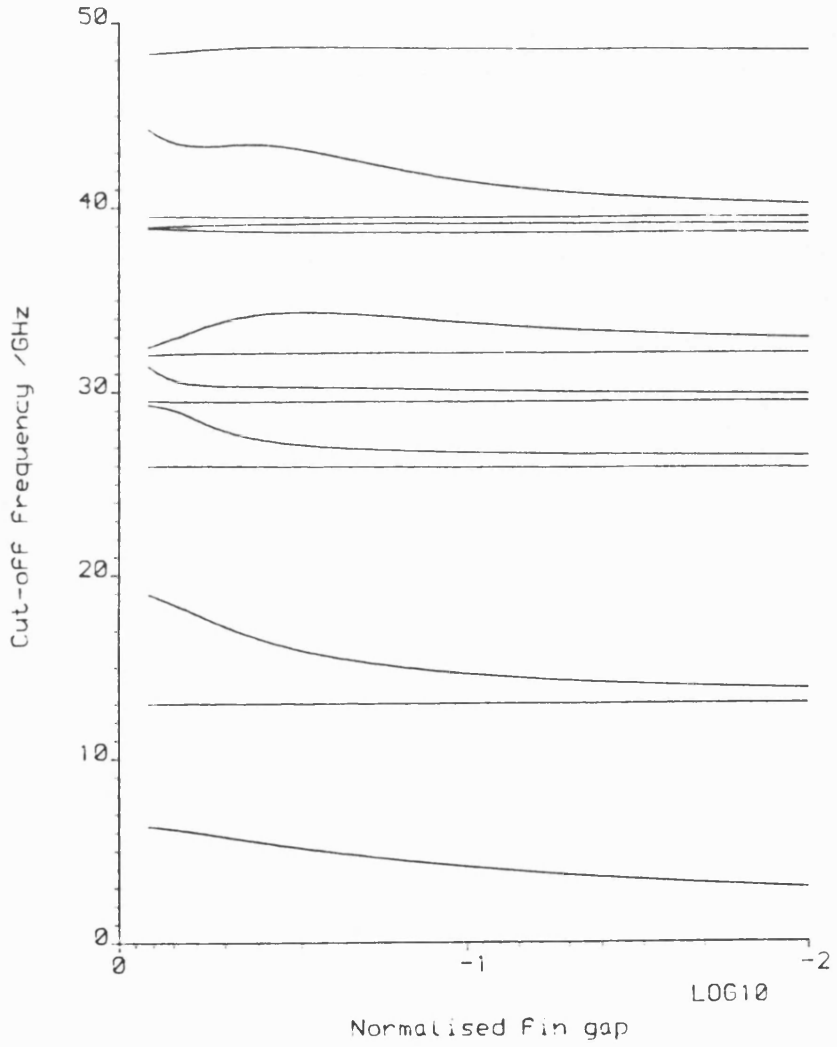

Figure (4.3.1) Cut-Off Frequencies of the LSE(0) Mode Family in X-Band Finline (ε_r = 2.20, guide dimensions a = 10.16, l = (h+s) =11.43mm, s = 0.254mm).

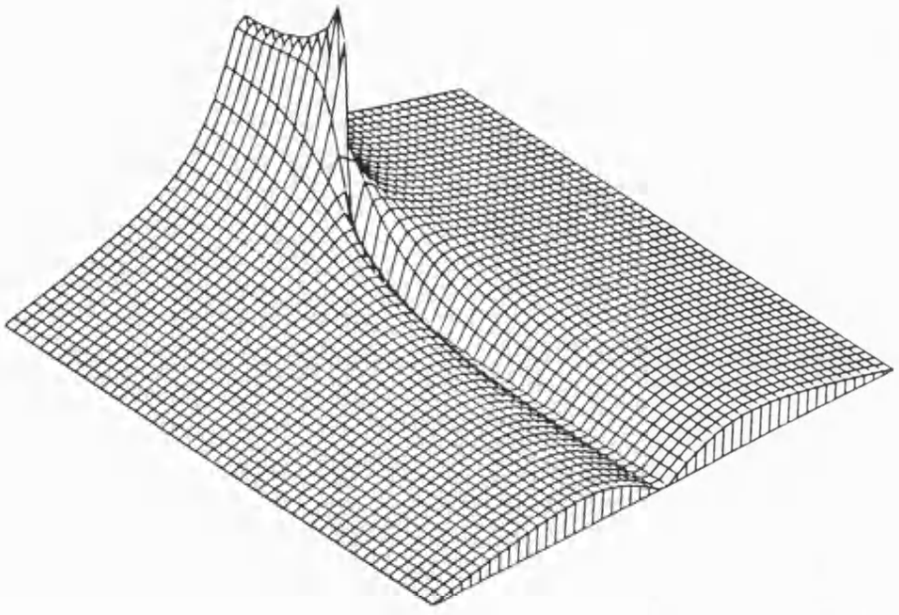

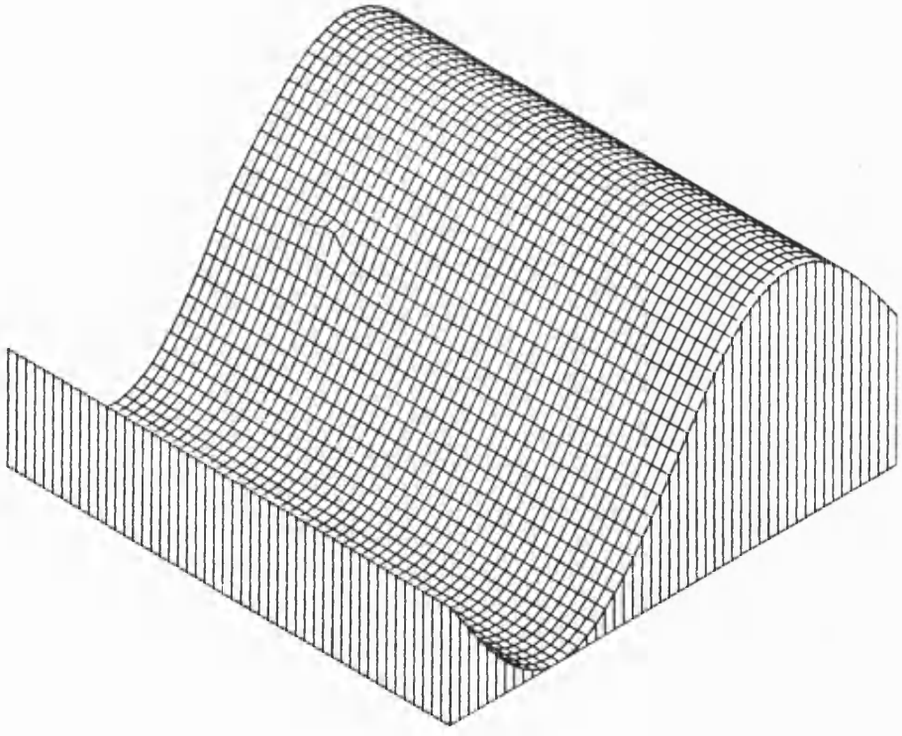

Figures (4.3.2a) and (4.3.2b) Ex Field For the $LSE(0)_1$ and $LSE(0)_2$ modes - Orientation(1) (see figure(A1) for orientation keys).

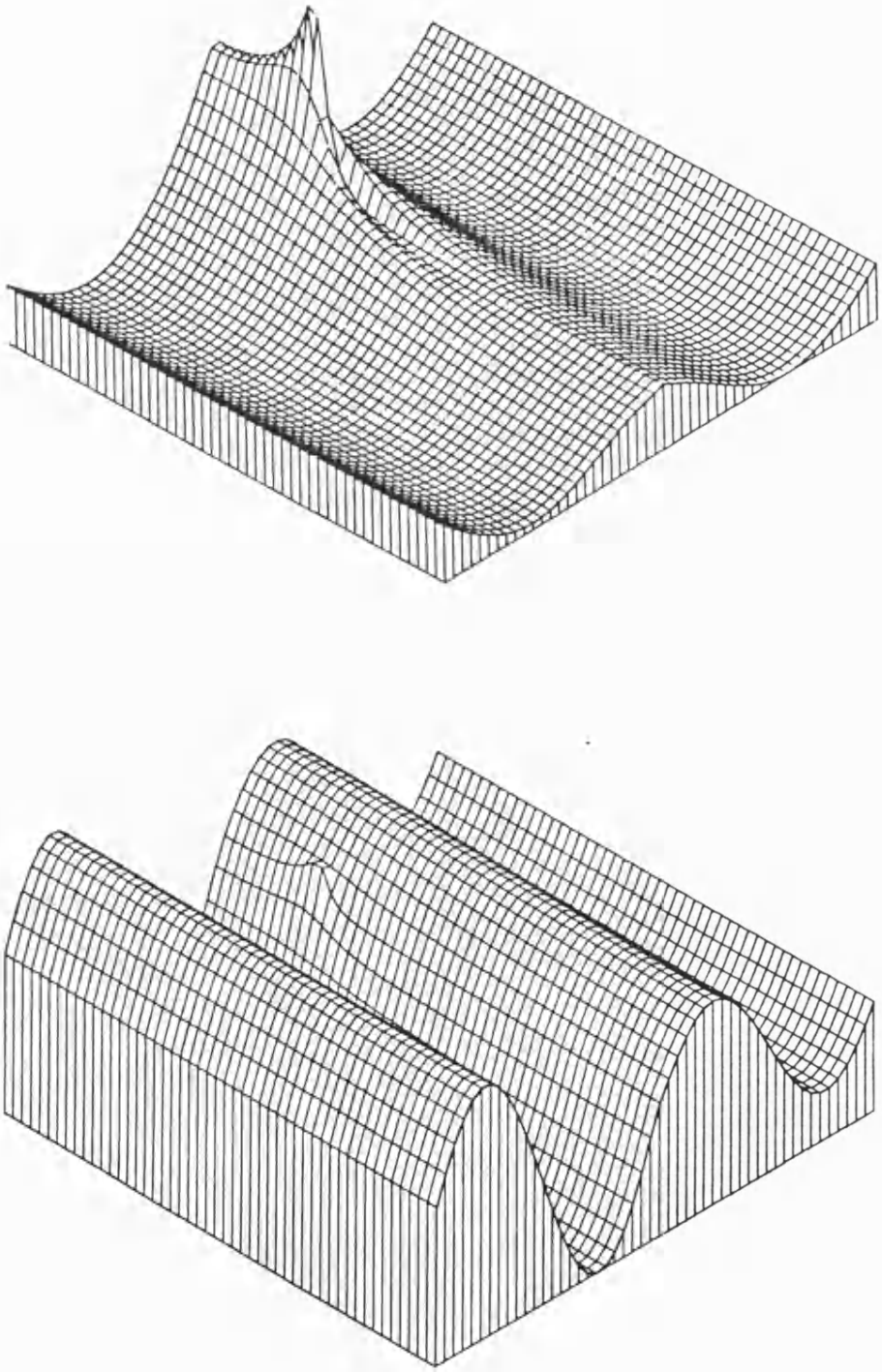

Figures (4.4.2a) and (4.4.2b) Ex Field For the $LSE(0)_3$ and $LSE(0)_4$ modes - Orientation(1)

between the cut-off behaviour of certain modes as predicted.

Figures (4.3.2a) and (4.3.2b) show the field Ex for the $LSE(0)_1$ and $LSE(0)_2$ modes respectively. The concentration of field in the gap region occurring in the fundamental mode is clearly seen. However the $LSE(0)_2$ mode experiences a realatively weak fin interaction. In general, modes which are LSE at cut-off and interact strongly with the fins experience a reduction the cut-off frequency with fin-gap, whilst the modes weakly coupled remain basically unaffected. Figures (4.3.3a) and (4.3.3b) confirm a continuation of these trends for the $LSE(0)_3$ and $LSE(0)_4$ modes.

For small fin gaps it is noted that cut-off frequencies of all finline modes begin to approach asymptotic values. This can be explained by the fact that when a large number of transverse modes are coupled to the fin gap field, the contribution of each to the overall admittance in equation (4.1.9) is small. Thus when poles occur in a particular admittance, introducing a rapid variation between $\pm\infty$, zeros corresponding to solutions of the cut-off equation tend to occur near to the poles. In general this pole zero clustering effect increases as more transverse modes are coupled to the fin.

The cut-off frequencies of the LSE(1) mode family are shown in figure (4.3.4) and are seen to behave in a similar manner. But since $n = 0$ x-variations are not present in the quasi-static gap field defining this mode family, LSE(1) modes do not occur until higher up in the mode spectrum. Furthermore, because this gap field couples to many more transverse modes, the zero-pole clustering effect is much more apparent. Cut-off frequencies to these modes approach asymptotic values very quickly as the fin gap is reduced. The cut-off frequencies of modes in higher slot mode families become asypmtotic even more quickly. In fact, without knowledge of these asymptotes,

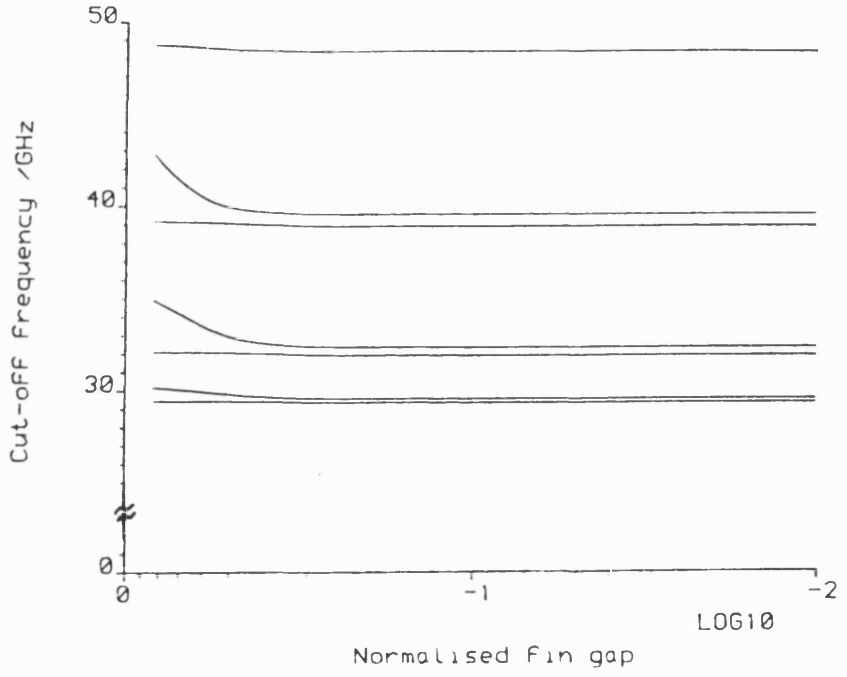

Figure (4.3.4) Cut-Off Frequencies of the LSE(1) Mode Family in X-Band Finline (guide parameters as figure (4.3.1)).

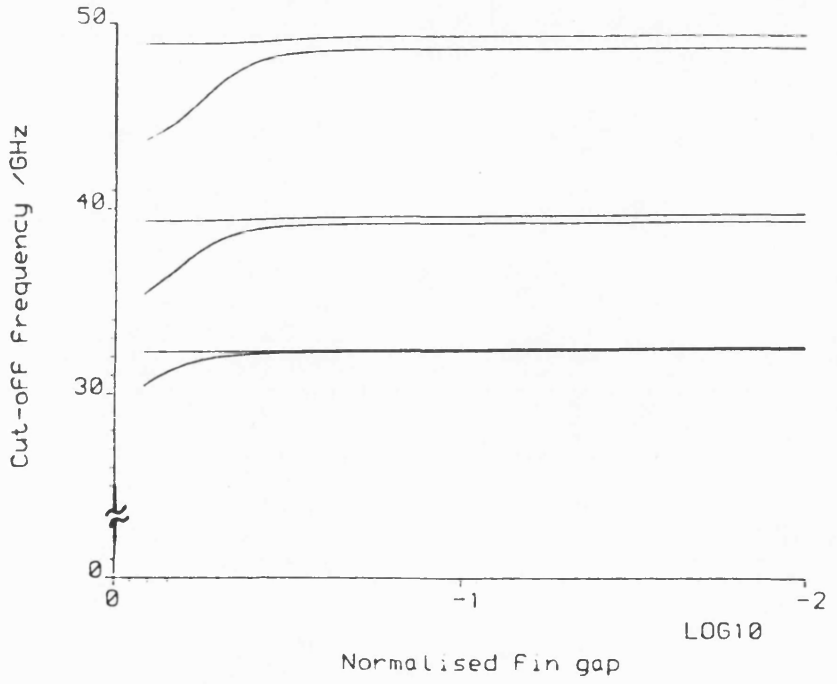

Figure (4.3.5) Cut-Off Frequencies of the LSM(1) Mode Family in X-Band Finline (guide parameters as figure (4.3.1)).

the proximity of poles to zeros can cause severe numerical problems.

Figure (4.3.5) shows the variation in calculated cut-off frequencies for the LSM(1) mode family. Since the transverse TE modes see the fins as an inductive obstacle, the cut-off frequencies of LSM(m) modes increase as the fin gap is reduced. However, the fin gap field couples to a great many transverse modes and hence asymptotic behaviour in cut-off is soon apparent.

The overall mode spectrum of finline is found as a superposition of all mode families. In general cut-off frequencies between individual LSE and LSM mode families only coincide in the asymptotic limit for an infinitely small fin gap. However, as seen in figure (4.3.6), there will frequently exist particular fin gaps where LSE and LSM modes share the same cut-off point giving rise to a degenerate mode. Furthermore, away from the cut-off points, a coupling between all of the mode families can be expected. In particular, whenever roots to the LSE and LSM modes are in close proximity to each other, complex mode behaviour may occur.

This effect may be easily seen from the mathematics by considering the matrices $\underline{\underline{Y}}_{11}$ and $\underline{\underline{Y}}_{22}$ which define LSE and LSM solutions at the cut-off point. Once $\beta \neq 0$ a coupled system of equations results from an equation of the form:

$$\det\left[\underline{\underline{Y}}_{11} - \underline{\underline{Y}}_{12} \, \underline{\underline{Y}}_{22}^{-1} \, \underline{\underline{Y}}_{21} \right] = 0 \qquad (4.3.1)$$

Zeros from the determinant of $\underline{\underline{Y}}_{22}$ define LSM modes, when they fall at or very near to the cut-off point, may cause the inverse $\underline{\underline{Y}}_{22}^{-1}$ to become singular, and hence they appear in equation (4.3.1) as poles. Figure (4.3.7) illustrates how such an interfering pole can causes a root to disappear from the real β axis leading to a complex mode

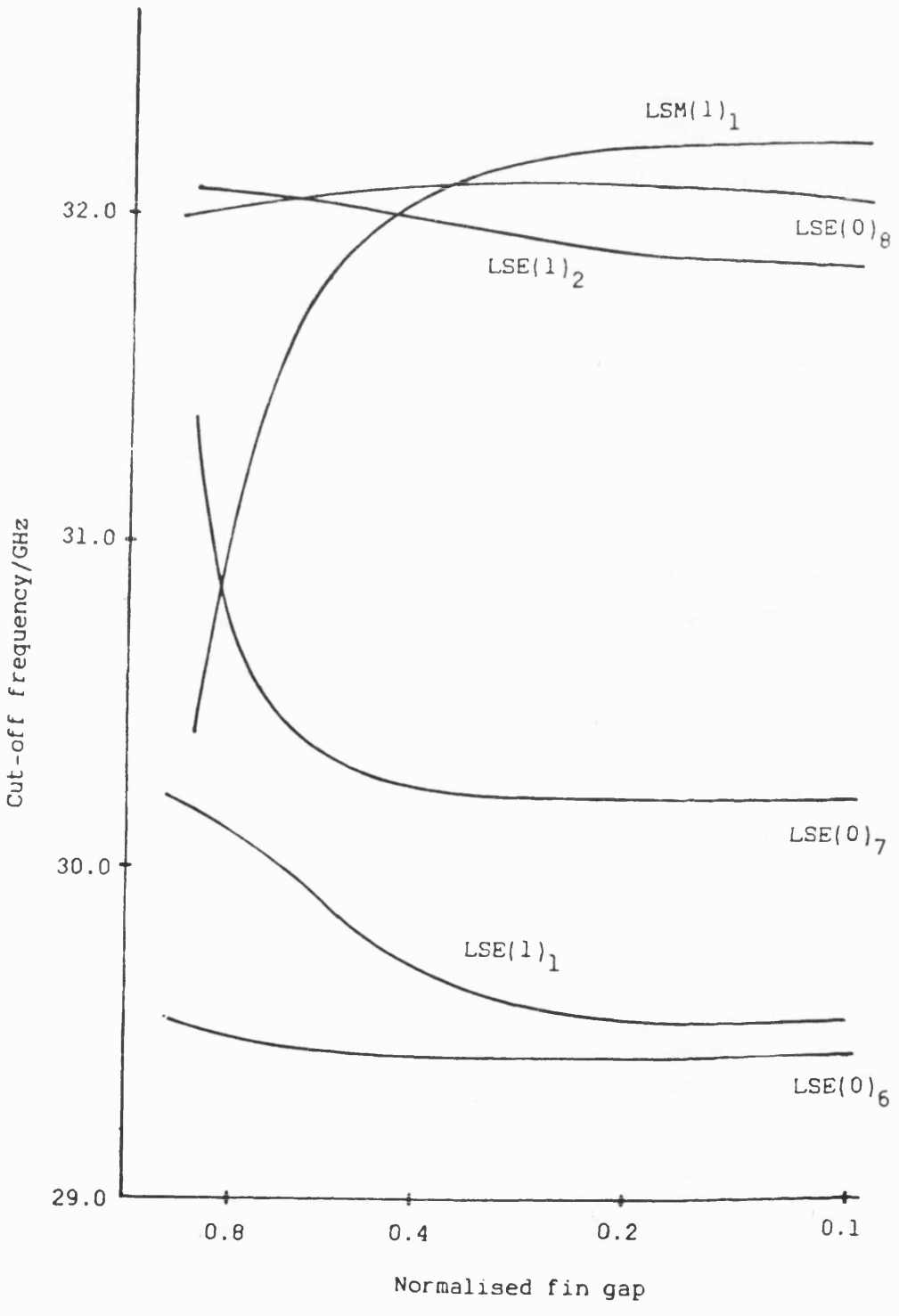

Figure (4.3.6) Section of the Overall Mode Spectrum in X-Band Finline (guide parameters as figure (4.3.1)).

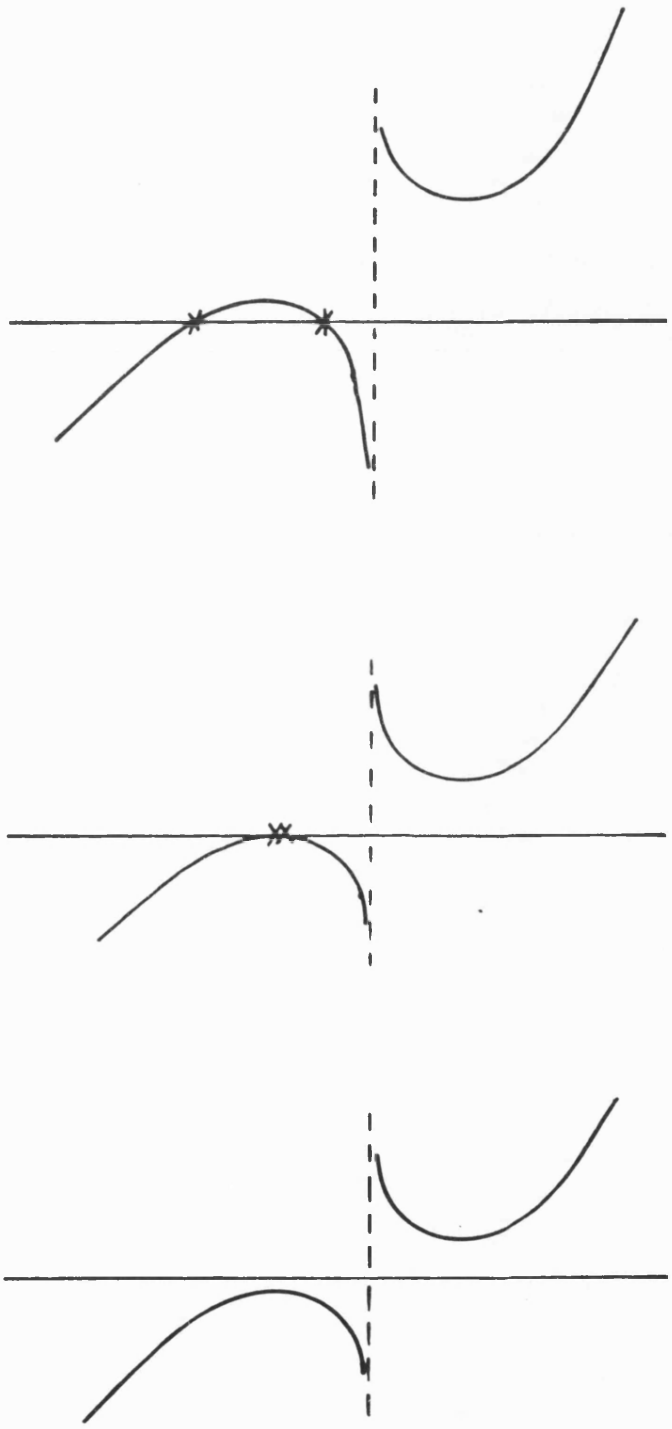

Figure (4.3.7) Illustration of Roots Vanishing From Real Axis.

pair.

From the results on the cut-off points of LSE and LSM type modes, it is apparent that the higher order slot mode families in particular have LSE and LSM solutions occurring very close together and complex mode behavior may therefore be expected to be widespread especially for narrow fin gaps.

4.4) Equivalence of Mode Families.

Consider the case of a field representation in terms of TE and TM components using the z-directed potentials, Ψ_{te} and Ψ_{tm}. At cut-off the fields are given as:

$$\underline{E} = \begin{bmatrix} \frac{\partial}{\partial y} \\ \frac{\partial}{\partial x} \\ 0 \end{bmatrix} \Psi_{te}(x,y) + \begin{bmatrix} 0 \\ 0 \\ k^2 \end{bmatrix} \Psi_{tm}(x,y) \qquad (4.4.1)$$

$$\underline{H} = \begin{bmatrix} \frac{\partial}{\partial y} \\ \frac{\partial}{\partial x} \\ 0 \end{bmatrix} \Psi_{tm}(x,y) + \begin{bmatrix} 0 \\ 0 \\ k^2 \end{bmatrix} \Psi_{te}(x,y) \qquad (4.4.2)$$

By comparing these fields components with those given by the LSE and LSM representation at cut off, it is seen that the two sets are equivalent, i.e. modes purely LSE at cut-off are also purely TE, and modes purely LSM are TM at cut-off. Thus if the fins vanish and the substrate permittivitty approaches unity, modes TE at the cut-off are able to remain purely TE as the finline structure reverts to a conventional rectangular waveguide. The n'th member of the LSE(m) mode family, the $LSE(m)_n$ mode, becomes the TE_{mn} mode, where n= 1,2,3.. , m= 0,1,2.. . Similarly the $LSM(m)_n$ mode becomes the TM_{mn}

mode, where n= 1,2,3.. , m= 1,2.. and in accordance with an dobservation made earlier, m=0 is not allowed for the TM case.

In fact, by considering the case of perfectly symmetrical finned waveguide, the vanishing of the matrices $\underline{\underline{Y}}_{12}$ and $\underline{\underline{Y}}_{21}$ implies that equation (3.6.9) in the aperture formulation gives solutions for TE modes only. Whilst, in the dual case of the obstacle formulation, the vanishing of the matrices $\underline{\underline{Z}}_{12}$ and $\underline{\underline{Z}}_{21}$ in equation (3.7.16) gives rise to solution for TM modes only. Thus under conditions of symmetry pure TE and TM modes will exist in a finned waveguide, in accordance with the boundary conditions of the edge alone [4].

4.5) Simplfied Dispersion Relation.

To complete the characterisation of finline modes, it is proposed to describe the dispersion of all modes near the cut-off point by a simple expression of the form:

$$\beta = \eta \sqrt{k_o^2 - k_c^2} \qquad (4.5.1)$$

where k_c is the cutoff wavenumber previously obtained. η is now to be determined.

It has been shown that in a lossless, reciprocal and uniform waveguide the propagation constant as a function of frequency can be expanded near cut-off as an odd series of $\sqrt{k_o^2 - k_c^2}$,[5]. In its simplest form this expansion is just (4.5.1) where η is a constant.

In order to determine η consider the limit $k_o^2 \longrightarrow 0$. At this point, the problem again becomes quasi-static, and since all finline modes are cut off in this limit, η can be determined from the decay coefficient, γ_o, and the cut-off wavenumber, k_c :

$$n = \frac{\gamma_o}{k_c} \qquad (4.5.2)$$

Before solving for γ_o, closer examination of the Green's admittance yields some useful simplifications which greatly ease correlating the γ_o with their respective k_c. As $k^2 \longrightarrow 0$ all TM admittances vanish. Furthermore from equations (AI.1) and (AI.2), defining the effective frequency variables u and w, it is observed that the air and substrate regions become indistinguishable to the remaining TE modes. Thus the effect of the dielectric is not felt and the problem becomes that of the static case in finned waveguide. If moreover the fins are centrally placed in the finline enclosure, as is usually the case for most practical finlines, then the symmetry causes the coupling operators Y_{12} and Y_{21} to vanish. The decoupled system allows solution for γ_o of the LSE(m) and LSM(m) mode families to proceed as before by exploiting knowledge of the fin gap field under quasi-static conditions.

Thus γ_o for the LSE(m) modes is given by:

$$\sum_{n=m}^{\infty} Y_{11n}(\gamma_o)\, P^2_{nm} = 0 \qquad (4.5.3)$$

and for the LSM(m) modes :

$$\sum_{n=m}^{\infty} Y_{22n}(\gamma_o)\, P^2_{nm} = 0 \qquad (4.5.4)$$

In fact, the assumption of a centrally placed fin does lead to discrepancies where the mode has a high order y variation. But since these modes tend to propagate much more in the air regions of the enclosure n, is sufficiently close to unity not to warrant further evaluation. Moreover for modes which experience a minimum in the E_x

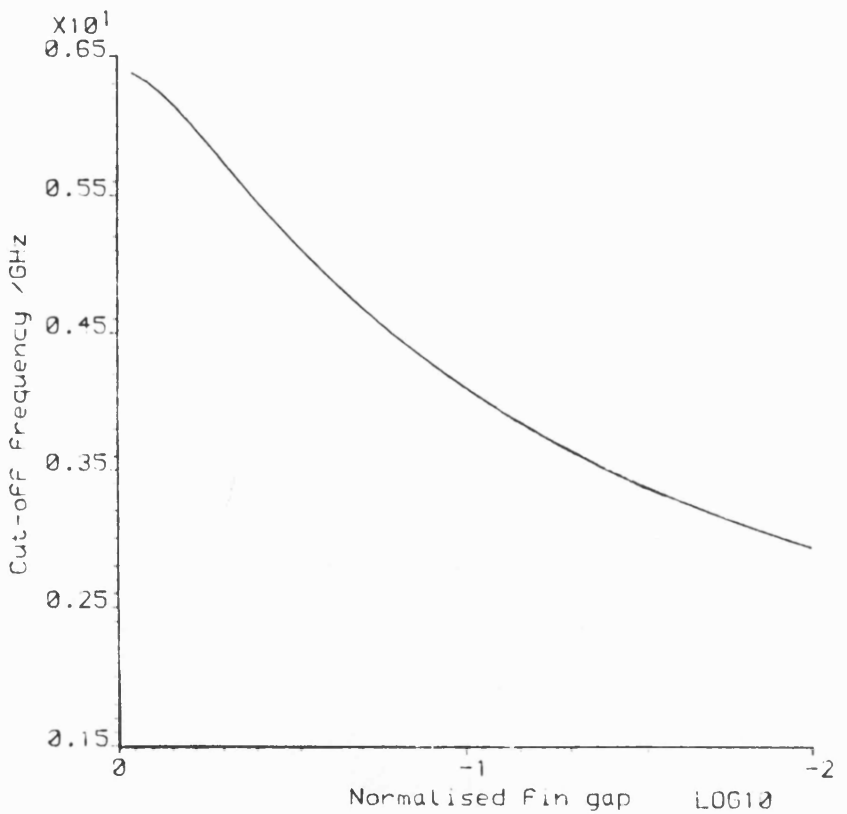

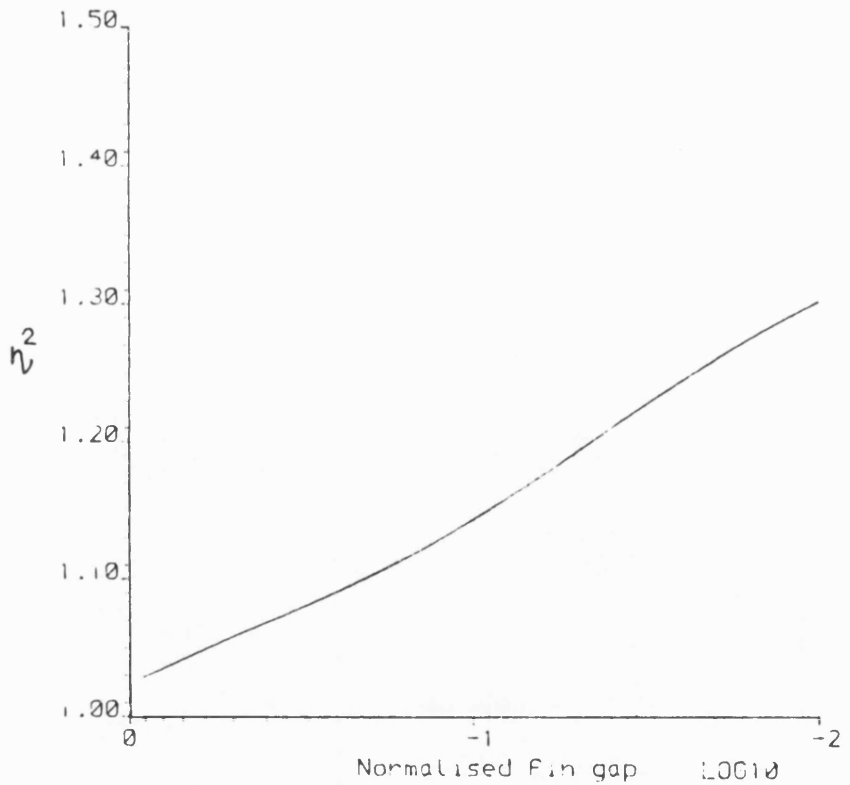

Figures (4.4.1a) and (4.4.1b) Parameters to the Dispersion Approximation for the Fundamental Mode in X-Band Finline (guide parameters as figure (4.3.1)).

field with y near to the fins, and consequently have a weak interaction, η is close to unity in any case. Thus in practice, η need only be evaluated for the fundamental and the third mode only where assuming $\eta = 1.0$ is not sufficiently accurate. Figures (4.4.1a) and (4.4.1b) show curves of η^2 and the cut-off frequency f_c for the fundamental mode. The parameter η^2 is seen to increase as the fin-gap narrows and more field is propagagtes within the vicinity of the fins i.e. within the dielectric.

Dispersion curves calculated for the first three modes give excellent agreement with results obtained using the rigorous analysis, as shown in figure (4.4.2a). Results for the dispersion of higher modes given simply by the cut-off are similarly very good as shown in figure (4.4.2b) . Table (4.1) shows a comparison between results obtained by Schunemann [6] using the Singular Integral Equation technique, the full Ritz-Galerkin solution of chapter (3), and the present approximation. It can been seen that even for higher order modes, the simple closed form approximation is within a few percent of the rigorous solutions.

These approximations near cut-off, of course, cannot be expected to describe the more hybrid behaviour of finline dispersion, but this may be possible by employing a more refined expansion, as in the original work by Rhodes ,[5]. However, it is the description of the fundamental mode dispersion which proves most useful to the circuit designer, and since this behaves in a simple manner, the one term approximation excellent for this purpose. A simplified description of the first few higher order modes may also be useful in the broadband modelling of interacting discontinuities.

As an application of the approximation to fundamental mode dispersion, consider the phase characterisation of a finline taper.

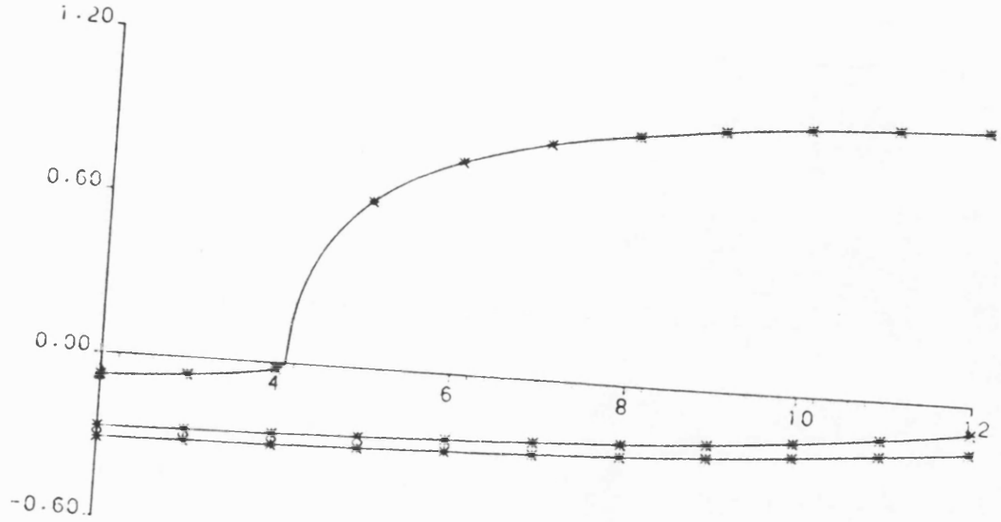

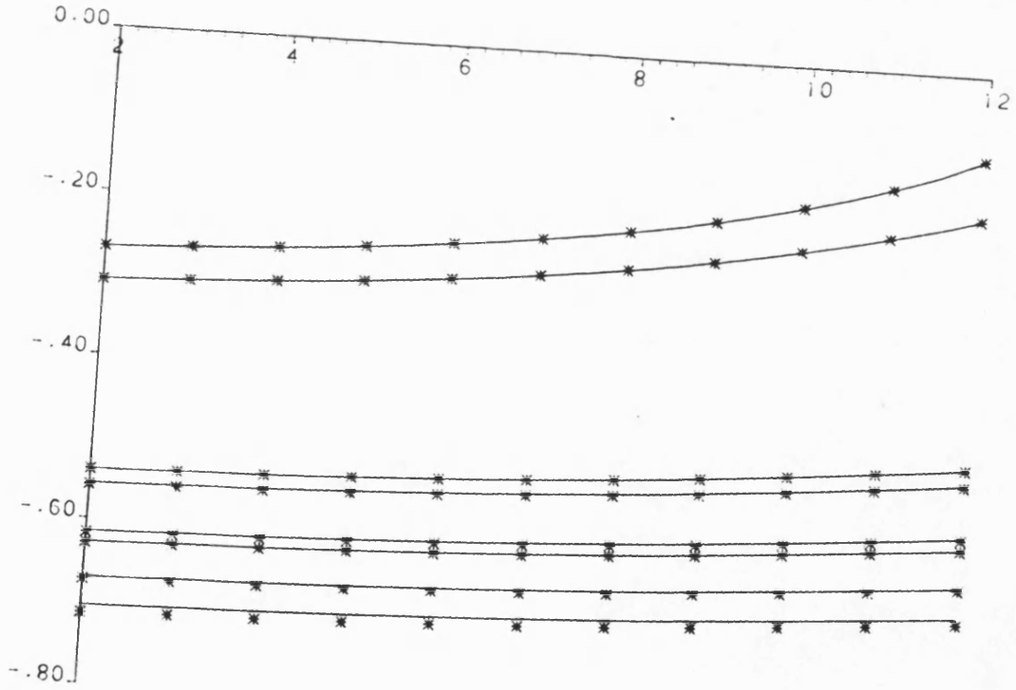

Figures (4.4.2a) and (4.4.2b) Comparison of Rigorous Spot Frequency Dispersion Points with Approximation Curves for the First Nine Modes in X-Band Finline (guide parameters as figure (4.3.1)).

Table 4.1) Comparison of fundamental

and higher order mode dispersion.

i) fin gap =0.2mm

Mode	Schunemann 9x9 matrix	Present theory 4X4 matrix	Present theory cut-off approx
1	0.6820	0.6819	0.677 (*)
2	-j 0.6067	-j 0.6065	-j 0.604
3	-j 0.7448	-j 0.7450	-j 0.739 (*)
4	-j 1.5955	-j 1.5650	-j 1.579
5	-j 1.6489	-j 1.6488	-j 1.619

ii) fin gap =1.0mm

Mode	Schunemann 9x9 matrix	Present theory 4X4 matrix	Present theory cut-off approx
1	0.5976	0.5970	0.595 (*)
2	-j 0.6154	-j 0.6153	-j 0.617
3	-j 0.8563	-j 0.8563	-j 0.854 (*)
4	-j 1.6031	-j 1.6025	-j 1.580
5	-j 1.6489	-j 1.6513	-j 1.628

iii) fin gap =3.0mm

Mode	Schunemann 9x9 matrix	Present theory 4X4 matrix	Present theory cut-off approx
1	0.4930	0.4929	0.492 (*)
2	-j 0.6207	-j 0.6207	-j 0.622
3	-j 1.1355	-j 1.1355	-j 1.134 (*)
4	-j 1.6489	-j 1.6463	-j 1.588
5	-j 1.6501	-j 1.6501	-j 1.646

(*) Full approximation. Others use $\eta = 1.0$.

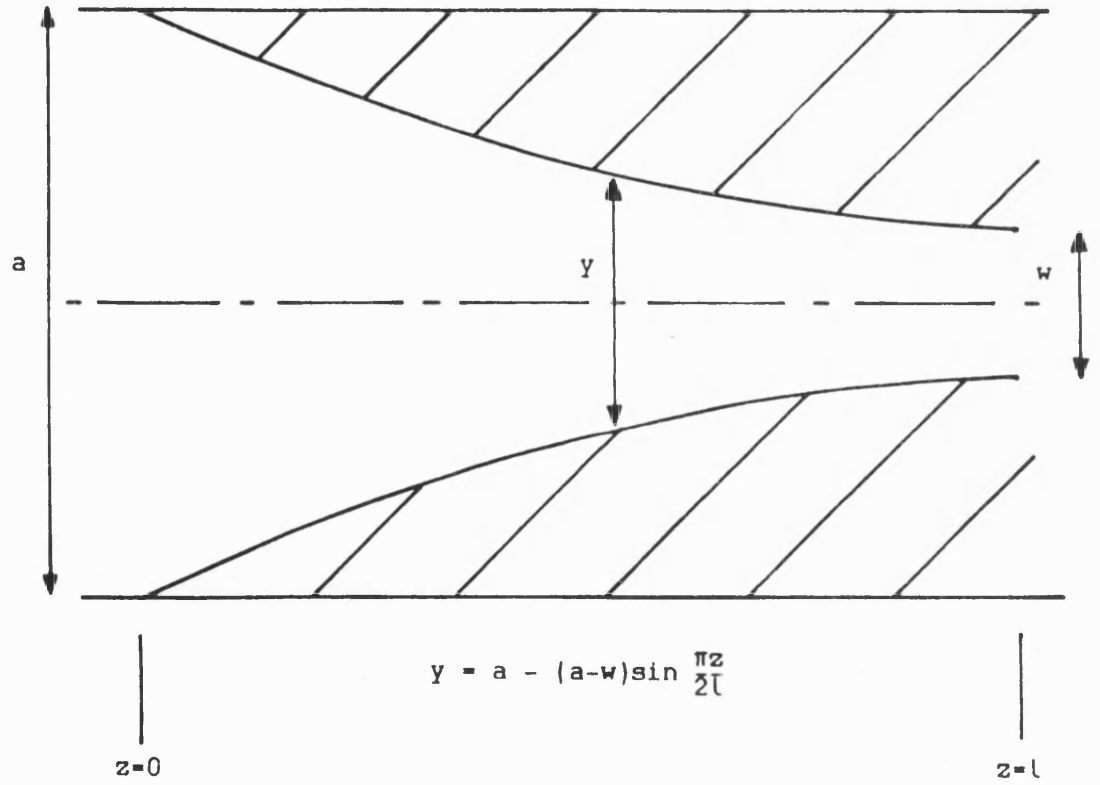

Figure (4.4.2) Details of "Cosine Taper".

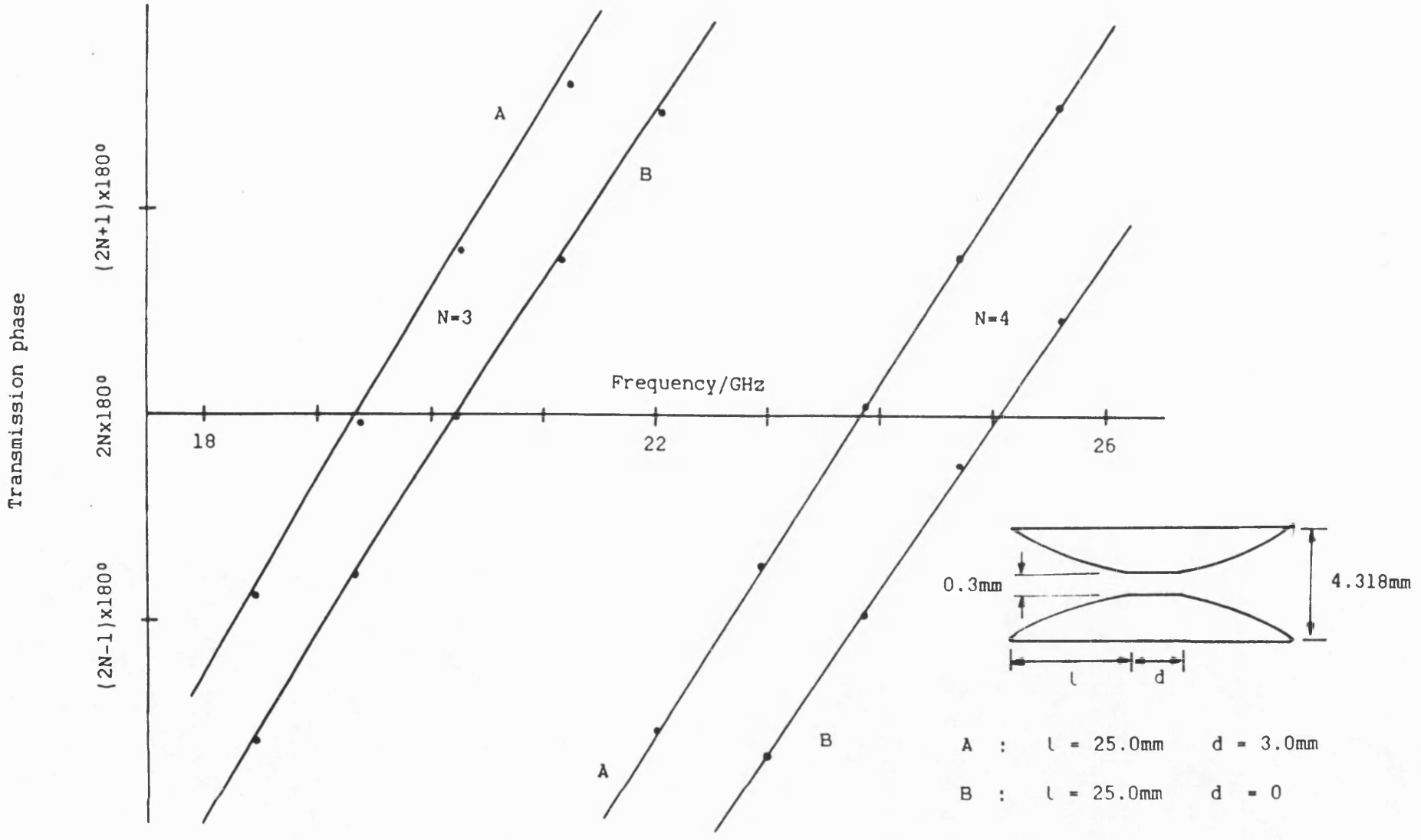

Figure (4.4.3) Comparison of Theoretical Phase Curves with Experimental Points.

Having precise knowledge of the taper profile, for instance as in figure(4.4.3), the overall phase shift produced in a propagating wave may be obtained from the summing the phase shifts encountered over a succession of short sections. To perform this calculation over a range of frequencies will require repeated calculation of the phase constant. However, from a knowledge of the taper profile and the cut-off frequencies and η over a range of fin gaps, this phase characterisation may be rapidly obtained over a range of frequencies.

Measured results of the transmitted phase through two back-to-back tapers, separated by a short uniform finline section, are compared with theoretical curves using 50 sections in the above method in figure (4.4.4). It can be seen that the agreement is again within a few percent.

References - Chapter (4)

1) Cohn, S.B.: 'Properties of ridged waveguide.' Proc IRE, 1947, pp 783-788.

2) Saad, A.M.K. and Begenmann G.,'Electrical performance of finlines of various configurations' IEE MOA, Jan 1977, vol 1 pp 81-88.

3) Omar, A.S. and Schunemann, K. , 'Space-Domain Decoupling of LSE and LSM Fields in Generalized Planar Guiding Structures.' IEEE trans, MTT-32, December 1984, pp 1626-1632.

4) Collin, R. E. and Zucker, F. J., ' Antenna Theory.' McGraw-Hill, New York, 1669, pp 18-19.

5) Rhodes, J. D. , 'General Constraints on Propagation Characteristics of Electromagnetic Waves in Uniform Inhomogeneous Waveguides.', Proc IEE, 1971, 118(7), pp 849-856

6) Omar, A.S. and Schunemann, K. , 'Formulation of the Singular Integral Equation Technique for Planar Transmission Lines.' IEEE trans MTT-33, December 1985, pp 1313-1321.

CHAPTER FIVE : FINLINE MODAL FIELDS, IMPEDANCE AND LOSS

Having developed a rigorous and numerically efficient analysis for first and higher order finline modes, attention now turns to the determination of the modal fields. Knowledge of the latter can then be used to evaluate the dissipation due the finite conductivity of housing and fin metallisation and that due to the loss tangent of the substrate. Further parameters of interest are the Finline impedance, defined in terms of the slot voltage and the total power flow, and the Q-factor, useful for the comparison with other transmission media.

5.1i) Determination of Finline Fields

From the aperture field the amplitude coefficients U_{hn} and U_{en} may be determined , then via substitution into the potentials, all six field components are obtained.

The expansion coefficients, X_m, may be obtained from equation (3.5.10); whilst Z_m are found from solution of equations (3.5.9a) and (3.5.9b) for $\underline{Z}$ giving:

$$\underline{Z} = - Yo\, E_{x0} \left[\underline{\underline{Y}}_{22} - \underline{\underline{Y}}_{21}\, \underline{\underline{Y}}_{11}^{-1}\, \underline{\underline{Y}}_{12} \right]^{-1} \underline{P}_0 \qquad (5.1.1)$$

choosing $E_{x0} = 1$, say.

The field amplitudes E_{xn} and E_{zn} follow using (3.5.6) and (3.5.7), which are repeated here using convenient vector notation as:

$$E_{xn} = \underline{P}_n^T \cdot \underline{X} \qquad (5.1.2)$$

$$E_{zn} = \underline{P}_n^T \cdot \underline{Z} \qquad (5.1.3)$$

Then solution of equations (3.2.19) and (3.2.21) for the equivalent transmission line currents and voltages:

$$I^{TM}_{nL,nR} \text{ and } V^{TE}_{nL,nR}$$

and substitution back into equations (3.2.5) and (3.2.6), gives the coefficients of the potentials as:

$$U^R_{hn} = \frac{1}{j\omega\mu} \frac{-j\beta E_{xn} + \left(\frac{n\pi}{a}\right) E_{zn}}{\sqrt{\left(\frac{n\pi}{a}\right)^2 + \beta^2}} \qquad (5.1.4)$$

$$U^R_{en} = \frac{Y^{TE}_{nR}}{j\omega\varepsilon} \frac{\left(\frac{n\pi}{a}\right) E_{xn} - j\beta E_{zn}}{\sqrt{\left(\frac{n\pi}{a}\right)^2 + \beta^2}} \qquad (5.1.5)$$

$$U^L_{hn} = \frac{1}{j\omega\mu} \frac{j\beta E_{xn} + \left(\frac{n\pi}{a}\right) E_{zn}}{\sqrt{\left(\frac{n\pi}{a}\right)^2 + \beta^2}} \qquad (5.1.6)$$

$$U^L_{en} = \frac{Y^{TE}_{nL}}{j\omega\varepsilon} \frac{\left(\frac{n\pi}{a}\right) E_{xn} + j\beta E_{zn}}{\sqrt{\left(\frac{n\pi}{a}\right)^2 + \beta^2}} \qquad (5.1.7)$$

The above coefficients are found to be purely real for all finline modes since the term $j\beta E_{zn}$ is always real. The coefficients E_{xn} are also always real. Since the fundamental finline mode is essentially TE in the slot, the ceofficients E_{zn} can sometimes be neglected altogether.

Substitution back into equations (3.1.5) and (3.1.6), together

with the appropriate y-dependence, gives the LSE and LSM potentials $\underline{\Pi}_h$ and $\underline{\Pi}_e$. The resulting spatial distributions of electric and magnetic field are found using equations (3.1.3) and (3.1.4). The resulting sets of expressions are of the form:

$$E_x(x,y) = \sum_{n=0}^{\infty} \psi_n(y)\, \phi_{hn}(x) \qquad (5.1.8)$$

$$E_y(x,y) = \sum_{n=1}^{\infty} \psi_n(y)\, \phi_{en}(x) \qquad (5.1.9)$$

$$E_z(x,y) = \sum_{n=1}^{\infty} \psi_n(y)\, \phi_{en}(x) \qquad (5.1.10)$$

whilst for the magnetic fields:

$$H_x(x,y) = \sum_{n=0}^{\infty} \psi_n(y)\, \phi_{en}(x) \qquad (5.1.11)$$

$$H_y(x,y) = \sum_{n=1}^{\infty} \psi_n(y)\, \phi_{hn}(x) \qquad (5.1.12)$$

$$H_z(x,y) = \sum_{n=1}^{\infty} \psi_n(y)\, \phi_{hn}(x) \qquad (5.1.13)$$

Where $\psi_n(y)$ describe the y-depedence of each field as defined in appendix AIII.

5.1i) Field Distributions

Using the above has enabled isometric field plots to be generated for the fundamental and higher order finline modes, providing a useful insight into many waveguide mechanisms.

Examples of the field E_x for the first few LSE(0) modes have

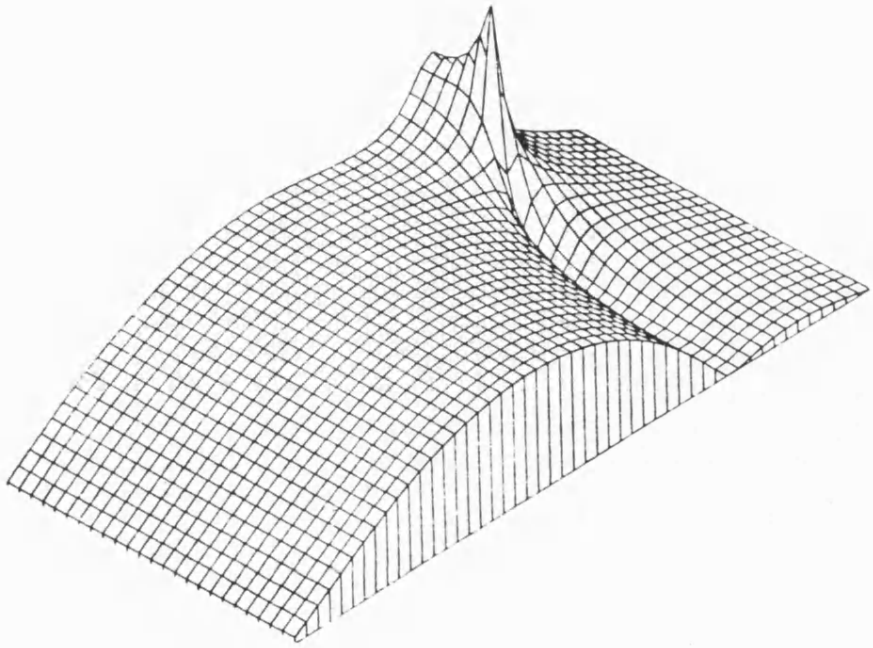

Figure (5.1.1) Ex Field for Displaced Substrate and Fin - Orientation(1) (See figures (A1a) and (A1b) for orientation keys).

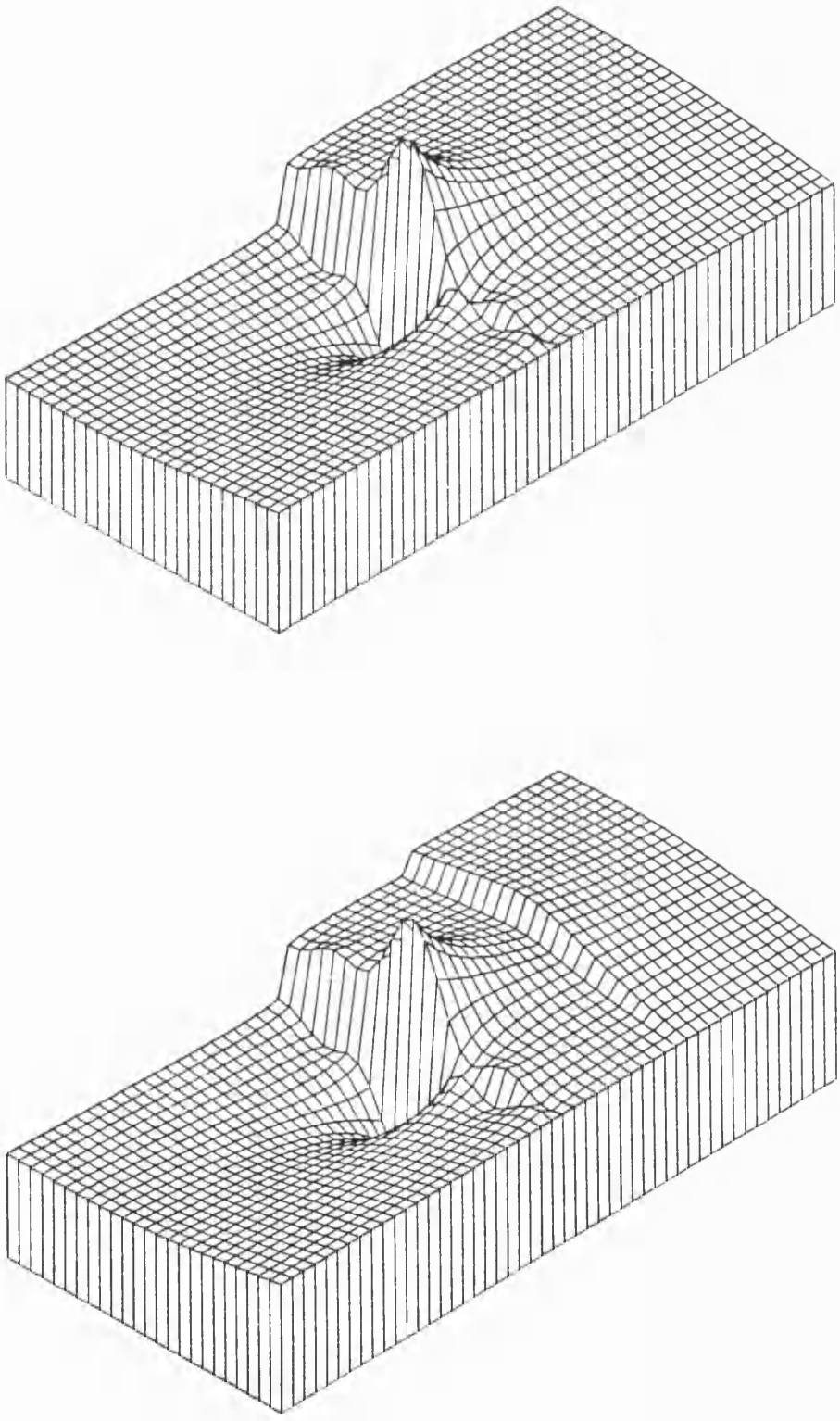

Figures (5.1.2a) and (5.1.2b) Ey Field Near Fin for εr = 1.0 and εr = 2.20 - Orientation(2).

already been given to illustrate their relative fin interaction. However, it is interesting to illustrate the effect of moving the plane of the fins away from the central position, if only to re-inforce the latter conclusions of chapter four. Figure (5.1.1) shows such a finline where the fundamental modes fin interaction is greatly reduced, and its TE_{10} character is much more in evidence.

Figures (5.1.2a) and (5.1.2b) show the electric field E_y in the vicinity of the fin-gap for the fundamental mode for two substrate permittivities. This field decays rapidly away from the fin edges as it is mainly generated by the field twisting occurring here. This expanded view also shows the discontinuity in field caused by the dielectric.

The dielectric is further seen to affect the z-directed fields. Figure (5.1.3a) shows the E_z field for a large fin-gap whilst figure (5.1.3b) shows the same field for a large fin-gap. The axis scaling has been inlcuded here to show that the amplitude of this field in the gap remains essentially constant, but the narrower gap promotes a large concentration of field on the far side of the dielectric (where there is no metallisation). It is believed that this effect represents a field twist caused by a combination of the dielectric and the fin edges. Figures (5.1.4a) and (5.1.4b) show the H_z field for both large and small fin-gaps. The fins are seen to cause a levelling of the field variation in the regions away from the fin whilst the dielectric promotes a rapid ramp of field, i.e. another field twist, adjacent to the fin-gap.

5.1ii) Wall Currents.

The field distributions can also be used to evaluate the wall currents for various finline modes.

The currents within a closed metallic waveguide fall into two

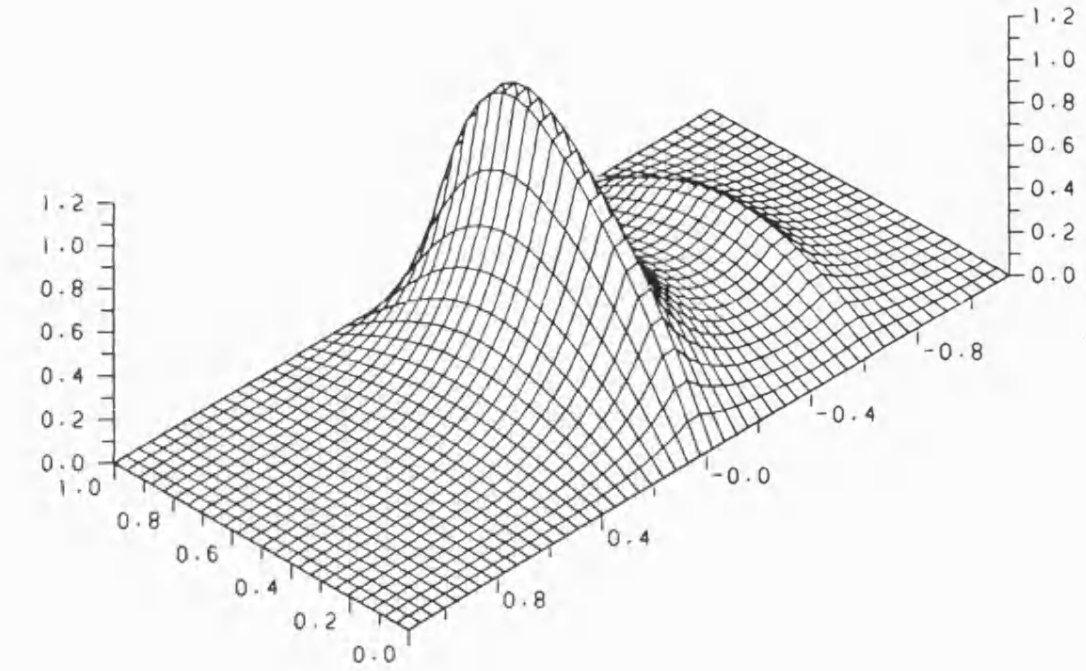

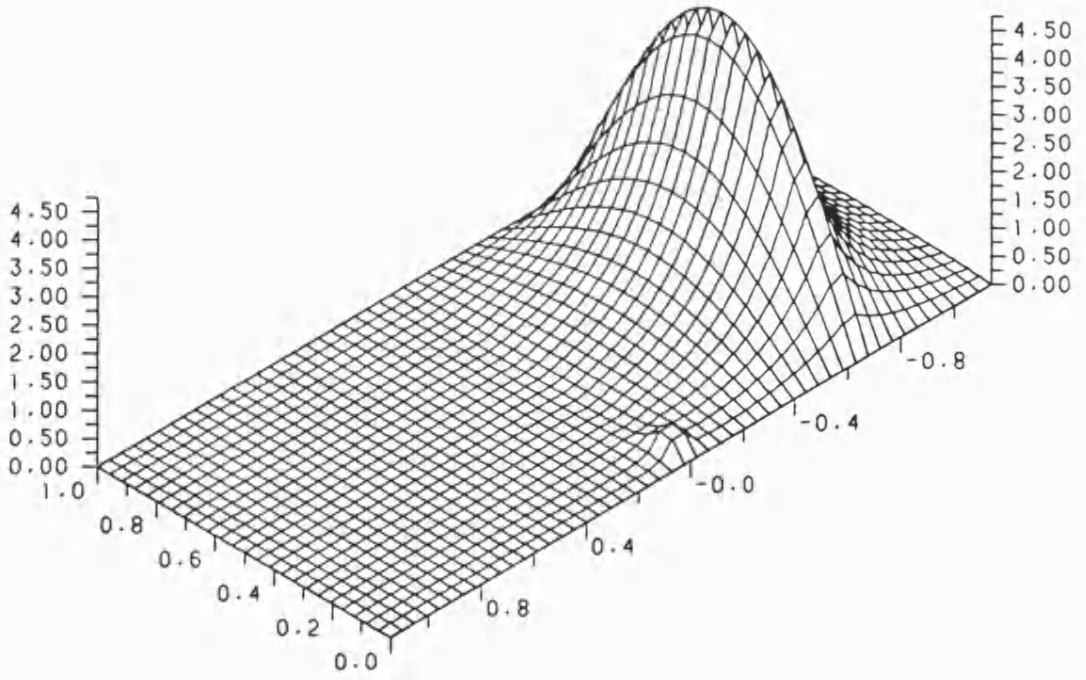

Figures (5.1.3a) and (5.1.3b) Ez Field for Large and Narrow Fin Gaps - Orientation(2).

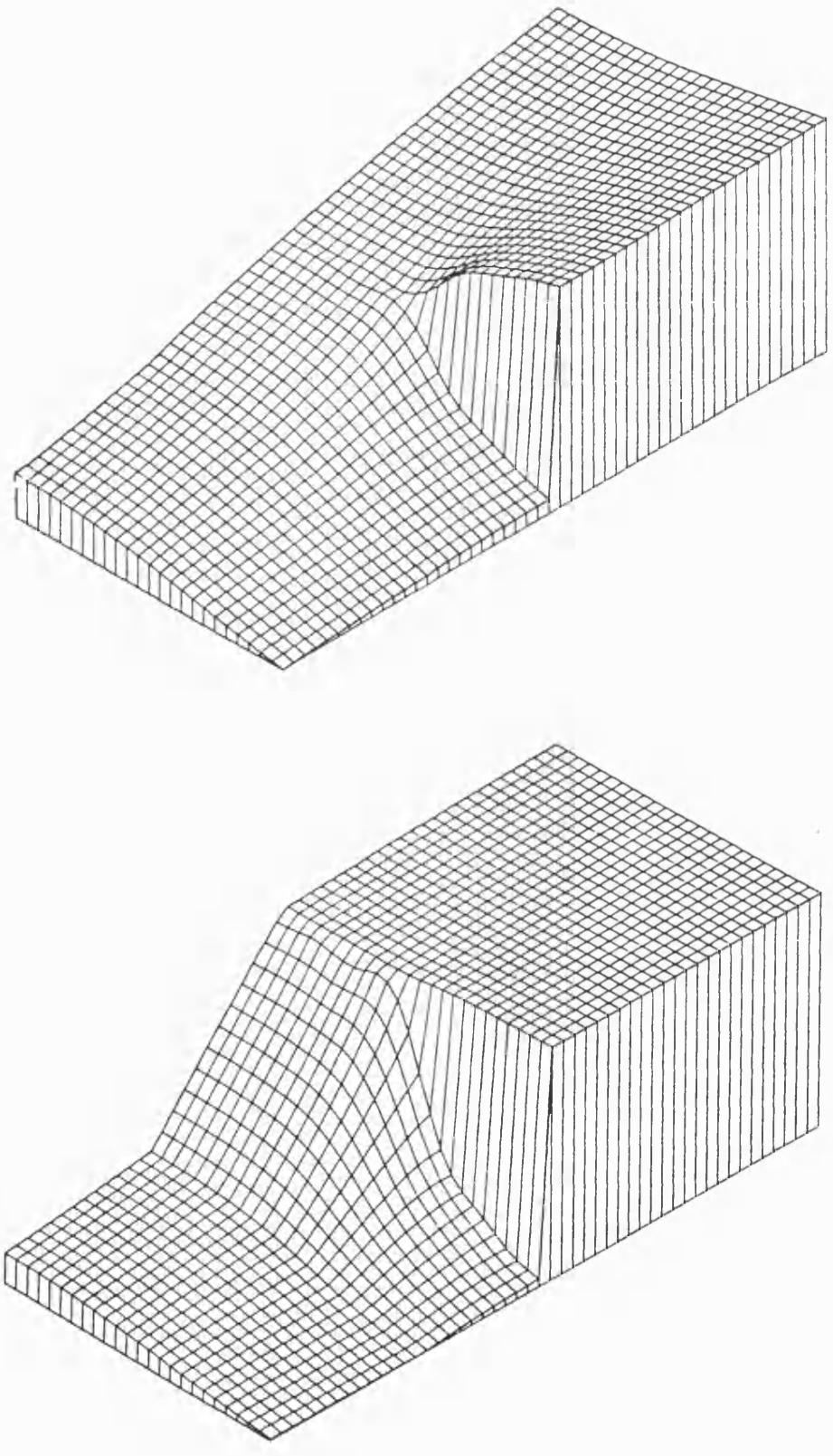

Figures (5.1.4a) and (5.1.4b) Hz Field for εr = 1.0 and εr = 2.20 - Orientation(1).

categories: the circulating currents induced by H_z at the metallic surfaces and axial currents induced by the transverse magnetic fields. In finline the former currents rise up from zero at the fin edge, divide at the intersection of the fins with the housing, and circulate around to the other fin edge, as illustrated by figure (5.1.5). For the fundamental mode the distribution of these currents show little variation around the guide apart from zeros of order $r^{0.5}$ at the fin edges. It is therefore apparent that the current node which is present in the broad wall of conventional waveguide operating in the fundamental TE_{01} mode, is displaced onto the edges of the intruding fins. This is of major practical significance, since the construction technique commonly employed with conventional waveguides utilises this node as the mating point between two machinings. This method, however, now is highly problematic when applied to finline because of the reason above and it requires in practice improved forms of choking.

The axial currents are found from H_x and H_y depending on the direction of the normal. Here the wall currents are modified in the opposite sense as shown in a schematic isometric form, figure (5.1.6). The central current maximum in the broad wall of the waveguide operating in the TE_{01} mode becomes split into two maxima with a node appearing at the intersection of the fins and the housing where x and y-directed magnetic field cannot exist. However, of more significance to the losses, is the edge condition on the fins which gives rise to a singularity of $r^{-0.5}$ in the transverse fields. It may be argued that the edge effect is weakened by the fact that the skin depth is much less than the metallisation thickness. However, there is evidence to suggest that at 10GHz where the skin depth in copper is approximately 1μm, the singularity is still in the order of $r^{-0.5}$

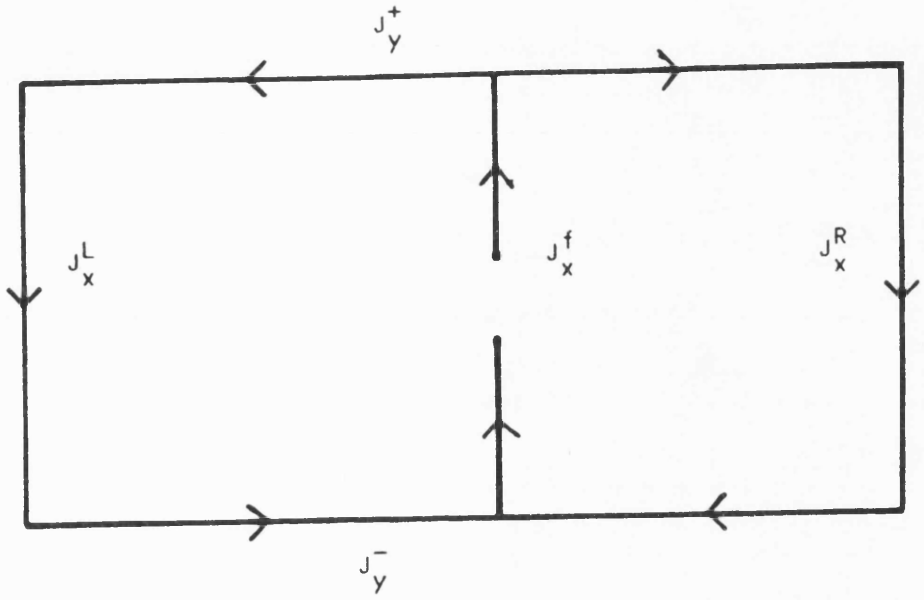

Figure (5.1.5) Schematic Diagram of Finline Circulating Currents.

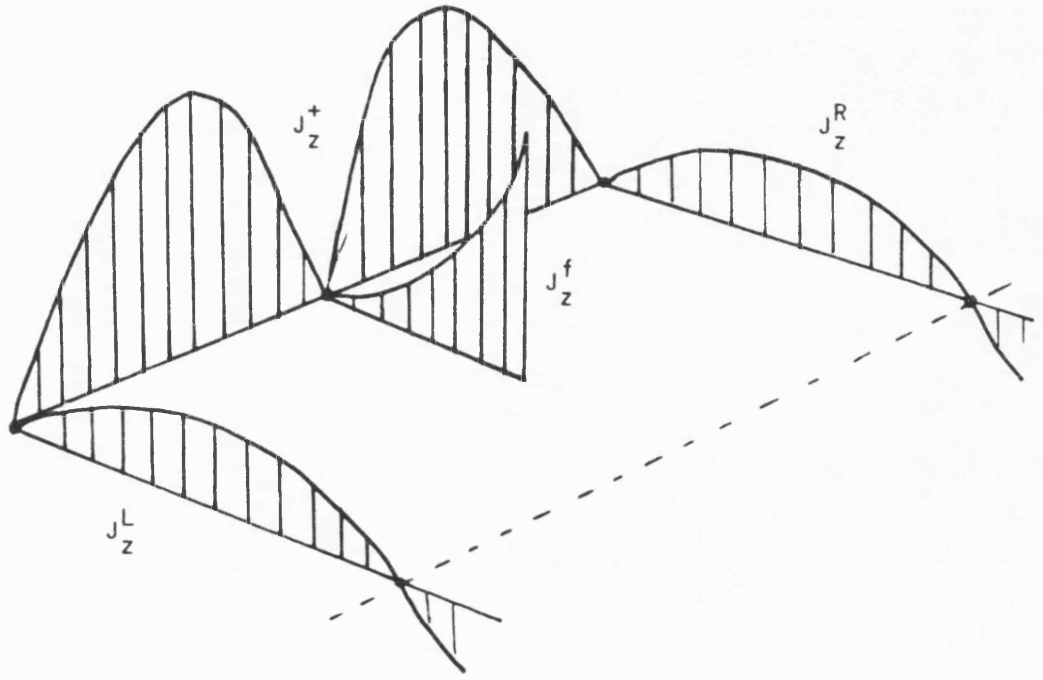

Figure (5.1.6) Schematic Isometric Diagram of Axial Currents - Orientation(2).

for a metallisation thickness of approximately 35μm (1 oz/ft^2). This will be presented shortly by comparing experimental and theoretical Q-factors.

5.2) Theory of Attenuation and Q-Factors.

Knowledge of the finline fields now allows power flow and loss calculations to be performed.

If it is assummed that the loss tangent of the dielectric region is small, and that the resistivity of the metallic surfaces is small, then fields obtained from the assumption of perfect dielectric and conductor will be very close to those in reality. A small resistivity will cause a correspondingly small tangential electric field to exist at the metal surfaces, whilst a non zero loss tangent will effectively cause small currents to flow in the dielectric. The former effect causes a fractional power flow into the metal surfaces since the normal Poynting vector is now non zero, decaying rapidly according to the skin depth. The latter effect gives rise to dissipation within the bulk of the dielectric.

5.2i) Attenuation Factors.

By assuming that the magnetic fields at the metallic walls are unperturbed by the small outward power flow, the tangential electric fields are thus expressed in terms of these magnetic fields and characteristic impedance of the metal. This is generally a complex quantity, but for loss purposes, only the real part is of interest. The real part of the Poynting vector giving the mean power flux into a metallic surface at a point, (x,y), as:

$$P_c(x,y) = \frac{1}{2} R_s H_t^2(x,y) \qquad (5.2.1)$$

where R_s is the real part of the characteristic impedance of the metal, often referred to as the surface resistance, given by:

$$R_s = \sqrt{\frac{\omega\mu}{2\sigma}} \quad ; \quad \sigma \text{ being the conductivity of the metal.}$$

It is often convenient to define the skin depth, t, from the above so that,

$$R_s = \frac{1}{\sigma t} \qquad (5.2.2)$$

and the dissipation in the metallic walls may be visualised as occurring only in a thin sheet of thickness, t, giving the effective depth to which electromagnetic field penetrates.

The total power dissipated in an infinitessimal length, Δz, is evaluated from the sum of integrals taken around all metal surfaces as:

$$W_c = \Delta z \quad \Sigma \int R_s \quad |H_t|^2 \, dl \qquad (5.2.3)$$

Dielectric loss arises from a phase lag in polarisation giving rise to a complex permittivity:

$$\varepsilon' = \varepsilon \exp(\delta) \qquad (5.2.4)$$

Inserting this into one of the Maxwell curl equations, and comparing with the case where currents are flowing gives:

$$\omega\varepsilon \sin\delta \; \underline{E} + j\omega\varepsilon \cos\delta \; \underline{E} = \underline{J} + j\,\omega\varepsilon \; \underline{E} \qquad (5.2.5)$$

If δ is small, $\cos\delta \sim 1.0$, and an equivalent conductivity of σ_e =

$\omega\varepsilon \sin\delta$ may be introduced. The mean dissipation density at a point x,y is thus obtained as:

$$\varepsilon\omega \sin\delta \quad \frac{1}{2} \quad E^2(x,y) \tag{5.2.6}$$

The total power dissipated over an infinitesimal length Δz is therefore given by the integral:

$$W_d = \frac{1}{2} \varepsilon\omega \sin\delta \iint |E|^2 \, dx \, dy \tag{5.2.7}$$

The attenuation factor, α, of a propagating mode is defined by the rate at which fields decay along the guide, the propagating power W_f therefore decays at twice this rate:

$$\frac{\partial}{\partial z} W_f = -2\alpha W_f \tag{5.2.8}$$

Thus over an infinitesimal length Δz the power dissipated may be directly equated to $2\alpha W_f \Delta z$. This will consist of the sum of conductor and dielectric losses over the distance Δz i.e.

$$2\alpha W_f = W_c + W_d \tag{5.2.9}$$

From which the overall attenuation factor can be separated into two components:

$$\alpha = \alpha_c + \alpha_d \tag{5.2.10}$$

where $\alpha_c = \frac{W_c}{2W_f}$ and $\alpha_d = \frac{W_d}{2W_f}$

The attenuation factor due to the conductor losses is thus obtained as:

$$\alpha_c = \frac{R_s \int |H_t|^2 \, dl}{2 \iint \underline{E} \times \underline{H} \cdot \hat{\underline{z}} \, dS} \qquad (5.2.11)$$

and for dielectric losses:

$$\alpha_d = \frac{\omega\varepsilon \sin\delta \int |E|^2 \, ds}{2 \iint \underline{E} \times \underline{H} \cdot \hat{\underline{z}} \, dS} \qquad (5.2.12)$$

5.2ii) Q-Factor.

A useful quantity to describe the overall loss performance of electrical and microwave circuits is the Q-factor defined by:

$$Q = \frac{2\pi \times \text{Total energy stored per unit length}}{\text{Total energy dissipated per unit length per cycle}} \qquad (5.2.13)$$

The denominator term in the above is given by the combined sum of (5.2.3) and (5.2.7), and the energy stored per unit length may be obtained from:

$$\bar{W} = \varepsilon \int |E|^2 dA \qquad (5.2.14)$$

taken over the guide cross-section.

The Q-factor is a particularly useful quantity since, provided the losses are not excessive, it may be found simply by operating the structure as a resonator and measuring the half power points at peaks in the frequency response.

If $\bar{W}$ denotes the stored energy then, $\bar{W}_d$, the energy

dissipated per cycle at the resonant frequency, ω_v, has the value:

$$\bar{W}_d = \frac{1}{\omega_v} \frac{d}{dt} \bar{W} \qquad (5.2.15)$$

therefore, $$Q = \omega_v \frac{\bar{W}}{\frac{d}{dt} \bar{W}}$$

Which gives a time response for a unit impulse of energy at time, $t = 0$, as:

$$\bar{W}(t) = \exp\left[- \frac{\omega_v}{Q} t \right] \qquad (5.2.16)$$

Thus the fields will have the form of a damped sinusoid decaying at half the rate of the energy, as:

$$f(t) = \exp(j\omega_v t) \exp\left[- \frac{\omega_v}{2Q} t \right] \qquad (5.2.17)$$

This oscillation may be considered as the envolope of a continuum of steady oscillations of frequencies $0 \leq \omega_v \leq \infty$.

Since $f(t) = 0$ for $t < 0$, the Fourier integral giving the distributions of frequency present is obtained as:

$$F(\omega) = \int_0^\infty \exp(j\omega_v t) \exp\left[- \frac{\omega_v}{2Q} t \right] \exp(j\omega t)\, dt \qquad (5.2.18)$$

which gives

$$F(\omega) = \frac{1}{2\pi} \frac{1}{\left[\frac{\omega_v}{2Q} - j(\omega_v - \omega) \right]^{1/2}} \qquad (5.2.19)$$

Taking the modulus of equation (5.2.19) gives rise to the well known resonance curve, where at frequencies $\omega = \pm \omega_v/2Q$ the response reaches $1/\sqrt{2}$ of the peak value. Thus the Q-factor at a resonant frequency, ω_v, is universally given by:

$$Q = \frac{\Delta\omega}{\omega_v} \qquad (5.2.20)$$

where $\Delta\omega$ is the frequency bandwidth between the half power points.

5.3) Evaluation of Finline Power Flow, Losses and Q-Factors.

This section considers in detail the numerical aspects of calculations required in order to generate finline loss results. Firstly the evaluation of the z directed component of the Poynting vector is considered.

This must be integrated over the waveguide cross-section. Since the finline field is defined over three regions and the z-directed Poynting vector contains components due to $E_x H_y$ and $E_y H_x$, this calculation can be subdivided into six parts.

For instance, over region (1):

$$P_{1a} = \iint E_x(x,y)\, H_y(x,y)\, dx\, dy \qquad (5.3.1)$$

$$P_{1b} = -\iint E_y(x,y)\, H_x(x,y)\, dx\, dy \qquad (5.3.2)$$

Similarly P_{2a}, P_{2b}, P_{3a}, and P_{3b} are defined over regions (2) and (3). These components are readily obtianed in an analytic form (see appendix AIV) leading to an efficient calculation of total power flow, which is given by the sum:

$$P = P_{1a} + P_{1b} + P_{2a} + P_{2b} + P_{3a} + P_{2b} \qquad (5.3.3)$$

The proportion of power propagting within the substrate region (2) may be readily obtained as:

$$Cd = \frac{P_{2a} + P_{2b}}{P} \times 100\% \qquad (5.3.4)$$

In addition, from knowledge of the power flow, the "finline impedance" may be easily obtained using the definition:

$$Z = \frac{V_s^2}{P} \qquad (5.3.5)$$

where V_s is the slot voltage obtained by integrating the field E_x over the gap region.

$$V_s = \int_{-w/2}^{w/2} E_x(x,y=0)\, dx = \frac{d}{a} E_{x0} + \sum_{n=0}^{\infty} \frac{\sqrt{2a}}{n\pi} \sin\frac{n\pi w}{a} E_{xn} \qquad (5.3.6)$$

Because all evaluations have been reduced to summations of analytic forms, computations of the finline impedance in particular can be performed very quickly on computer. Figure (5.3.1) shows a set of finline impedance curves obtianed using the above theory. These calculations are found to be in good agreement with other workers, [1] and [2]. It will, however, be shortly seen that finline loss calculations require an increased computational effort and lead to dissagreement between workers, since results are now critically dependant on the edge effect.

To proceed with conductor loss calculations, consider firstly the circulating currents on the housing. On the side walls corresponding to $x = \pm a/2$ the y directed current densities are given by:

Figure (5.3.1) Finline Impedance for Various Normalised Fin Gaps at Q-Band (a = l - (h+s) = 3.556mm, s=0.254mm).

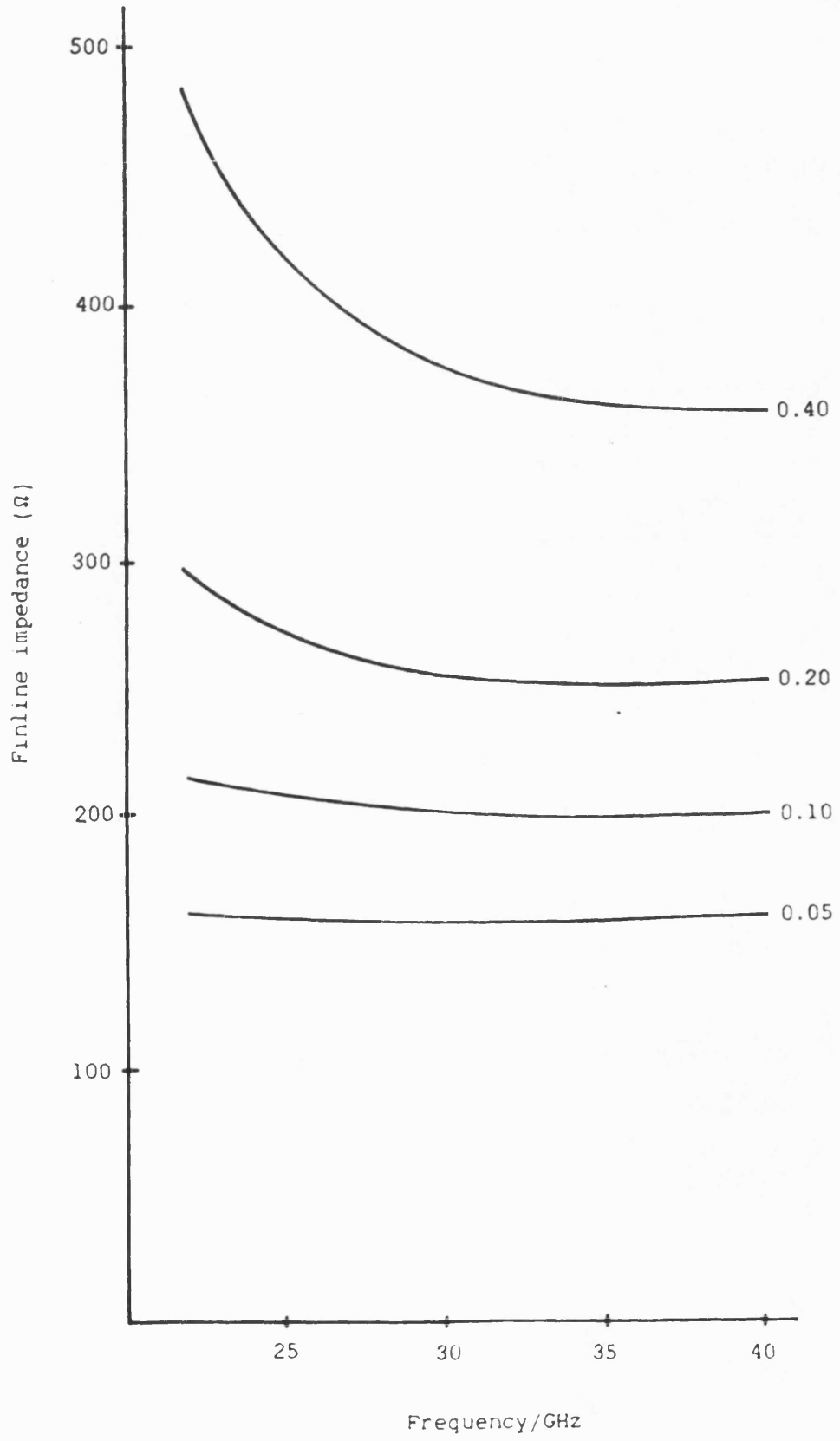

$$J_y^+(y) = H_z(x=+a/2,y) = \sum_{n=0}^{\infty} H_{zn}(y)\sqrt{\frac{\delta n}{a}}\,(-1)^n \qquad (5.3.7)$$

and

$$J_y^-(y) = H_z(x=-a/2,y) = -\sum_{n=0}^{\infty} H_{zn}(y)\sqrt{\frac{\delta n}{a}}\,(-1)^n \qquad (5.3.8)$$

where δn is the Neumann delta and the functions $H_{zn}(y)$ are obtained from appendix AIII.

On the end walls corresponding to $y = -(h+s)$ and $y = l$ the x-directed current densities are given by:

$$J_x^L(x) = H_z(x,y=-[h+s]) = \sum_{n=0}^{\infty} H_{zn}(y=-[h+s])\sqrt{\frac{\delta n}{a}}\cos\frac{n\pi x}{a} \qquad (5.3.9)$$

and

$$J_x^R(x) = -H_z(x,y=l) = -\sum_{n=0}^{\infty} H_{zn}(y=l)\sqrt{\frac{\delta n}{a}}\cos\frac{n\pi x}{a} \qquad (5.3.10)$$

Whilst on the fins, currents induced by the magnetic field H_z are given by:

$$J_x^f(x) = H_z^L(x,y=0) - H_z^R(x,y=0) = \sum_{n=0}^{\infty}\left[H_{zn}^L(y=0) - H_{zn}^R(y=0)\right]\sqrt{\frac{\delta n}{a}}\cos\frac{n\pi x}{a} \qquad (5.3.11)$$

To evaluate conduction loss, these current density functions must be squared and integrated with respect to the appropriate ordinate. For currents expressed in terms of the coordinate, x, this integration reduces to an infinite sum, due to the orthogonality of $\Phi_{hn}(x)$. This, however, does not apply to integrals over the coordinate, y. These have to be numerically evaluated. This task is

relatively easy to carry out on a computer at the expense of an increase in computational effort, further details of which are not given here.

The z-directed current flows are given as follows:-

On the housing walls given by $x = \pm a/2$ these currents are given by:

$$J_z^+(y) = H_y(x=+a/2,y) = \sum_{n=2}^{\infty} H_{yn}(y)\sqrt{\frac{2}{a}}\,(-1)^n \qquad (5.3.12)$$

and

$$J_z^-(y) = H_y(x=-a/2,y) = -\sum_{n=2}^{\infty} H_{yn}(y)\sqrt{\frac{2}{a}}\,(-1)^n \qquad (5.3.13)$$

On the end walls corresponding to $y = -(h+s)$ and $y = l$ the z-directed currents are given by:

$$J_z^L(x) = H_x(x,y=-[h+s]) = \sum_{n=2}^{\infty} H_{xn}(y=-[h+s])\sqrt{\frac{2}{a}}\sin\frac{n\pi x}{a} \qquad (5.3.14)$$

and

$$J_z^R(x) = -H_x(x,y=l) = -\sum_{n=2}^{\infty} H_{xn}(y=l)\sqrt{\frac{2}{a}}\sin\frac{n\pi x}{a} \qquad (5.3.15)$$

Whilst on the fins, currents induced by the magnetic field H_x are given by:

$$J_z^f(x) = H_x^L(x,y=0) - H_x^R(x,y=0) = \sum_{n=2}^{\infty}\left[H_{xn}^L(y=0) - H_{xn}^R(y=0)\right]\sqrt{\frac{2}{a}}\sin\frac{n\pi x}{a} \qquad (5.3.16)$$

The evaluation of the corresponding losses proceeds as outlined before, except that now caution must be exercised when considering

the z-directed fin current. Following from section (2.3) the field H_x will exhibit an integrable singularity inducing an infinite current density filament on the fin edge. If the dissipation integral applying to this particular current is not evaluated analytically to form simple sumations, severe problems can arise when employing numerical integration. Previous workers, [1], who encountered these problems, terminated the range of integration just before the edge. Others, [2], who did obtain an analytic summation result did not employ Schwinger functions and argued that the sumation in equation had to arbritarily truncated acording to a realistic concentration of field at the edge in order produce a finite result.

However, since the Schwinger functions have been derived by using a conformal mapping giving the slot fields in terms bounded parallel plate modes, the sumations here will converge. Figure (5.3.2) shows the convergence behaviour of the Schwinger functions squared, for a relatively narrow fin gap. The summation of the fundamental variation, m=0, is seen to converge after aproximatly 150 terms (this will reduce for wider gaps) and is closely related to the sumation required for conduction loss on the fins.

In order to assess the relative importance of the fin edge effects, the parameter C_f is calculated. Defined as:

$$C_f = \frac{\text{Conduction loss occurring on fins}}{\text{Total conduction loss}} \times 100\% \qquad (5.3.17)$$

The effects of edge rounding, found in practice, imply that conduction loss on the fins will be overestimated, especially at the higher millimetric frequencies, where the metallisation thickness is relatively greater. In fact, without exact knowledge of the fin profile all finline loss calcuations can become somewhat limited in absolute accuracy.

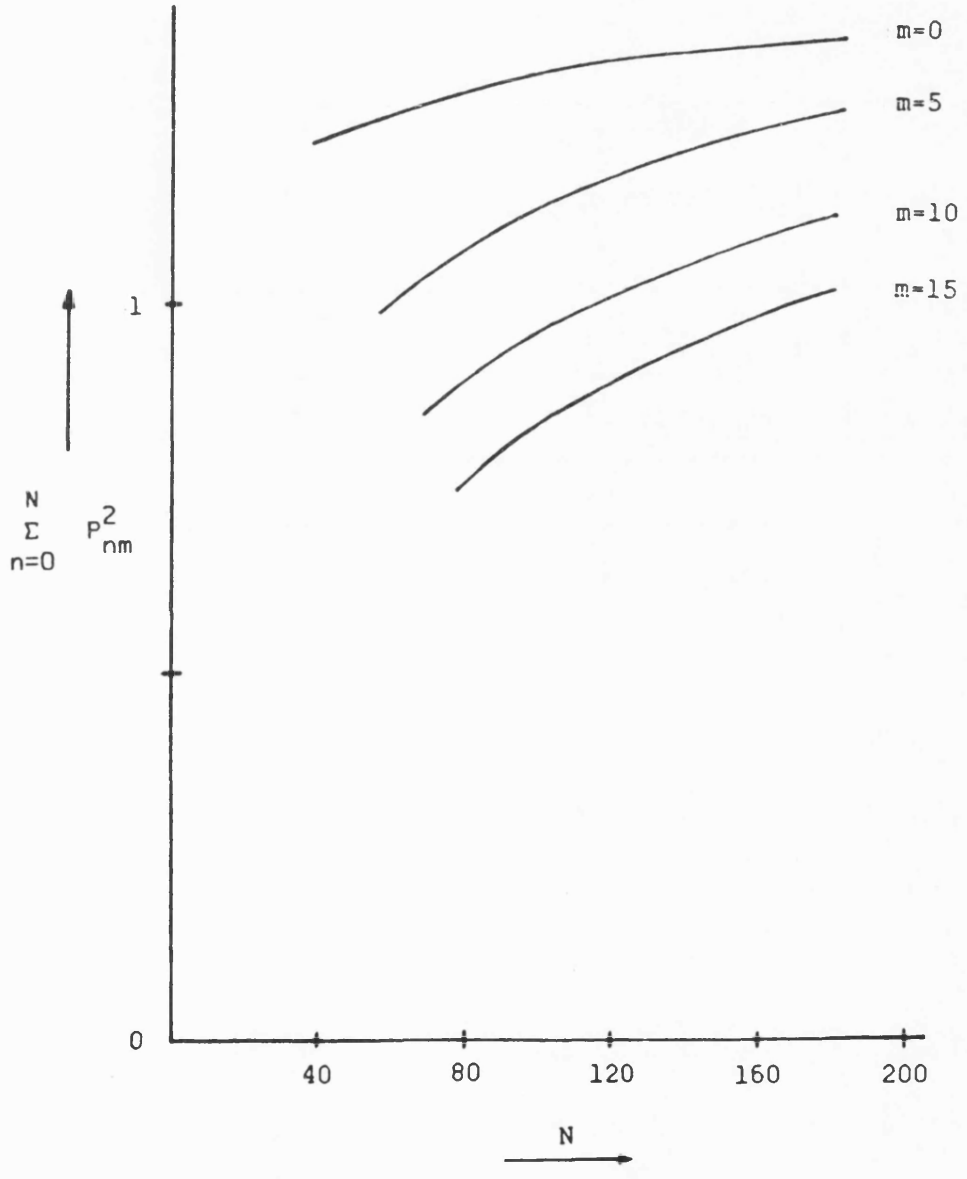

Figure (5.3.2) Convergence of Schwinger Functions Squared.

Dielectric loss calculations require evaluating the integral:

$$\int_{-a/2}^{a/2} \int_{s}^{0} |E\ (x,y)|^2\ dx\ dy \qquad (5.3.18)$$

for each of the fields E_x, E_y and E_z.
The orthogonality of the functions $\phi_{hn}(x)$ and $\phi_{en}(x)$ again resolves integration in the coordinate x to a simple summation, whilst the resulting integration in y can be performed analytically, calling on results given previously.

Finally, for the computation of transmission line Q factor , the value of total time averaged stored energy is required. The electric component of this is given by:

$$\Sigma \quad \frac{\varepsilon}{2} \iiint |E\ (x,y,z)|^2\ dV \qquad (5.3.19)$$

for each of the fields E_x, E_y and E_z.
But since the z-variation is common to all fields within the resonator section, stored energy per unit length need only be evaluated. Furthermore, since in a resonator the net stored energy is equally distributed between electric and magnetic fields, the total time averaged stored energy per unit length is given by:

$$\Sigma\ \varepsilon \int_{-a/2}^{a/2} \int_{-(h+s)}^{l} |E\ (x,y)|^2\ dx\ dy \qquad (5.3.20)$$

This again reduces to a summation of integrals in y for each of the electric field components covering the three regions (1), (2) and (3).

5.4) Finline loss results.

Calculations were performed for an X-band finline so that a comparison with experimental results can be made. The case of a Q-band finline (more commonly encountered in practice) was also analysed to enable a comparison with other workers. Losses at the higher frequency band are expected to increase as the skin depth reduces and the also as the phase lag in dielectric polarisation increases. However, there is a further change which has been found from detailed qualitative studies [3]. Namely, beyond X-band frequencies the effects of metallic surface roughness dramatically increase. This causes an increase in the effective surface resistance which is generally quantified by empirical corrections . This limits the absolute accuracy of theoretical calculations since there exists a high variance in conductor loses dependent on surface finish.

5.4i) Theoretical Results.

Figure (5.4.1) shows calculated loss per wavelength in Q-band finline with copper fins and housing, Cu-Cu, and copper fins with aluminium housing, Cu-Al, using effective conductivities of 30 μ ohm/m^2 and 65 μ ohm/m^2 for copper and aluminium respectively. During the course of evaluating the conduction loss it was possible to make a distinction between losses due to the fins and those due to

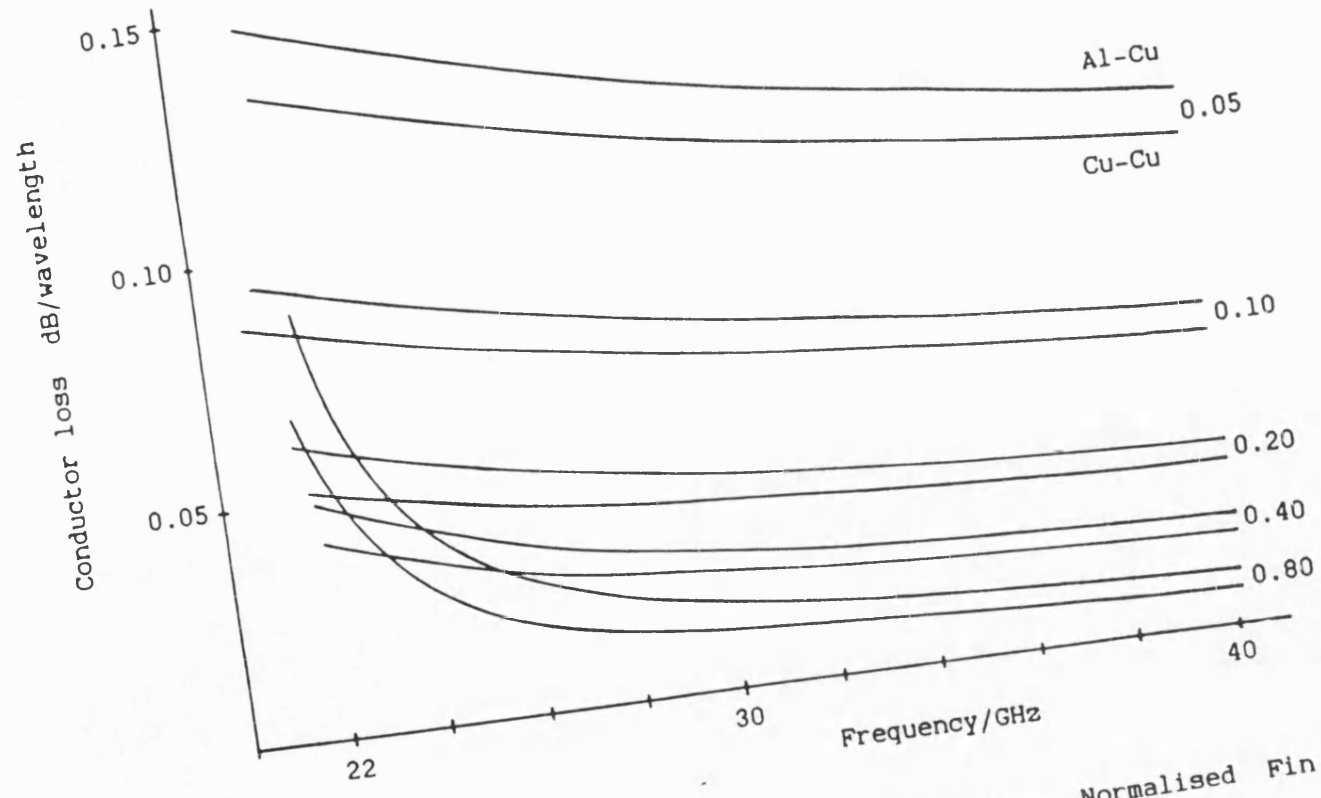

Figure (5.4.1) Theoretical Loss Curves for Various Normalised Fin Gaps and Housing-Fin metals (Guide Dimensions as figure (5.3.1)).

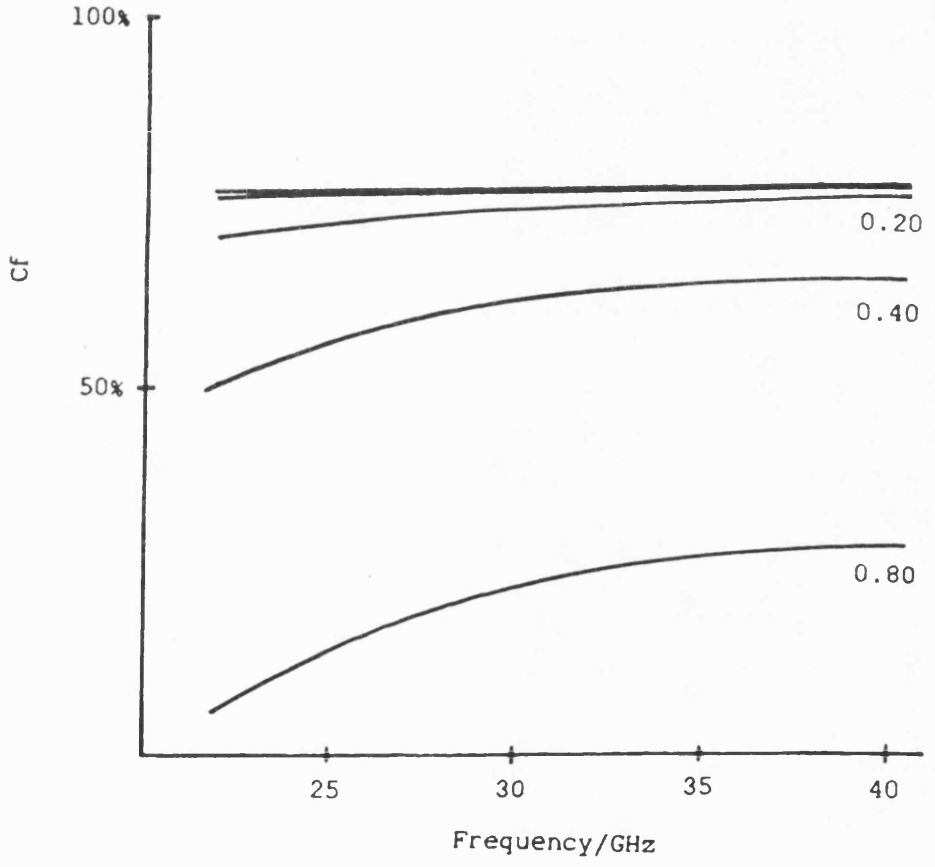

Figure (5.4.2) Curves of Cf, the Proportion of Power Dissipated on the Fins for Various Normalised Fin Gaps, Copper Housing and Fins (Guide Dimensions as figure (5.3.1)).

the housing. Figure (5.4.2) shows the proportion of power dissipated on the fins for various fin-gaps against frequency. As expected, this proportion increases rapidly as the fins intrude into the guide. However, reducing the normalised fin-gap below 0.2, i.e. within the range of fin-gaps found in practice, produces little further change. A smaller fin-gap will increasingly concentrate the fields to the gap region with increased fin currents, but in order to support these currents the housing currents must increase consequently. This effect results in a fixed ratio between the two losses. The housing material does therefore have an appreciable influence on conduction losses, those due to the singularity at the fin edges do not swamp all others.

Figure (5.4.3) shows results of calculated dielectric loss at Q-band based on a commercailly available low loss substrate material with ε_r = 2.20 and tan δ = 0.0006. These losses are clearly an order of magnitude lower than the conduction losses in finline. Figure (5.4.4) shows the proportion of power flow within the substrate. This increases very slightly with frequency and only exceeds 10% for very narrow fin-gaps.

Further calculations have been performed to investigate the effect of the substrate dielectric constant on finline characteristics. The basic effects on dispersion have been discussed previously, a reduction in cut-off frequency associated with a general reduction in guided wavelength. But the dielectric region must also exert an influence on the field configuration affecting the other finline characteristics in some manner. For these investigations an X-band finline was chosen with a normalised fin gap fixed at 0.1 and the frequency of operation set at 10GHz.

Figure (5.4.5) shows the variation of the parameters Cd and Cf

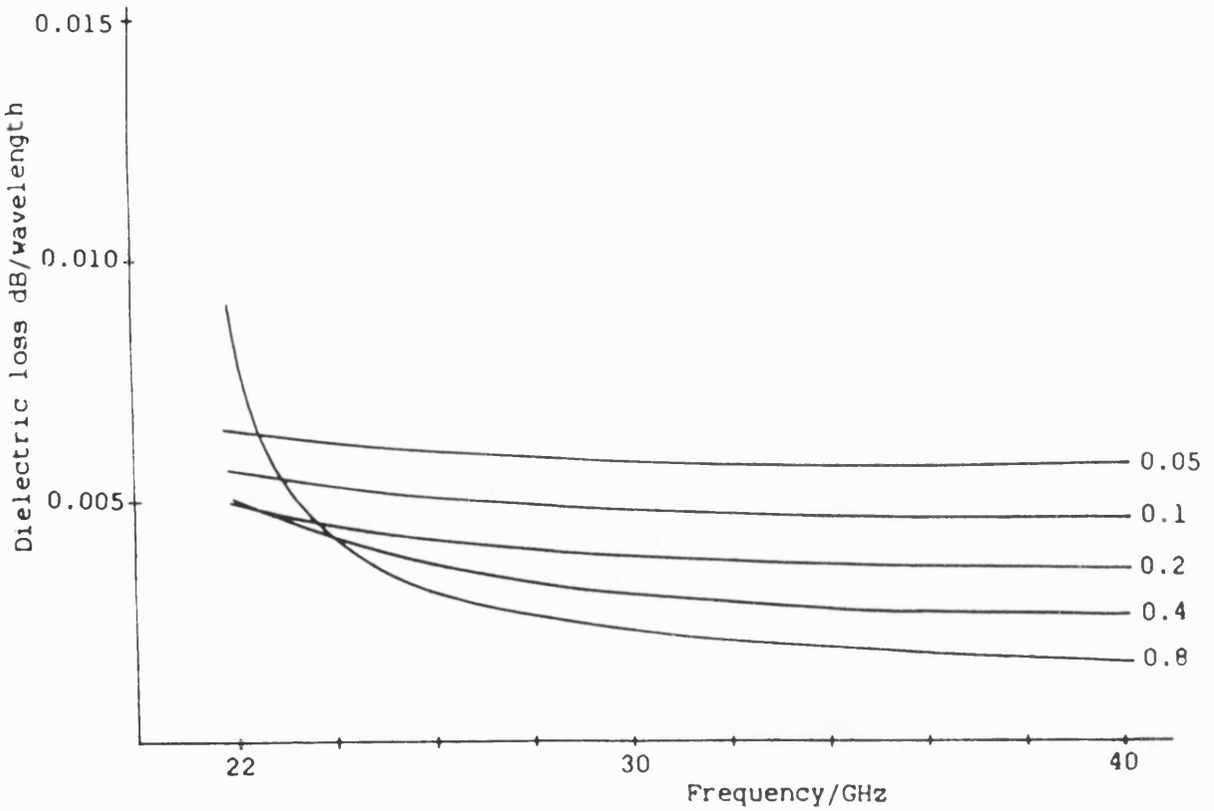

Figure (5.4.3) Theoretical Loss Curves for Various Normalised Fin Gaps (Guide Dimensions as figure (5.3.1)).

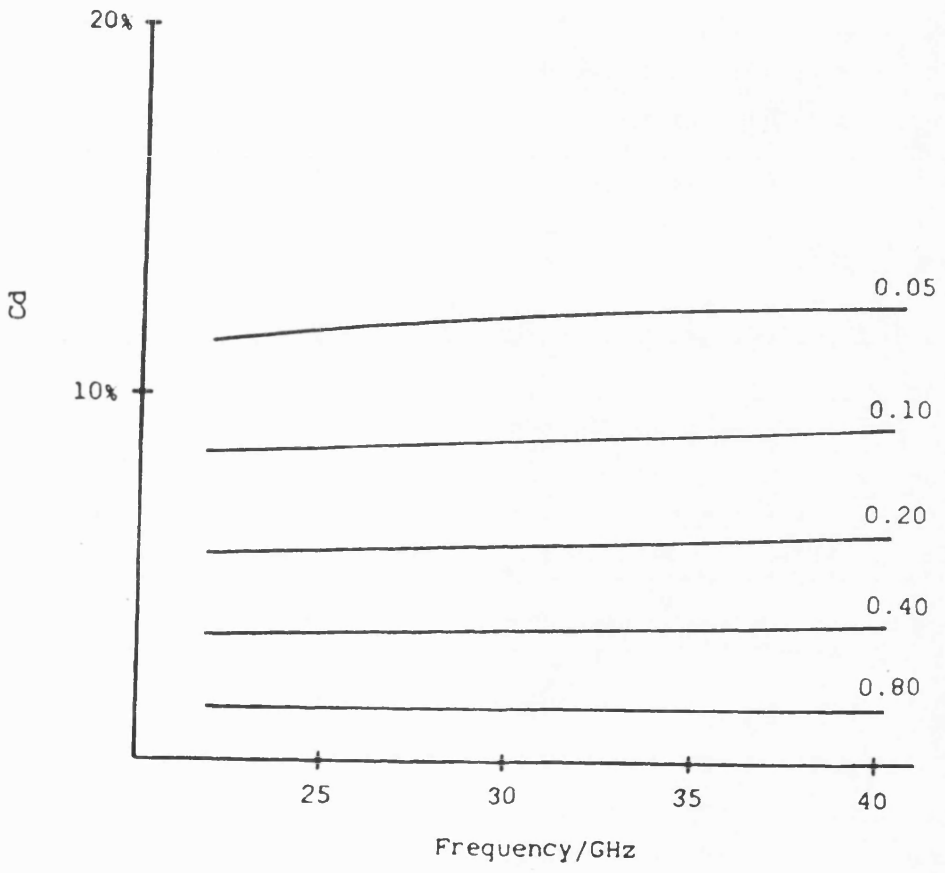

Figure (5.4.4) Curves of Cd, the Proportion of Power propagating in the Substrate for Various Normalised Fin Gaps (Guide Dimensions as figure (5.3.1)).

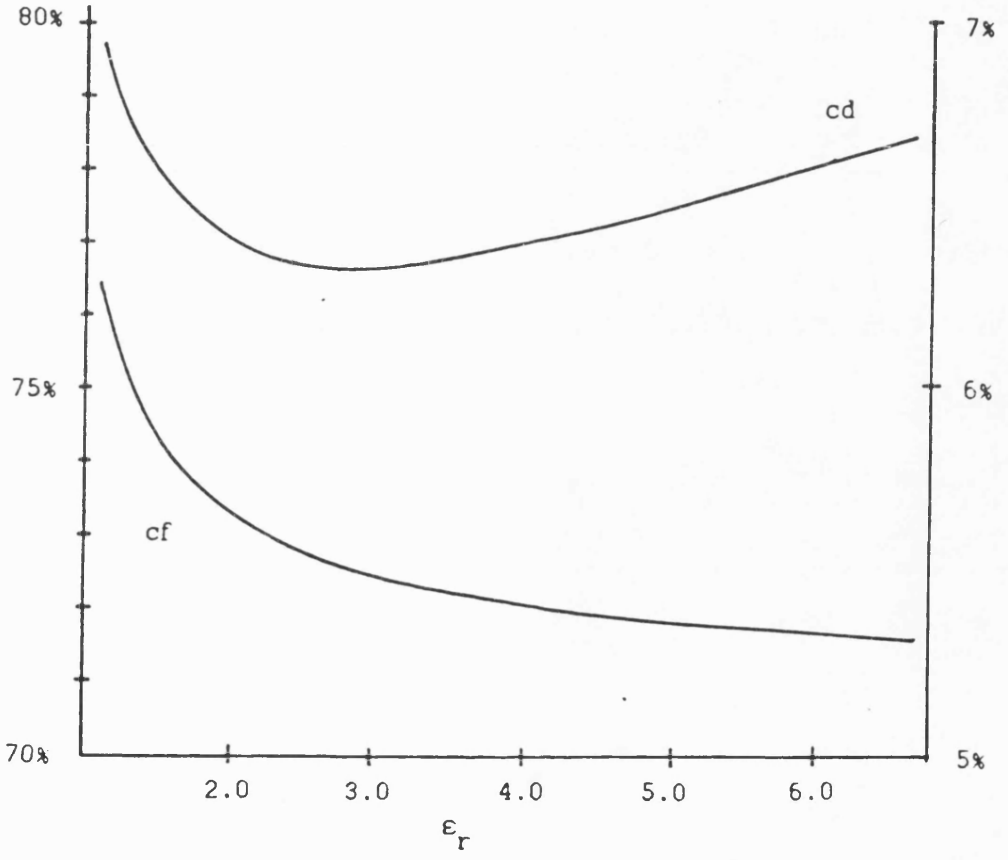

Figure (5.4.5) Variation of the Parameters Cd and Cf With Substrate Permittivity in X-Band Finline (Frequency = 10Ghz, w/a = 0.1, guide dimensions as figure (3.5.2)).

as defined in section (5.3) with the substrate relative permittivity, ε_r. It can be seen that initially an increase in ε_r reduces the proportion of power flow near to the fins, but once greater than 3.0, this proportion increases. Whilst the proportion of power dissipated on the fins reduces slightly to some asymptotic value. The variation of finline impedance with ε_r, as shown in figure (5.4.6), reaches a maximum corresponding to the minimum in Cd and then reduces as power flow concentrates in the fin gap region. These effects are all very minor but do seem to indicate a slight incompatibility between the guiding mechanisms of the fin-gap and that of the dielectric slab.

Finally, figure (5.4.7) shows the variation of finline losses with ε_r. By assuming a fixed loss tangent, the dielectric losses are seen to increase linearly with ε_r , but even remain at least an order of magnitude down on the conductor losses which increase only fractionlly as power is concentrated nearer to the fins.

5.4ii) Q-Factor Results and Experimental Verification

In order to allow a comparison with experiment, the Q-factor was calculated for the two experimental X-band finlines, since this is easily measured. The Q-factor also provides a useful quantity when applied to (evanescent) higher order modes as well as for comparison between transmission media.

Figure (5.4.8) presents results on calculated Q-factor verus frequency for the first few finline modes (normalised fin-gap = 0.227) in X-band finline. The cut-off points in the first three modes can be seen from the small peaks in the curves, although this effect seems to become less pronounced as mode order increases. Within the

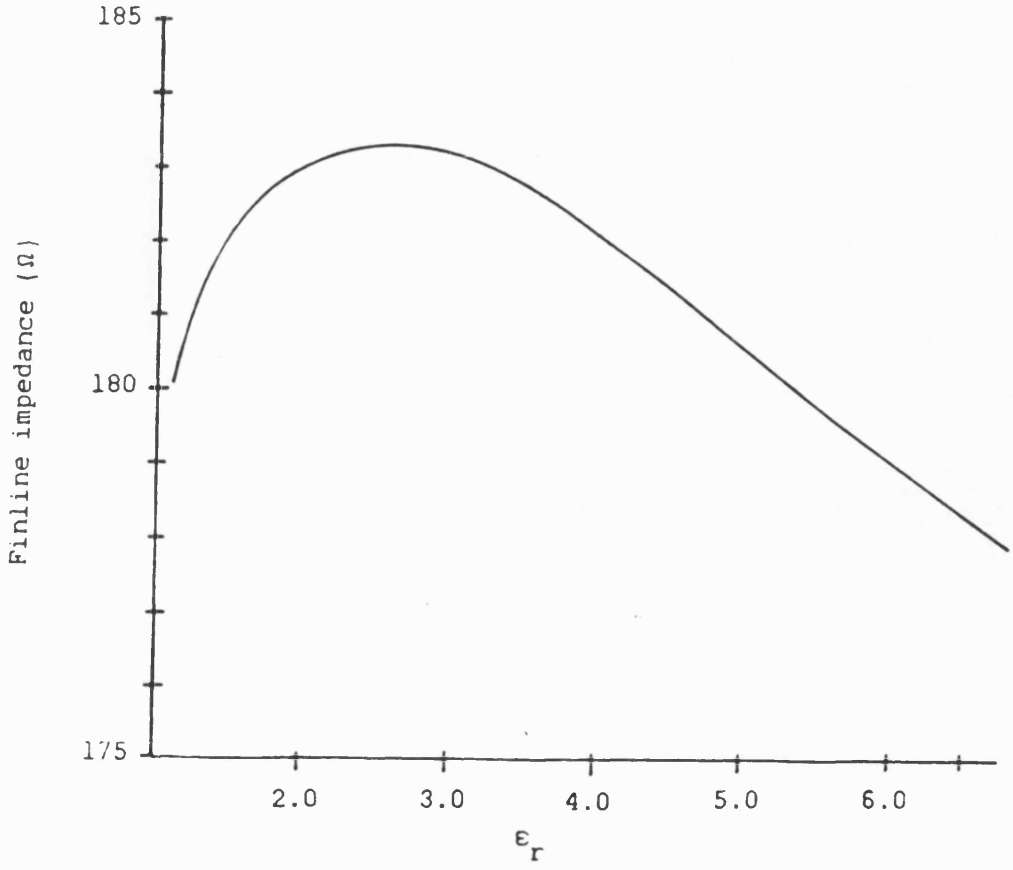

Figure (5.4.6) Variation of Finline Impedance With Substrate Permittivity in X-Band Finline (Frequency = 10Ghz, w/a = 0.1, guide dimensions as figure (3.5.2)).

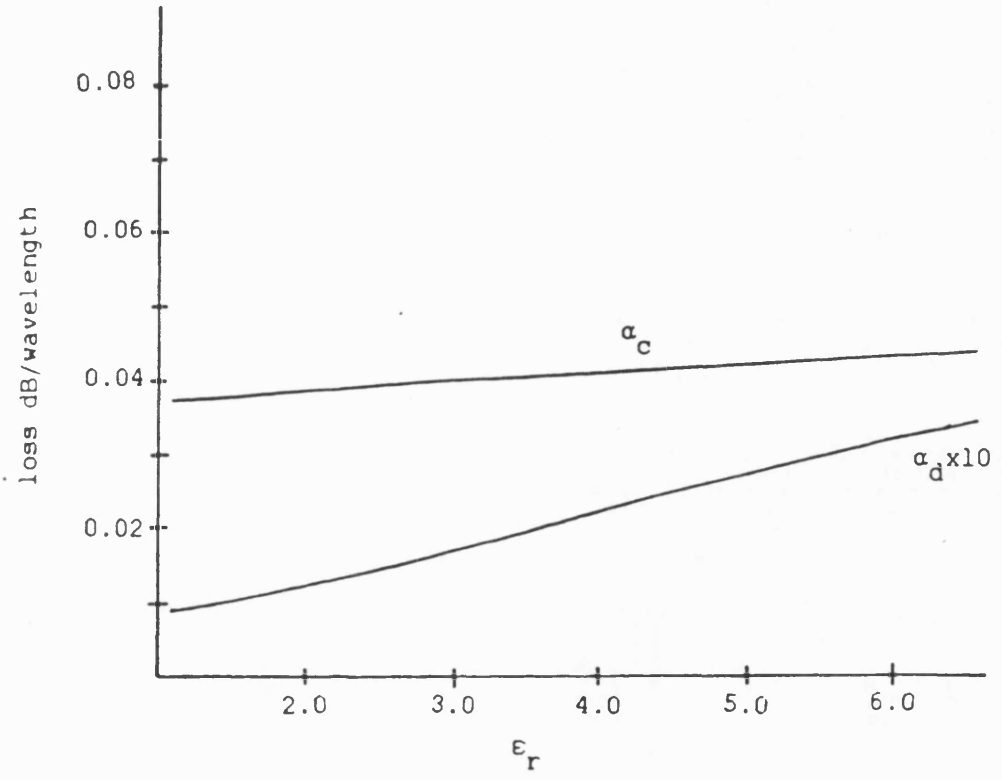

Figure (5.4.7) Variation of Finline Conductor and Dielectric Loss With Substrate Permittivity in X-Band Finline (Frequency = 10Ghz, w/a = 0.1, guide dimensions as figure (3.5.2)).

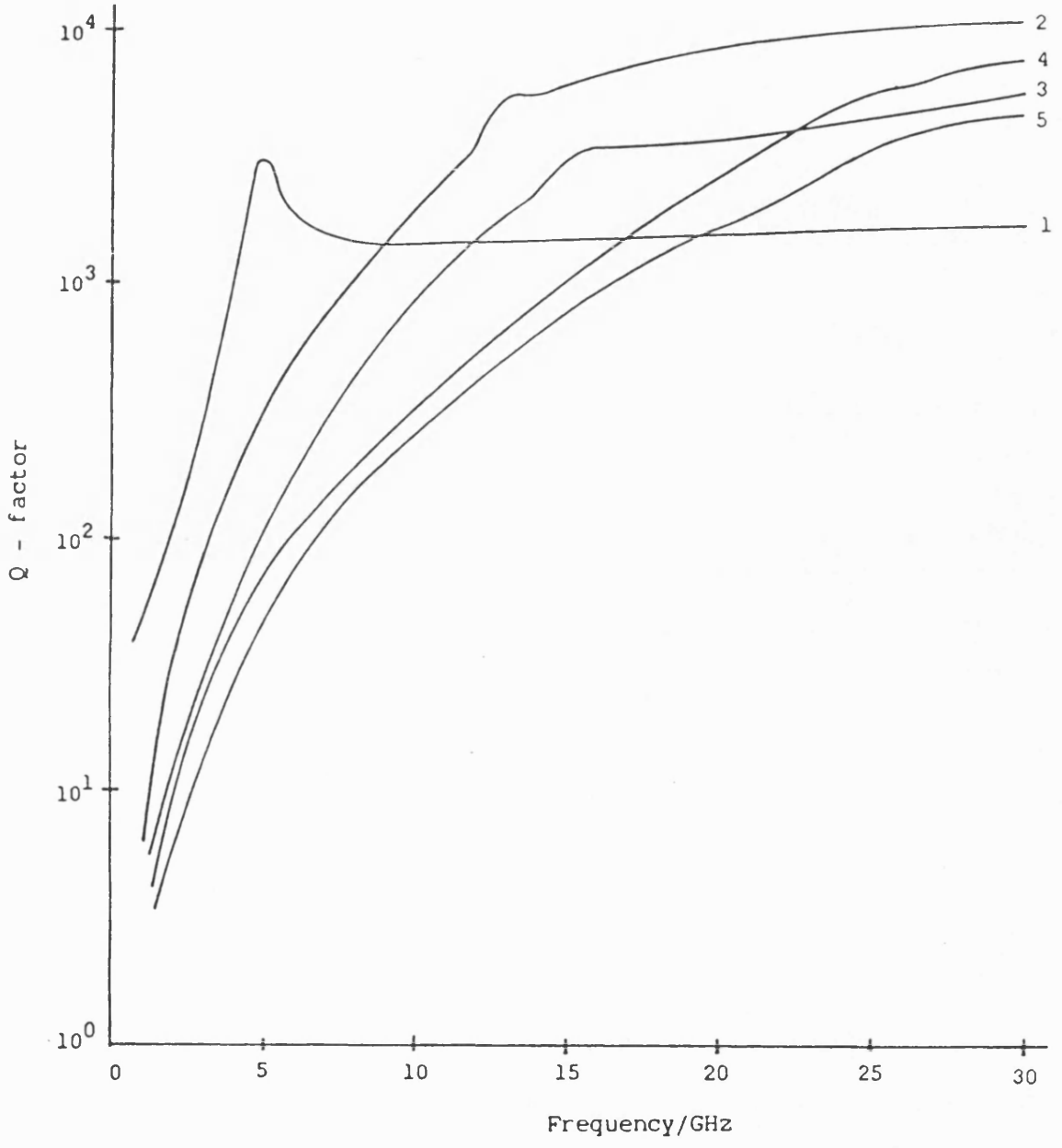

Figure (5.4.8) Q-Factors for the First Five Modes in X-Band Finline (guide dimensions as figure (3.5.2)). w = 2.31mm

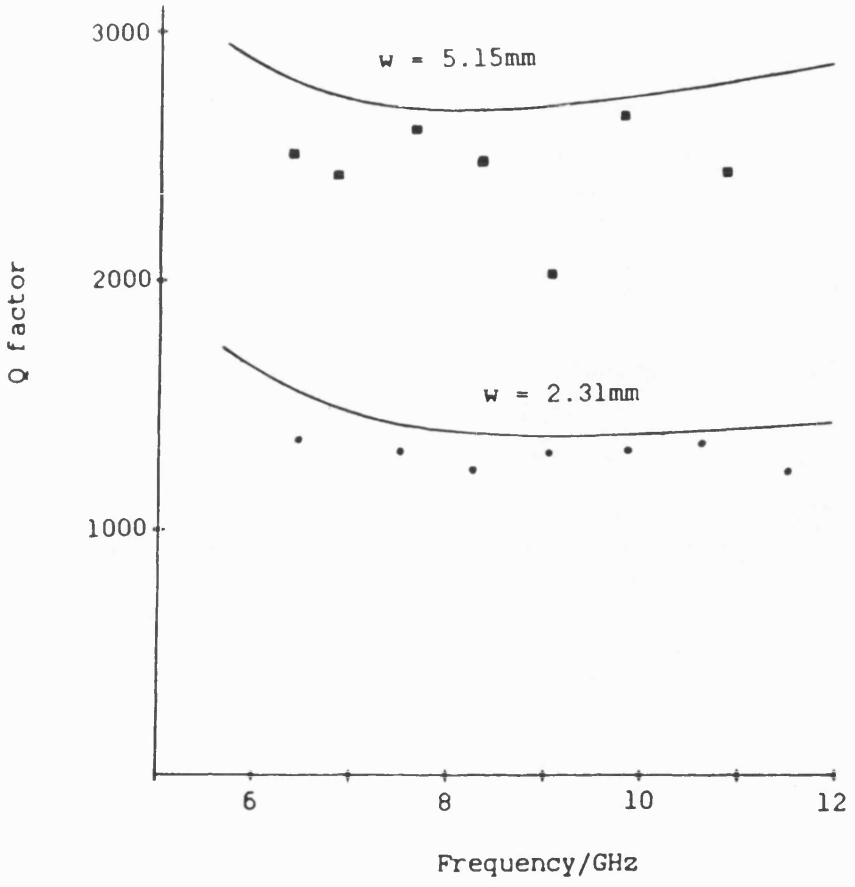

Figure (5.4.9) Theoretical Q-Factors Compared With Experimental Points (guide dimensions as figure (3.5.2)).

operating range of the fundamental mode, the higher order modes Q-factors are increasing rapidly from the very low value below cut-off. The second mode in particular has a very high Q-factor, once propagating, due to its very small interaction with the fins.

Figure (5.4.9) shows a comparison between calculated and measured Q-factor in X-band finline. It can be seen that there is a very good agreement with theory for the narrower fin gap giving a Q-factor in the order of 1000. For the wider fin gap the Q-factor is predicted to be in the order of 2500. It is apparent, therefore, that miscellaneous losses have a much greater impact. Although an improved form of choke virtually eliminated leakage along the structure, problems did still remain with the end shorts required to form the finline resonator producing the greater variance in results for the wider fin gap. However, these results do at least show finline losses to be in the order of those predicted.

References - Chapter (5)

1) Schmiidt, L. P., Itoh, T. and Hofmann, H. : 'Characteristics of Unilateral Fin-Line Structures with Arbitrarily Located Slots.' IEEE trans MTT-29, 1981, pp 352-355

2) Mirshekar-Syahkal, D. and Davies, J.B. , 'An Accuate, Unified Solution to Various Fin-line Structures of Phase Constant Characteristic Impedance and Attenuation.' IEEE trans MTT-30 Nov 1982 pp 1854-1861.

3) Benson, F.A. , 'Millimetre and Submillimetre Waves.' Iliffe Books, London, 1969, ch14.

4) Argence, E. and Kahan, T. , 'Theory of Waveguides and Cavity Resonators.' Blackie and Son , London, 1967, ch22.

CHAPTER SIX : FINLINE STEP DISCONTINUITY

6.1) Introduction and Discussion.

The step discontinuity in a waveguide system is the most fundamental building block from which filter structures and matching networks are constructed. In order to optimise designing such circuits with the help of C.A.D. synthesis, a simple yet accurate analysis of the step discontinuity is required.

The first reported treatment of the finline step discontinuity was given by Helard [1]. Having implemented the spectral domain technique to solve for the fundamental and first few higher order modes, the mode matching method of Wexler [2] was applied to the finline step. Good results for effects of the discontinuity on the fundamental mode were obtained, but because of the lack of the appropriate higher order modes, calculations for the reactance associated with the step failed to converge.

Realising the difficulties in obtaining a sufficient number of finline modes Sorrentino and Itoh [3] converted the problem into that of determining resonator eigenvalues. By performing a numerical experiment to determine three resonant lengths of a cavity structure containing the finline discontinuity, the Z matrix of the discontinuity at a particular frequency is obtained. The method is highly versatile, but does require large amounts of computing time.

Omar and Schunemann [4], applied both the modal expansion techniques of [2] and introduce the conservation of complex power approach [5] with a view to analysing large cascaded networks.

Finally, Web and Mittra [6] introduce a novel variational

approach whereby a trial magnetic current is solved via an iterative loop, however, only a few higher order modes were included within the analysis and this lead to relative convergence difficulties.

Although a number of theoretical treatments are reported above, the lack of a clear understanding of the finline mode spectrum has lead to excessive computational effort and poor convergence. The problem of obtaining higher order modes is avoided in the resonator type solution, but this still necessitates a complex and time consuming analysis. Whilst results obtained from such large computations can be included in design curves and look up tables, the scope of application is inevitably limited.

However, the finline mode spectrum is now known and higher order modes can be readily obtained. But in order to provide a numerically efficient solution, the detailed knowledge of the finline mode spectrum can be used to decide on simplifications to the problem. To this end some discussion on the physics of the problem is needed so that the dominant mechanisms of scattering can be identified.

The similarity between finline and ridge waveguide has been observed by numerous workers. Much of the field is concentrated under the ridge and very little field is outside. Because of this, a step in ridge waveguide can be compared to a step change in height within a parallel plate guide, and this may be rigorously solved from the quasi-static solution, [7], by employing the conformal mapping:

$$z = \ln t \qquad (6.1.1)$$

From the above solution, two distinct effects can be identified, namely:

i) The edge effects associated with the obtuse 90 degree bend in the waveguide walls (see figure (6.1.1)). This causes a localised

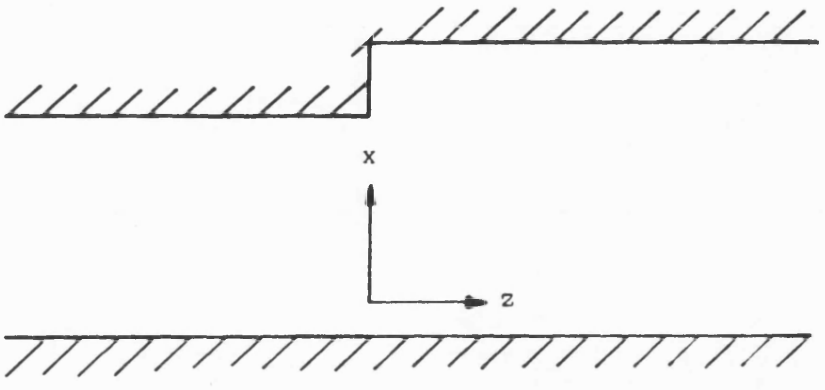

Figure (6.1.1) Step Discontinuity in Parallel Plate Waveguide.

concentration of electric fields within the x-z plane, whilst in accordance with the behaviour of wall currents here, all magnetic fields must vanish on the point.

ii) The acute 90 degree bend will essentially operate in the opposite manner, intensifying the y-directed magnetic field and causing a zero in x-z electric fields.

Now consider the limiting case of ridge waveguide and the step discontinuity in a finned waveguide. As the discontinuity is only located in the x-z plane, distortions to the y variation of fields are minimal. It is, therefore, reasonable to assume that the discontinuity essentially excites modes with y-variations similar to that of the incident wave. These include the fundamental mode of the other side of the step, and the first few members of higher order families. The concept of a mode family was introduced in chapter (4) as being identified by the same field variation in the gap (x-variation). However, since y-variations of different mode families and of different modes in the same family are different, the excitation of other modes will also occur at a secondary level. Moreover, since the ridge is now infinitely thin, an additional effect must be considered:

iii) The step in finned waveguide affects the y-z electric and magnetic fields as a current concetration builds on the metallisation edge.

The scattering mechanisms of a finline step, including the addition of a substrate layer, can therefore be seen to be highly complex and to involve all six fields. With exact knowledge of the higher order modes this problem may be reduced to a two dimensional

problem and solved rigorously by imposing the continuity of transverse magnetic and electric fields over the waveguide cross-section. However the relationship between transverse electric and magnetic fields is not straightforward, necessitating the use of dyadic impedances, especially within the dielectric region. The absence a unique wave impedance can be overcome in formulations such as [2] at the expense of computer time, which is further increased by the fact that many of the higher order modes will exhibit complex propagation constants.

However, since there is no discontinuity of the dielectric at the step, the problem can be considerably simplified by neglecting the effect of the dielectric. This simplification obviously does not allow for a fully rigorous electromagnetic solution especially if the dielectric constant is large and the dielectric region thick which are not normal conditions anyway. On the other hand, it does simplify the mode spectrum. From the previous work on the characterisation of finline modes it was observed that for purely symmetrical finned waveguide, modal solutions reduce to five field components (TE and TM in fact), and importantly also, the coupling between solutions LSE and LSM components which produce hybrid and complex propagation, vanishes. It is possible to put these effects into further perspective. Since for most practical applications the dielectric constant is in the region of 2.0 and the substrate thickness a few per cent of the guide breadth, the dielectric region in general has little effect on the finline field configuration. (Although the concentration of field in the dielectric in the gap has a significant effect on dispersion.)

6.2) Variational Formulation.

Bearing in mind the previous discussion, it is proposed to employ a Ritz-Galerkin variational formulation for the analysis of the step discontinuity in finline metallisation as given by figure (6.2.1a). The trial field expansion over the step region neglects the y dependence which is assumed common to all modes excited. This formulation readily yields an equivalent circuit for the step discontinuity as seen by the fundamental mode, and can also be used to consider the case of interaction between adjacent discontinuities as illustrated by figure (6.2.1b).

Accepting that the dielectric only plays a minor role in the finline field configuration, its main effect is on the dispersion characteristic which can be accurately described using expressions as given in section (4.4). Furthermore, if the fins are now assumed to be centrally placed in the housing, it has been shown that the LSE and LSM mode families become purely TE and TM to z. For the case of symmetrical finned waveguide operating in a TE mode, the spatial variation of the transverse fields are given by:

$$E_x(x,y) = \sum_{n=0}^{\infty} E_{xn}\, \phi_{hn}(x)\, \frac{\sinh k_n^a(l-y)}{\sinh k_n^a l} \qquad (6.2.1)$$

$$H_y(x,y) = \sum_{n=0}^{\infty} \frac{\beta}{\omega\mu}\, E_{xn}\, \phi_{hn}(x)\, \frac{\sinh k_n^a(l-y)}{\sinh k_n^a l} \qquad (6.2.2)$$

$$E_y(x,y) = \sum_{n=0}^{\infty} -\frac{n\pi}{a}\, E_{xn}\, \phi_{en}(x)\, \frac{\cosh k_n^a(l-y)}{k_n^a \sinh k_n^a l} \qquad (6.2.3)$$

$$H_x(x,y) = \sum_{n=0}^{\infty} \frac{n\pi}{a}\, \frac{\beta}{\omega\mu}\, E_{xn}\phi_{en}(x)\, \frac{\cosh k_n^a(l-y)}{k_n^a \sinh k_n^a l} \qquad (6.2.4)$$

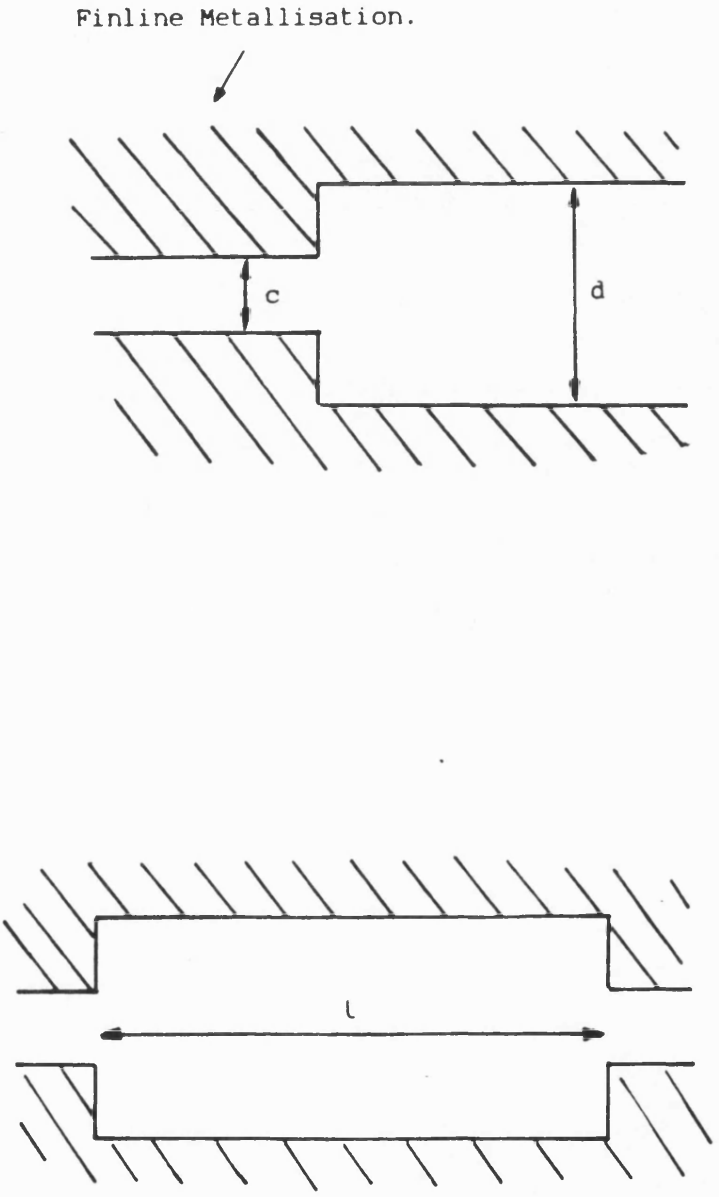

Figures (6.2.1a) and (6.2.1b) Finline Single Step and Double Step Discontinuities.

Note the occurrence of a scalar wave impedance linking Ex-Hy and Ey-Hx fields. Furthermore, by adopting modified field quantities:

$$E'_y = \int \frac{\partial}{\partial y} E_y \, dx \quad \text{and} \quad H'_x = \int \frac{\partial}{\partial y} H_x \, dx$$

all boundary conditions are rendered uniform, so that the transverse fields of a finned waveguide may be written in terms of a common set of spatial functions:

$$E_x(x,y) = \sum_{n=0}^{\infty} E_{xn} \, \sigma_n(x,y) \qquad (6.2.5)$$

$$H_y(x,y) = \frac{\beta}{\omega\mu} \sum_{n=0}^{\infty} E_{xn} \, \sigma_n(x,y) \qquad (6.2.6)$$

$$E'_y(x,y) = -\sum_{n=1}^{\infty} E_{xn} \, \sigma_n(x,y) \qquad (6.2.7)$$

$$H'_x(x,y) = \frac{\beta}{\omega\mu} \sum_{n=1}^{\infty} E_{xn} \, \sigma_n(x,y) \qquad (6.2.8)$$

where

$$\sigma_n(x,y) = \phi_{hn}(x) \, \frac{\sinh k_n^a (l-y)}{\sinh k_n^a l}$$

and $k_n^a = \sqrt{\left(\frac{n\pi}{a}\right)^2 + \beta^2}$ for a given mode of phase constant β.

Moreover, the disappearance of the n-coefficients in the infinite sums has the beneficial effect of ensuring proper convergence of the summation which are to follow.

TM modes can also be expressed in terms of the slot field Ex, but with $\beta/\omega\mu$ replaced by $\omega\varepsilon/\beta$.

Since all transverse fields are now of an identical form, a discontinuity analysis can proceed by satisfying the continuity of Ex and Hy fields using the appropriate scalar wave impedance.

Furthermore, if the discontinuity is assumed to have little effect on the y variation of fields, the trial field may be chosen so that y-integrals become trivial. i.e. the discontinuity field expansion is given by:

$$F(x,y) = \delta(0,y)\, F(x) \qquad (6.2.9)$$

where $\delta(0,y)$ is the Dirac delta function, so that:

$$\iint F(x,y)\, dx\, dy = \int F(x)\, dx \qquad (6.2.10)$$

However, despite the apparent resolution of the finline step discontinuity into a one dimensional problem involving a step change in waveguide height, the trial function F(x) must be chosen very carefully. A trial field based upon an expansion for the electric field in the smaller gap does not produce satisfactory results, whilst including the appropriate edge condition may make matters worse. The reason for the failure of this approach is that the magnetic fields behave in almost the opposite manner to that of the electric fields. In fact, within the framework of an integral equation formulation, an adequate choice of trial field for the field at the discontinuity is provided by the modal field of an intermediate fin gap close to the geometric mean.

A simple sketch of static fields shows that the discontinuity need excite only TM modes, to provide the required Ez components, with higher order variations across the fin gap. From a knowledge of the cut-off frequencies, the characteristic admittances of these modes are given by:

$$Y = \frac{j\omega\varepsilon}{\gamma} \qquad \text{where} \quad \gamma = \sqrt{k_c^2 - k_o^2} \qquad (6.2.11)$$

(The coefficient n being unity for all modes in finned waveguide.)

It is now assumed that the gap field of each mode present is given exactly by just one Schwinger function. This is found to be reasonably true for the fundamental mode, and increasingly true for the higher order modes. Although the Schwinger functions are intrinsically orthonormal, when expressed in terms of a finite expansion of the eigenfunctions $\phi_{hn}(x)$ these properties may be lost, especially for very narrow fin gaps. Therefore, one assumes their orthogonality when constructing Green's functions but it is necessary to re-normalise the slot variations producing two sets of othonormal functions as follows:

$$\varsigma_m(x) = \frac{\sum_{n=0}^{Nt} Pc_{mn}\, \phi_{hn}(x)}{uc_m} \quad , \text{ where, } \quad uc_m = \sum_{n=0}^{Nt} Pc_{mn}^2 \qquad (6.2.12)$$

where Pc_{mn} are the coefficients linking the m'th Schwinger function of slot width c to the n'th eigenfunction $\phi_{hn}(x)$,

$$\xi_m(x) = \frac{\sum_{n=0}^{Nt} Pd_{mn}\, \phi_{hn}(x)}{ud_m} \quad , \text{ where, } \quad ud_m = \sum_{n=0}^{Nt} Pd_{mn}^2 \qquad (6.2.13)$$

where Pd_{mn} are the coefficients for slot width d.

From chapter (2), the variational expressions for the elements of the equivalent T network of the discontinuity are obtained as:

$$Z_{11} = \frac{\langle F(x)\, \varsigma(x)\rangle^2}{\langle F(x)\, Y(x,x')\, F(x')\rangle} = \underline{c}^T \cdot \underline{\underline{Y}}^{-1} \cdot \underline{c} \qquad (6.2.14)$$

$$Z_{12} = Z_{21} = \frac{\langle F(x)\ \varsigma(x)\rangle\langle F(x)\ \xi(x)\rangle}{\langle F(x)\ Y(x,x')\ F(x')\rangle} = \underline{C}^T \cdot \underline{\underline{Y}}^{-1} \cdot \underline{D} \qquad (6.2.15)$$

$$Z_{22} = \frac{\langle F(x)\ \xi(x)\rangle^2}{\langle F(x)\ Y(x,x')\ F(x')\rangle} = \underline{D}^T \cdot \underline{\underline{Y}}^{-1} \cdot \underline{D} \qquad (6.2.16)$$

where $F(x)$ is the trial field over the discontinuity and the Green's admittance is given by:

$$Y(x,x') = \sum_{m=1}^{Mc} Yc_m\ \varsigma_m(x)\ \varsigma_m(x') + \sum_{m=1}^{Md} Yd_m\ \xi_m(x)\ \xi_m(x')$$

with Yc_m and Yd_m as the characteristic admittances of the m'th TM mode in guides c and d respectively.

Equations (6.2.14) to (6.2.16) also include the Ritz-Galerkin results obtained from the expansion onto a basis set. In this chapter the expansion is only taken over one basis, $F(x)$, giving scalar equations for the elements of the impedance matrix.

The T network described by the above impedance matrix is connected to a simple transmission line as in figure (6.2.2a). However, because the discontinuity is located in a transverse plane, the resulting Z matrix is singular as the discontinuity network may be represented by a pure shunt element. Figure (6.2.2b) shows this simplified representation where the single shunt element, jb , and an ideal transformer of turns ratio, r, are given by:

$$jb = \frac{1}{Z_{11}} \quad , \quad r = \frac{Z_{11}}{Z_{22}} \qquad (6.2.17)$$

The evaluation of the stationary expressions for Y and r is straightforward once an appropriate choice of $F(x)$ has been made and this function has been expressed in terms of the set $\phi_{hn}(x)$.

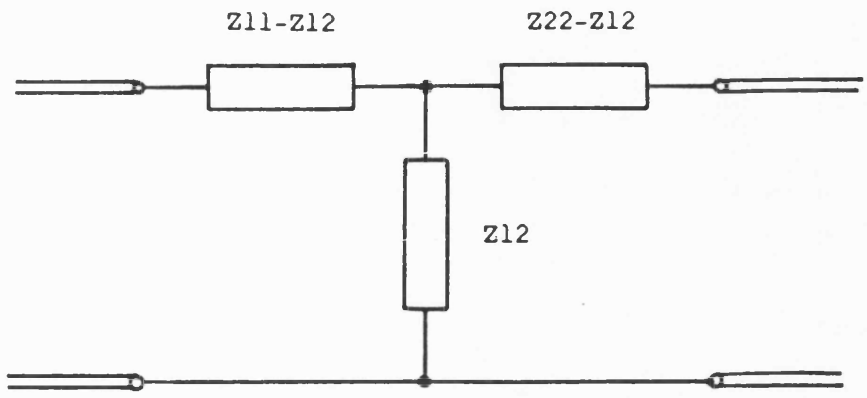

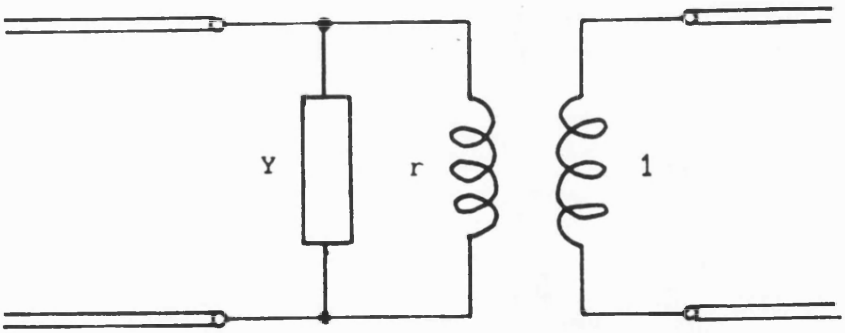

Figures (6.2.2a) and (6.2.2b) Equivalent Circuits of the Finline Single Step.

If, $F(x) = \sum_{n=0}^{\infty} Q_n \phi_{hn}(x)$, then by orthogonality:

$$\langle F(x)\, \zeta(x) \rangle = C = \frac{\sum_{n=0}^{Nt} Q_n Pc_{0n}}{uc_0} \qquad (6.2.18)$$

$$\langle F(x)\, \xi(x) \rangle = D = \frac{\sum_{n=0}^{Nt} Q_n Pd_{0n}}{ud_0} \qquad (6.2.19)$$

and

$$\langle F(x)\, Y(x,x')\, F(x') \rangle = Y =$$

$$\sum_{m=1}^{Mc} \frac{Yc_m}{(uc_m)^2} \left[\sum_{n=0}^{Nt} Q_n Pc_{mn} \right]^2 + \sum_{m=1}^{Md} \frac{Yd_m}{(ud_m)^2} \left[\sum_{n=0}^{Nt} Q_n Pd_{mn} \right]^2 \qquad (6.2.20)$$

Thus the parameters of the finline step may be quickly evaluated. Figures (6.2.3) to (6.2.5) show predictions of the return loss given by the above theory, those given by the "finline impedance" mismatch and a comparison with measured points at X-band. It can be seen that the above theory gives reasonable agreement in all cases, whilst the simple finline impedance method gives an excessive mismatch prediction especially for the most abrupt step. Furthermore, the impedance calculation requires a comparable computational effort to that of the discontinuity formulation which in addition gives values for the step reactance.

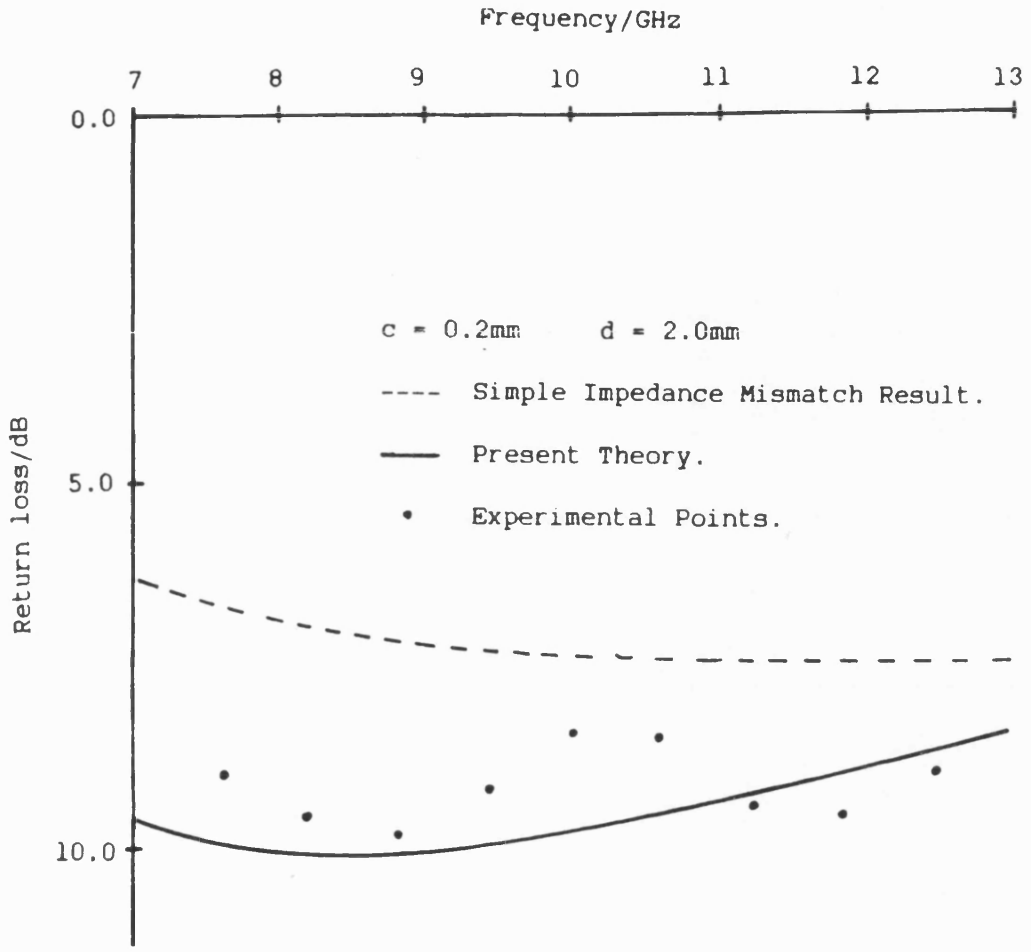

Figure (6.2.3) Comparison of Theoretical Return Loss Curves With Experiment at X-Band (εr = 2.20 , guide dimensions, a = 10.16mm, l = (h+s) = 11.43mm, s = 0.254mm).

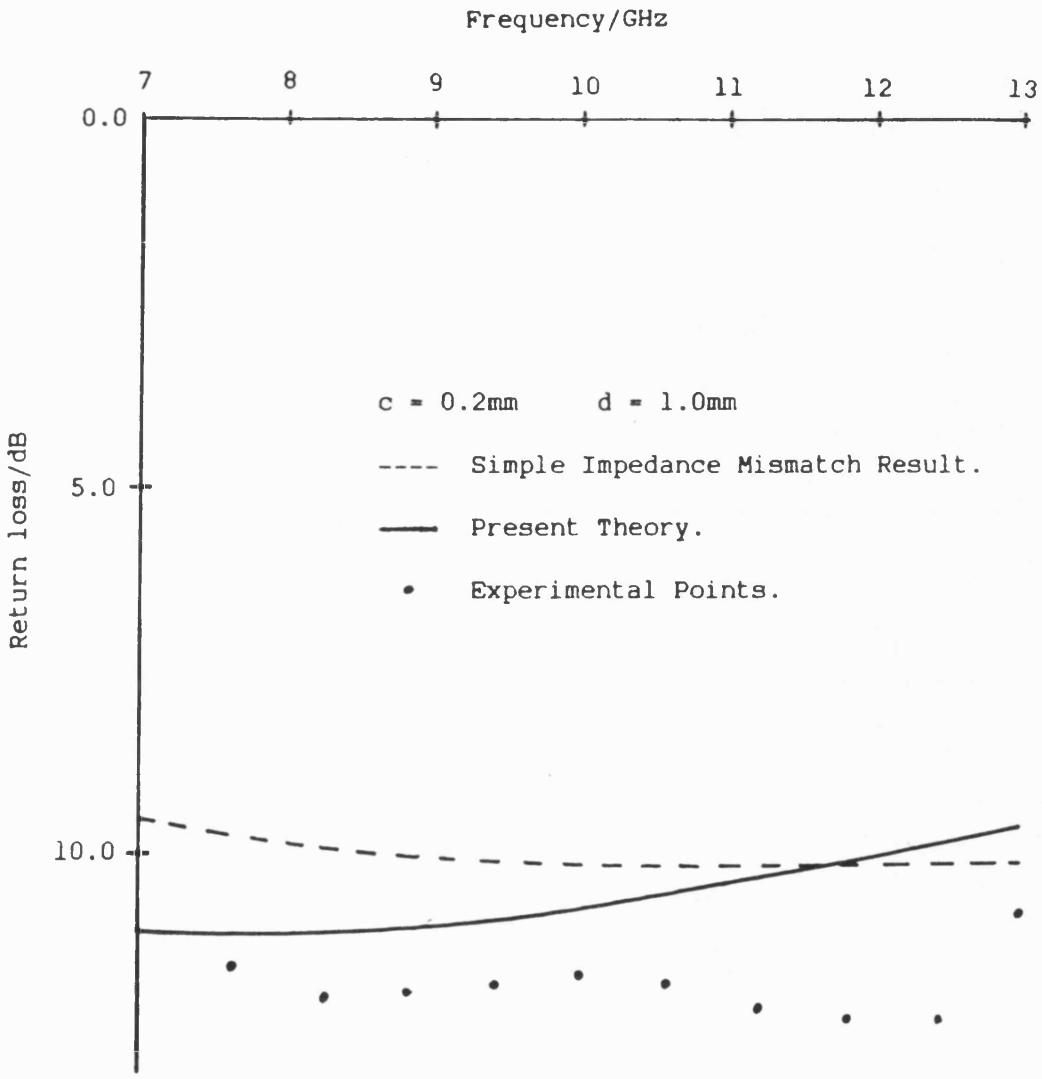

Figure (6.2.4) Comparison of Theoretical Return Loss Curves With Experiment at X-Band (other guide parameters as figure (6.2.3)).

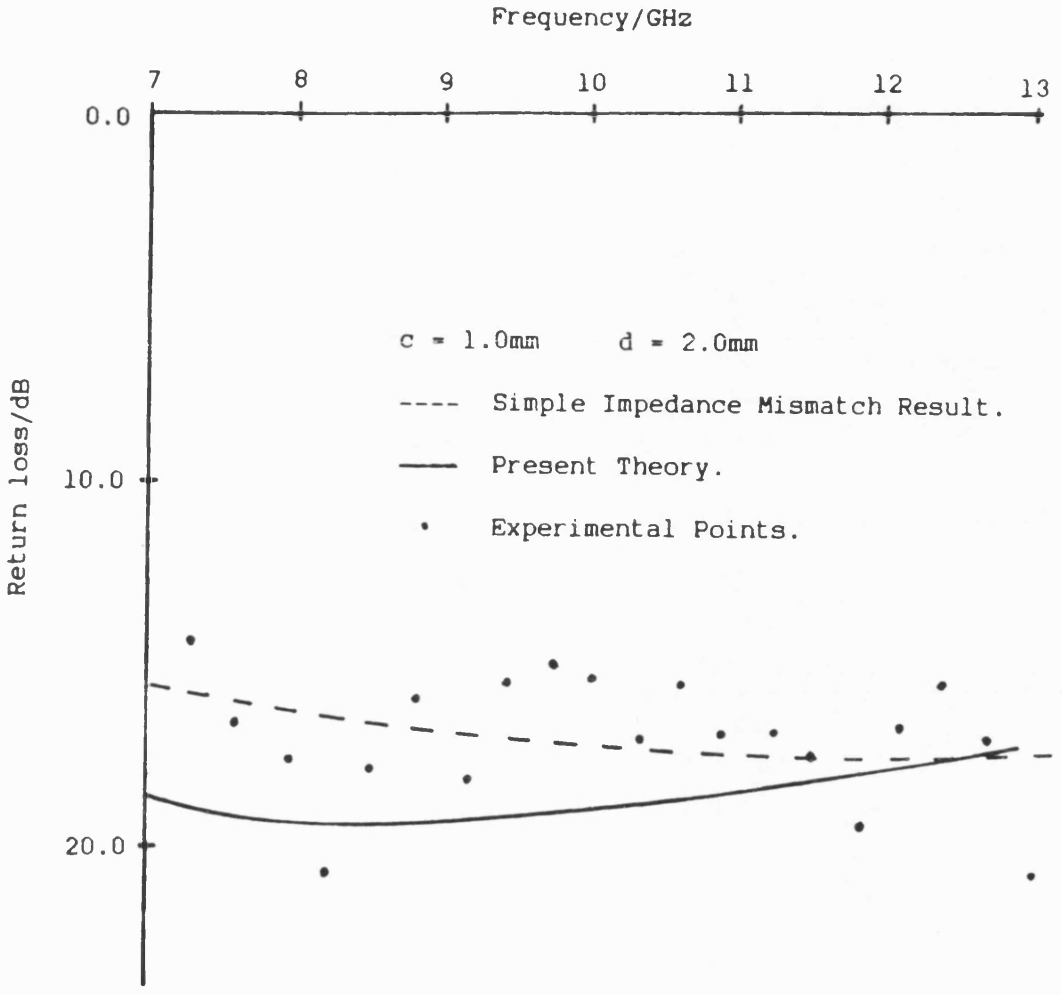

Figure (6.2.5) Comparison of Theoretical Return Loss Curves With Experiment at X-Band (other guide parameters as figure (6.2.3)).

6.3) Simple Finline Filter.

To further test the finline step analysis, a simple filter structure was considered. Two such filter were constructed, based on the slot pattern as given by figure (6.2.1b). At this stage the theory had not been extended to cope with the interacting case, and hence the distance l had to be sufficiently long to ensure higher order mode coupling did not occur. Since the smallest decay constant of the first TM mode is in the region of 0.5 Np/mm this minimum spacing was set at 10mm.

The filter network is seen to consist of a cascade of five distinct sections, which can be easily analysed using transmission matrix theory. Denoting the step transformer ratio r, the shunt susceptance, b, and the characteristic impedances of the line section and the encompassing line system by Z2 and Z1 respectively, as in the equivalent circuit of figure (6.3.1), the overall transmission matrix is obtained by evaluating:

$$\begin{bmatrix} A & B \\ C & D \end{bmatrix} =$$

$$\begin{bmatrix} 1/r & 0 \\ 0 & r \end{bmatrix} \begin{bmatrix} 1 & 0 \\ jb & 1 \end{bmatrix} \begin{bmatrix} \cos\theta & jZ2\sin\theta \\ j(1/Z2)\sin\theta & \cos\theta \end{bmatrix} \begin{bmatrix} 1 & 0 \\ jb & 1 \end{bmatrix} \begin{bmatrix} r & 0 \\ 0 & 1/r \end{bmatrix} \qquad (6.3.1)$$

where θ is the electrical length of the line section $= 2\pi\, l/\lambda_g$.

The overall two port scattering parameters are obtained from [8] as :

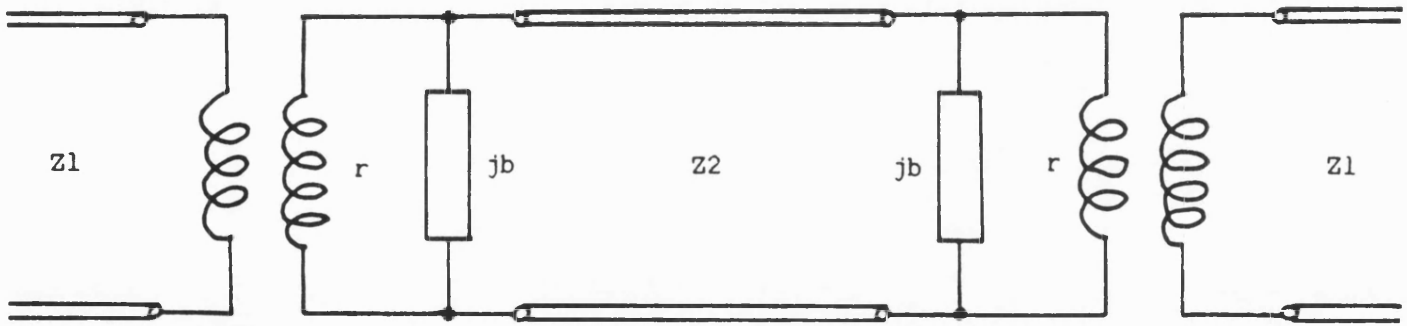

Figure (6.3.1) Equivalent Circuit of Widely Spaced Double Step.

$$s11 = \frac{A' + B' - C' - D'}{A' + B' + C' + D'} \qquad (6.3.2)$$

$$s12 = \frac{2\,(A'D' - B'C')}{A' + B' + C' + D'} \qquad (6.3.3)$$

$$s21 = \frac{2}{A' + B' + C' + D'} \qquad (6.3.4)$$

$$s22 = \frac{-A' + B' - C' + D'}{A' + B' + C' + D'} \qquad (6.3.5)$$

where for the case of identical input and output lines,

$$A' = A, \quad B' = B/Z1, \quad C' = C\,Z1, \quad D' = D$$

Theoretical plots of s11 and s12 for together with measured results for two filters are shown in figures (6.3.2) and (6.3.3). Comparison with theory shows good agreement, although frequency shift discrepancies can be observed. Results indicate that the calculated shunt reactance is of the same order as the true value. Furthermore since the step separation was large enough to prevent interaction via the TM modes, but not so large as to prevent interaction via the first higher order TE modes. For instance, at 12GHz the decay in the first higher order mode ammounts to 25dB over a distance of 30mm (the step seperation considered here). From the shape of the frequency responses obtained it can, threfore, be concluded that the first few TE finline modes are not strongly excited by the step.

The frequency shift discrepancy is believed to be mainly due to the crude construction techniques employed, giving poor definition of the fin-gap, and an unsatisfatory choking arrangment. Bearing in mind

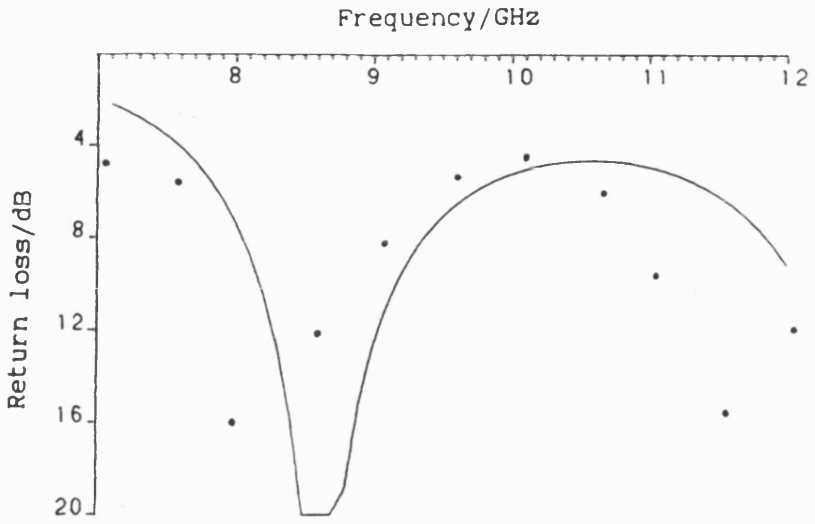

c = 1.5mm d = 10.0mm ℓ = 30.0mm

• Experimental Points.

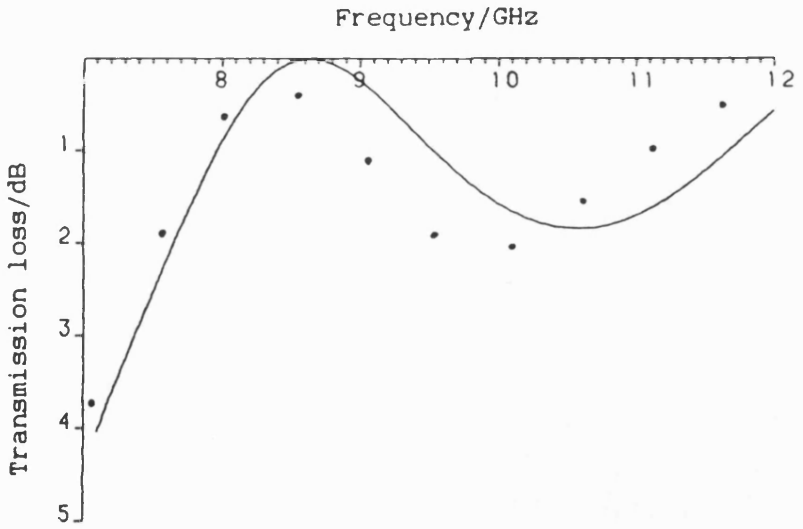

Figure (6.3.2) Comparison of Theoretical Return and Transmission Loss With Experiment for the Double Step at X-Band (other guide parameters as figure (6.2.3)).

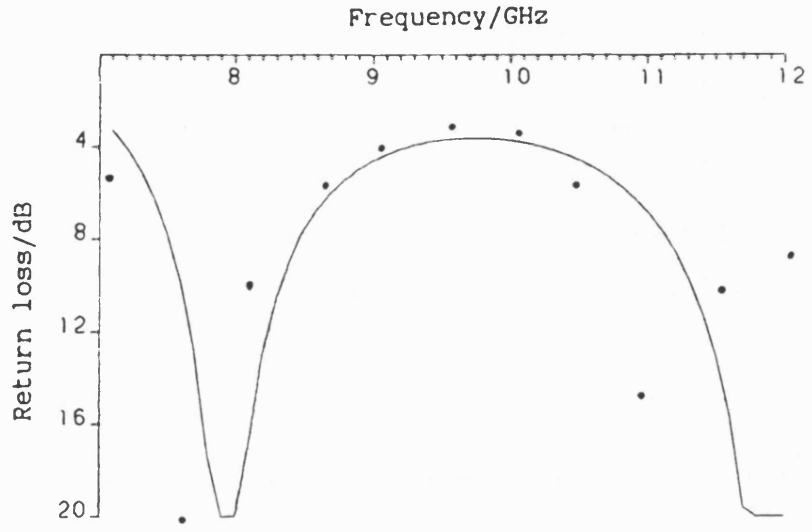

c = 1.5mm d = 6.0mm l = 30.5mm

Experimental Points.

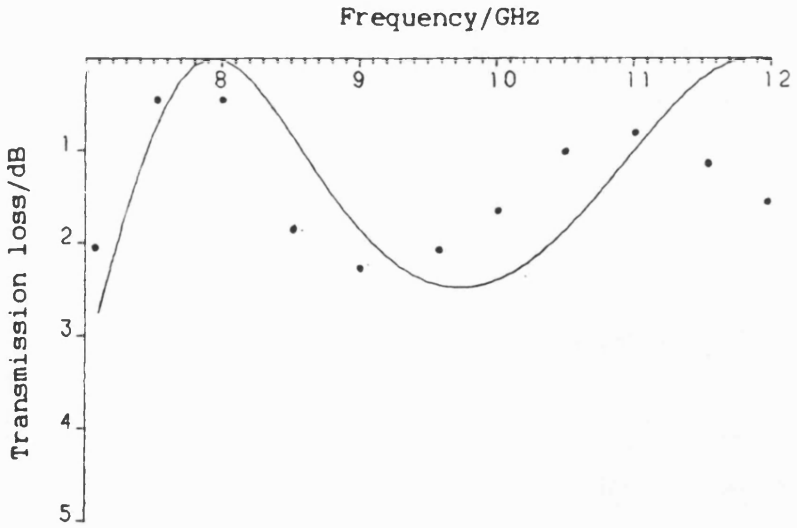

Figure (6.3.3) Comparison of Theoretical Return and Transmission Loss With Experiment for the Double Step at X-Band (other guide parameters as figure (6.2.3)).

that relatively large fin-gaps were employed, it is notable that the experimental results given in chapter (3) showed a greater deviation from theory when considering large fin-gaps. It is therefore believed that the performance of wider gap finlines is highly susecptible to the effects of asymmetry and the excitation of anti-symmetric modes. These effects are further compounded by the difficulty in maintaining adequate continuity of the currents at the intersection of the fins with the guide housing, failure to do so will allow a TEM mode to exist between the now isolated fins as illustrated by figure (6.3.4).

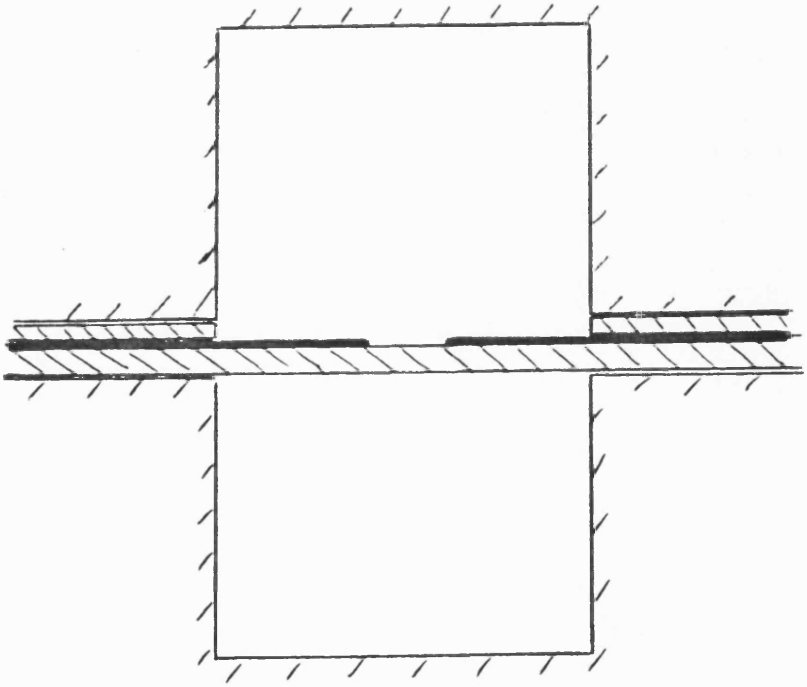

Figure (6.3.4) Isolated Finline.

References - Chapter (6)

1) Helard, M. , Citerne, J. , Picon, O. and Fouad Hanna, V. 'Exact Calculations of Scattering Parameters of a Step Slot Width Discontinuity in a Unilateral Fin-Line.' Electron Let, vol 19, pp 537-539, July 7th, 1983.

2) Wexler, A. 'Solution of Waveguyide Discontinuities by Modal Analysis', IEEE Trans MTT-15, No 9, pp 508-517, Sept 1967

3) Sorrentino, R. and Itoh, T. 'Transverse Resonance Analysis of Finline Discontinuities', IEEE Trans MTT-33, No 10, pp 1633-1638, Oct 1985.

4) Omar, A. S. and Schunemann, K. 'Transmission Matrix Representation of Finline Discontinuities', IEEE Trans MTT-33, No 9, pp 765-770, Sept 1985.

5) Safavi-Naini, R. and Macphie, R. H. 'On Solving Waveguide Junction Scattering Problems by the Conservation of Complex Power Technique', IEEE Trans MTT-29, No 2, pp 337-343, Apr 1981.

6) Webb, K. and Mittra, R. 'Solution of the Finline Step-Discontinuity Problem Using the Generalized Variational Technique', IEEE Trans MTT-33, No 9, pp 1004-1010, Oct 1985.

7) Schwinger, J. and Saxon, D.S. 'Discontinuities in Waveguides.' Gordon and Breach, New York, 1968, pp 114-124.

8) Altman, J. L. 'Microwave Circuits.' D.Van Nostrand, New York, 1964, pp399-402.

CHAPTER SEVEN : CONCLUSION

7.1) General Remarks.

This thesis has applied the Transverse Resonance Diffraction method to unilateral finline. Starting from a classical field representation in terms of Hertzian vector potentials, it was shown how a transverse equivalent network in interpretation arises. This was then used to generate the Green's functions used within a system of integral equations describing the effects of the fin. These effects were taken into explicit account by employing the Schwinger mapping to generate a set of functions to expand the fields within the fin gap. It was shown that when considering the fundamental mode, which is predominantly TE in character, only one field component need be considered. Expanded in terms of the zeroth Schwinger function, reasonably accurate results were obtained with minimal computational effort. Furthermore, this lead directly to a convenient transverse equivalent network interpretation, involving two short circuited transmission lines and a lumped fin admittance.

The general Ritz-Galerkin formulation was then developed, leading to an exact solution for the fin gap field and giving highly accurate results for all finline modes. At this stage it was instructive to develop the dual formulation employing an expansion for the fin currents in terms of appropriate Gegenbauer polynomials in order to introduce the correct edge condition. Whilst results of the two approaches were in good agreement, the Schwinger expansion leads to a higher degree of numerical efficiency.

Clearly, therefore, the general method can be used to formulate for a wide range of E-plane structures, and in view of the

aformentioned advantages, the Schwinger expansion for aperture fields may well find further application. However, in cases where an expansion of the current density seems more natural, the Gegenbauer polynomials can be employed.

With a view to simplfying the complicated mode spectrum which was appearing, the cut-off condition in finline was then considered. This lead to a decoupling of LSE and LSM components, and since the Schwinger functions closely approximate the quasi-static field in the gap, a further decoupling was observed. This then enabled finline modes to be characterised in a systematic manner in terms of modes families.

Following from this, with the cut-off frequencies readily available it was possible to describe finline dispersion in terms of simple square-root expressions. But in order to do this the quasi-static limit $k_0 \longrightarrow 0$ had to be investigated. However, by accepting the assumption of fins being exactly midway between the two end walls, simplifications could be made here as well.

Having obtained a satisfactory means of describing finline dispersion, attention was then directed towards determining finline attentuation loss. This was a further area where a clear understanding had been lacking. In published literature to date workers have failed to recognise that any singularities of field existing at metallic edges as in finline must be integrable for the system to contain finite energy. By employing Schwinger functions this requirement is satisfied implicitly, thus allowing new results on finline loss and Q-factor to be generated. In addition, the behaviour of the wall and fin currents was investigated. Here it was seen that the continuity of current between the fin and housing must be maintained for satisfactory operation of the waveguide.

The effect of the dielectric substrate on finline characteristics was also investigated. But since the substrate region is generally small in comparison, its effects are mainly second order. Furthermore, since a low permittivity material is usually employed its effect on finline fields can almost be ignored.

Bearing in mind the above remarks, the problem of the finline step discontinuity was addressed. To further simplify the problem the case of fins midway between the two end walls was again considered since the discontinuity exists only on the metallisation and practical finlines are relatively symmetric. It was then found from the results of chapters (3) and (4) that under such conditions of total symmetry both the aperture and obstacle formulations become degenerate. The resulting mode spectrum now consists of purely TE and TM mode families. Thus the E-plane finline step is seen to be an impedance step with an associated capacitance. By employing a very simple trial field reasonable results were obtained with very little computational effort.

7.1) Further Work.

It was the objective of this thesis to provide reasonably accurate analyses suitable for desk top comupter optimisation and design of finline circuits, and in this respect, the simplified description of dispersion is highly satisfactory. Even the general solution, employing a low expansion order, in conjunction with an evaluation of finline impedance would constitute a useful design package. However, it is the analysis of discontinuities, for the design of matching networks and filters which is of most interest to the designer and it is here that improvements can be made.

Whilst the discontinuity analysis presented in chapter (6) gave

an agreement with experiment, it could be improved by employing a Ritz-Galerkin formulation to optimise the trial field. Further improvements could be made by employing a full cross-sectional analysis, rather than one dimensional across the fins. Both will increase computational effort, but not to the extent of a full mode matching approach including the effects of the dielectric.

However, as has been consistently observed in experiments, the non-ideal finline structure, which is empoloyed in practice, can lead to significant deviations from theory. Until this choking problem is solved, E-plane filters are perhaps best realised using all metal inserts, the theory of which is already well known, [1]. But finline is still highly actractive for integration with active diode devices, and matching of these devices into circuits does require a suitable analysis of finline discontinuities. Although relatively simple matching networks, employing series stubs, can be sucessfully designed using dispersion data alone.

Further theoretical work on the characterisation of finline modes should be extended to cover anti-symmetric modes, and the general case of a non central fin gap position, so that circuit designers are not restricted to purely symmetrical circuits.

Whilst the causes of complex mode propagation were observed in chapter (4), the general solution was not implemented to solve in the complex plane. This could be easily done using complex arithmetic on a large computer. Although complex finline modes only arise when a dielectric substrate is introduced into finned waveguide, and since the dielectric is generally thin these modes may not be of much practical significance.

References - Chapter (7)

1) Bornemann, J., Vahldiek, R., Arndt, F. and Grauerholz D. "Optimized Waveguide E-plane Metal Insert Filters for Millimetre-Wave Applications". IEEE trans, MTT-31, Jan 1983, pp 65-69

APPENDICES

Appendix AI) Normalised Frequency, Admittances and Quasi-static Admittances.

The variational formulation developed in Chapter (3) requires the solution of a transcendental equation containing an infinite sum. Clearly this can only be performed by a computer, and it is the purpose of this appendix to develop the formulation so that numerical problems are avoided by introducing normalised quanties. In addition, it shown how the choice of a Schwinger function expansion for the aperture field enables certian infinite sums to be evaluated analytically, vastly improving the numerical efficiency.

AI.1) Normalised frequencies

Firstly, it is convenient to introduce normalised frequencies. These greatly simplify the expressions for the propagation coefficients which, moreover, change slowly with the solution points. For this latter reason, one of the following will be the preferred variable for iteration when solving for transverse resonance. Defining:

$$w^2 = \left[\frac{a}{\pi}\right]^2 (k_o^2 - \beta^2) \qquad \text{(AI.1)}$$

$$u^2 = \left[\frac{a}{\pi}\right]^2 (\varepsilon_r k_o^2 - \beta^2) \qquad \text{(AI.2)}$$

so that,

$$k_n^a = \sqrt{n^2 - w^2}\ \frac{\pi}{a} \qquad \text{(AI.3)}$$

$$k_n^s = \sqrt{n^2 - u^2}\ \frac{\pi}{a} \qquad \text{(AI.3)}$$

The variables u and w are so normalised that the n'th y directed transverse mode in the substrate region is propagating if u > n, and

in the air region if $w > n$. From the wave equation the relationship between the two normalised frequency variables is found to be:

$$u^2 = w^2 + (\varepsilon_r - 1)\, k_o^2 \left(\frac{a}{\pi}\right)^2 \qquad \text{(AI.4)}$$

Thus u^2 is always greater than w^2 giving three possible states for the n'th transverse mode:

i) Decay in both the air and substrate regions , $n < u$.

ii) Decay in the air region only, $w < n < u$.

iii) Propagation in both air and substrate regions, $w > n$.

AI.2) Normalised admittances

To avoid the occurence of unwieldy numbers and to remove the common frequency variation in expressions such as (3.4.16), it is convenient to normalise all admittances to the characteristic admittance of the fundamental TE in, say, the substrate region. Thus all admittances denoted up to now by the uppercase, Y, may be replaced by the normalised counterpart, lowercase y.

TE admitances seen looking right of the fins may therefore be written as:

$$y_{nR}^{TE} = g_{na} \coth k_n^a h \qquad \text{(AI.5)}$$

where $g_{na} = \dfrac{\sqrt{n^2 - w^2}}{ju}$

TE admittances to the left become:

$$y_{nL}^{TE} = g_{ns} \frac{g_{na} \coth k_n^a h \coth k_n^s s + g_{ns}}{g_{na} \coth k_n^a h + g_{ns} \coth k_n^s s} \qquad \text{(AI.6)}$$

where $g_{ns} = \dfrac{\sqrt{n^2 - u^2}}{ju}$

Whilst TM admittances seen looking right of the fins become:

$$y_{nR}^{TM} = q_{na} \coth k_n^a h \qquad \text{(AI.7)}$$

where $q_{na} = \frac{k^2}{u^2} \frac{ju}{\sqrt{n^2 - w^2}}$, $k = \frac{a}{\pi} k_o$

and TM admittances left become:

$$y_{nL}^{TM} = q_{ns} \frac{q_{na} \coth k_n^a q \coth k_n^s s + q_{ns}}{q_{na} \coth k_n^a h + q_{ns} \coth k_n^s s} \qquad \text{(AI.8)}$$

where $h_{ns} = \varepsilon_r \frac{k^2}{u^2} \frac{ju}{\sqrt{n^2 - u^2}}$

AI.3) Quasi-static admitances

It is now instructive to examine the asymptotic behaviour of the normalised transverse admittances with large n. This will enable much of the frequency dependence of the admittance operators to be extracted expicitly as quasi-static sums.

Clearly the term n^2 will dominate the square root terms appearing in the characteristic admittances since u will be small in comparison. The same term will also dominate the transverse wavenumbers appearing in the hyperbolic terms so that they become large, positive and nearly frequency independent. Once the arguments of these terms exceed 3 or 4, the hyperbolic variation can be neglected completely (althougth some caution must be exercised when considering the difference between admittances). Thus for large n, (AI.5), (AI.6) and (AI.7) may be writen as:

$$y_{nR}^{TE} = \frac{n}{ju} e_4 \quad , \quad y_{nL}^{TE} = \frac{n}{ju} e_3 \quad \text{and} \quad y_{nR}^{TM} = \frac{k^2}{u^2} \frac{ju}{n} e_2 \qquad \text{(AI.9)}$$

Where the coefficients e are completely independent of frequency and rapidly independant of n . For present purposes they may be considered constant:

$$e_4 = e_3 = e_2 = 1$$

However, for thin substrates, as is generally the case in finline, the remaining TM admittance is found not to reach asymptotic behaviour with n as rapidly. In order to extract as much frequency variation as possible and hence achieve fast convergence, (AI.8) may be writen as:

$$y_{nL}^{TM} = \frac{k^2}{u^2} \frac{ju}{n} e_1 \qquad \text{(AI.10)}$$

where $e_1 = \varepsilon_r(1-S_n)$; $S_n = \dfrac{2}{\left[\dfrac{\varepsilon_r + 1}{\varepsilon_r - 1}\right] \exp(2n\pi s/a) + 1}$

Thus $e_1 \longrightarrow \varepsilon_r$ once the decay across the substrate region becomes large.

Expressing Y_{11n} in terms of normalised admittances gives the field coupling admittance involved in the variational solution (3.4.16) as:

$$y_{11n} = \cos^2\tau_n (y_{nL}^{TM} + y_{nR}^{TM}) + \sin\tau^2_n (y_{nL}^{TE} + y_{nR}^{TE})$$

whilst expanding the terms $\cos^2\tau_n$ and $\sin^2\tau_n$ in terms of the normalised frequency variable u gives:

$$y_{11n} = \frac{n^2}{k^2 - u^2 - n^2} (y_{nL}^{TM} + y_{nR}^{TM}) + \frac{k^2 - n^2}{k^2 - u^2 - n^2} (y_{nL}^{TE} + y_{nR}^{TE})$$

which for large n gives the coupling admittance as:

$$y_{11n} \longrightarrow ju\frac{2}{n} + \frac{k^2}{jun} (1 - \frac{1}{\varepsilon r} + S_n) \qquad \text{(AI.11)}$$

and when $S_n \longrightarrow 0$, the asymptotic form of the quasi-static admittance is obtained as:

$$y_{11n} \longrightarrow \frac{y_{s11}}{n} \quad , \text{ where } \quad y_{s11} = j2u + \frac{k^2}{ju}\left(1 - \frac{1}{\varepsilon_r}\right) \qquad \text{(AI.12)}$$

The infinite sum within (3.4.16) can be evaluated exactly by removing this quasi-static component from the summation:

$$yo + \sum_{n=1}^{nd} \left(y_{11n} - \frac{y_{s11}}{n}\right) P_{n0}^2 + y_{s11} \sum_{n=1}^{\infty} \frac{1}{n} P_{n0}^2 = 0 \qquad \text{(AI.13)}$$

Once the admittance y_{11n} assumes asymptotic behaviour, the first summation in the above may be succesfully truncated.

It will now be shown how the second summation occurring in (AI.13) may be obtained analytically. Consider the summation elements A_{mk}:

$$A_{mk} = \sum_{n=1}^{\infty} \frac{1}{n} P_{nm} P_{nk} \qquad \text{(AI.15)}$$

From (3.3.10) and the orthogonality of the functions f_m the coefficients P_{nm} and P_{nk} may be expressed as integrals, giving:

$$A_{mk} = \sum_{n=1}^{\infty} \frac{1}{n} \int_0^{\pi}\int_0^{\pi} \phi_{hn}(x(\theta))\, f_m(\theta)\, \phi_{hn}(x(\theta'))_m f\,(\theta')\, d\theta\, d\theta'$$

Writing the eigenfunctions more explicitly so as to consider only the even case, and interchanging the order of summation and integration,

$$A_{mk} = \delta_m \delta_k \frac{4}{a\pi} \int_0^{\pi}\int_0^{\pi} \sum_{n=1}^{\infty} \frac{1}{n} \cos\frac{2n\pi}{a} x(\theta))\, \cos\frac{2n\pi}{a} x(\theta'))$$

$$\cos m\theta \cos k\theta \; d\theta\, d\theta'$$

so that the identity:

$$\sum_{n=1}^{\infty} \frac{1}{n} \cos nx \cos ny = -\frac{1}{2} \ln 2|\cos x - \cos y| \qquad \text{(AI.16)}$$

may be used to convert the infinite summation (AI.15) into a straightforward integral. Thus the Schwinger mapping gives:

$$A_{mk} = \sqrt{\delta_m \delta_k}\ \frac{4}{a\pi} \int_0^{\pi}\int_0^{\pi} -\frac{1}{2} \ln \alpha_2 |\cos\theta - \cos\theta'| \cos m\theta \cos k\theta \ d\theta\, d\theta' \qquad \text{(AI.17)}$$

For the particular case m = k = 0,

$$A_{00} = \frac{-1}{a\pi} \int_0^{\pi}\int_0^{\pi} \ln \alpha_2 + \ln 2\,|\cos\theta - \cos\theta'|\, d\theta\, d\theta'$$

but since only constant terms give any contribution to the integral over the range 0 - π, the result required for the variational solution is obtained as:

$$A_{00} = \frac{\pi}{2a} \ln \frac{1}{\alpha^2} = \frac{1}{2} P_{00}^2 \ln \frac{1}{\alpha^2} \qquad \text{(AI.18)}$$

In order to prepare for the general solution and its asociated quasi-static summations, the remaining results are derived as follows. Expanding (AI.17) into two distinct integrals,

$$A_{mk} = \frac{4}{a\pi} \int_0^{\pi}\int_0^{\pi} \frac{-1}{2} \ln \alpha_2 \cos m\theta \cos k\theta'\, d\theta\, d\theta'$$

$$+ \quad \frac{4}{a\pi} \int_0^{\pi}\int_0^{\pi} \frac{-1}{2} \ln 2\,|\cos\theta - \cos\theta'|\cos m\theta \cos k\theta \, d\theta \, d\theta'$$

Unless $m = k = 0$ the first integral is incidentally zero, whilst applying the identity (AI.16) to the second leads to:

$$A_{mk} = \frac{4}{a\pi} \int_0^{\pi}\int_0^{\pi} \sum_{l=1}^{\infty} \frac{1}{l} \cos l\theta \cos l\theta' \cos m\theta \cos k\theta \, d\theta \, d\theta'$$

which gives the results:

$$A_{mk} = 0 \qquad \text{for} \qquad m \neq k \qquad \text{(AI.19)}$$

and

$$A_{mm} = \frac{\pi}{a}\frac{1}{m} = P_{00}^2 \frac{1}{m} \qquad \text{for} \qquad k = m > 0 \qquad \text{(AI.20)}$$

Results (AI.17-19) may be more conveniently expressed as:

$$\sum_{n=1}^{\infty} \frac{1}{n} \underline{P}_n \cdot \underline{P}_n^T = \underline{\underline{A}} = P_{00}^2 \begin{bmatrix} \frac{1}{2}\ln\frac{1}{\alpha^2} & 0 & . & . & 0 \\ 0 & 1 & 0 & . & 0 \\ 0 & 0 & \frac{1}{2} & 0 & . \\ & & & & \end{bmatrix} \qquad \text{(AI.21)}$$

Where $\underline{P}_n$ is a colum vector of elements P_{nk}, and $\underline{\underline{A}}$ is the matrix of elements A_{mk}.

Appenidx AII) Admittance Poles in the Mixed Dielectric Region.

When considering the determination of admittance poles in chapter (4), it was seen that when looking right of the fin these poles were obtained by inspection. However, when looking to the left of the fin into the mixed dielectric region, admittance poles cannot be determined analytically. For instance:

$$Y_{nL}^{TM} = j\,\varepsilon_r \frac{\sqrt{\varepsilon_r}\,k_c}{\sqrt{n^2-\varepsilon_r k_c^2}} \frac{\varepsilon_r\sqrt{\frac{n^2-k_c^2}{n^2-\varepsilon_r k_c^2}} + \coth\sqrt{n^2-k_c^2}\,\frac{\pi h}{a}\coth\sqrt{n^2-\varepsilon_r k_c^2}\,\frac{\pi s}{a}}{\varepsilon_r\sqrt{\frac{n^2-k_c^2}{n^2-\varepsilon_r k_c^2}}\coth\sqrt{n^2-\varepsilon_r k_c^2}\,\frac{\pi s}{a} + \coth\sqrt{n^2-k_c^2}\,\frac{\pi h}{a}} \qquad \text{(AII.1)}$$

Poles from this admittance are only found zeros in the denominator:

$$\varepsilon_r\sqrt{\frac{n^2-k_c^2}{n^2-\varepsilon_r k_c^2}}\coth\sqrt{n^2-\varepsilon_r k_c^2}\,\frac{\pi s}{a} + \coth\sqrt{n^2-k_c^2}\,\frac{\pi h}{a} = 0 \qquad \text{(AII.2)}$$

since poles in the numerator of equation (AII.1) are always cancelled by poles in the denominator. However, roots to equation (AII.2) are located between poles due to both:

$$\sqrt{k_c^2-n^2}\,\frac{\pi h}{a} = N\pi \qquad \text{(AII.3a)}$$

and

$$\sqrt{\varepsilon_r k_c^2-n^2}\,\frac{\pi s}{a} = M\pi \qquad \text{(AII.3b)}$$

where N and M are arbritary ingeters.

Values of k_c obtained from the above must then be sorted, to allow a systematic determination of admittance poles. However, since the substrate thickness, s, is generally small when compared to, h, the extent of the air region (1), poles due to $M\pi$ occur less often

and are not usually required when considering only the first few cut-off's.

TE admittance poles seen looking to the right of the fins are simarly obtained from the solution of:

$$\sqrt{\frac{n^2 - k_c^2}{n^2 - \varepsilon_r k_c^2}} \coth\sqrt{n^2 - \varepsilon_r k_c^2}\,\frac{\pi s}{a} + \coth\sqrt{n^2 - k_c^2}\,\frac{\pi h}{a} = 0 \qquad \text{(AII.4)}$$

in place of equation (AII.7). This is because the dielectric has a different effect on TE admittances.

Appendix AIII) Field Functions.

Here the functions $\chi_n(y)$ describing the y-variation of fields in chapter (5) are given in full:

1) For the field E_x in region (1) ; $-(h+s) < y < -s$.

$$\psi_n(y) =$$

$$\frac{n\pi}{a}\ \frac{\coth(k_n^s s + \theta_{en})}{k_n^s}\ \frac{\frac{n\pi}{a}E_{xn} + j\beta E_{zn}}{k_n^2}\ \frac{\varepsilon_r \cosh\theta_{en}\ k_n^a \sinh k_n^a(y+h+s)}{\cosh k_n^a h\ \ \cosh(k_n^s s + \theta_{en})}$$

$$+\ \omega\mu\beta\ \ \frac{j\beta E_{xn} + \frac{n\pi}{a}E_{zn}}{j\omega\mu\ k_n^2}\ \frac{\sinh\theta_{hn}}{\sinh k_n^a h}\ \frac{\sinh k_n^a(y+h+s)}{\sinh(k_n^s s + \theta_{hn})} \qquad \text{(AIII.1)}$$

in region (2) ; $-s < y < 0$,

$$\psi_n(y) =$$

$$\frac{n\pi}{a}\ \frac{\coth(k_n^s s + \theta_{en})}{k_n^s}\ \frac{\frac{n\pi}{a}E_{xn} + j\beta E_{zn}}{k_n^2}\ \frac{k_n^s \sinh[k_n^s(y+s) + \theta_{en}]}{\cosh(k_n^s s + \theta_{en})}$$

$$+\ \omega\mu\beta\ \ \frac{j\beta E_{xn} + \frac{n\pi}{a}E_{zn}}{j\omega\mu\ k_n^2}\ \frac{\sinh[k_n^s(y+s) + \theta_{hn}]}{\sinh(k_n^s s + \theta_{hn})} \qquad \text{(AIII.2)}$$

in region (3) ; $0 < y < l$

$$\psi_n(y) = E_{xn}\ \frac{\sinh k_n^a(l-y)}{\sinh k_n^a l} \qquad \text{(AIII.3)}$$

2) For the field E_z in region (1) ; $-(h+s) < y < -s$.

$$\psi_n(y) =$$

$$-j\beta\ \frac{\coth(k_n^s s + \theta_{en})}{k_n^s}\ \frac{\frac{n\pi}{a}E_{xn} + j\beta E_{zn}}{k_n^2}\ \frac{\varepsilon_r \cosh\theta_{en}}{\cosh k_n^a h}\ \frac{k_n^a \sinh k_n^a(y+h+s)}{\cosh(k_n^s s + \theta_{en})}$$

$$+ j\omega\mu \frac{n\pi}{a} \frac{j\beta E_{xn} + \frac{n\pi}{a} E_{zn}}{j\omega\mu k_n^2} \frac{\sinh \theta_{hn} \sinh k_n^a(y+h+s)}{\sinh k_n^a h \sinh(k_n^s s + \theta_{hn})}$$

(AIII.4)

in region (2) ; $-s < y < 0$,

$$\psi_n(y) =$$

$$-j\beta \frac{\coth(k_n^s s + \theta_{en})}{k_n^s} \frac{\frac{n\pi}{a} E_{xn} + j\beta E_{zn}}{k_n^2} \frac{k_n^s \sinh[k_n^s(y+s) + \theta_{en}]}{\cosh(k_n^s s + \theta_{en})}$$

$$+ j\omega\mu \frac{n\pi}{a} \frac{j\beta E_{xn} + \frac{n\pi}{a} E_{zn}}{j\omega\mu k_n^2} \frac{\sinh[k_n^s(y+s) + \theta_{hn}]}{\sinh(k_n^s s + \theta_{hn})}$$

(AIII.5)

in region (3) ; $0 < y < l$

$$\psi_n(y) = E_{zn} \frac{\sinh k_n^a(l-y)}{\sinh k_n^a l} \qquad \text{(AIII.6)}$$

3)for the field E_y in region (1) ; $-(h+s) < y < -s$.

$$\psi_n(y) =$$

$$\frac{\coth(k_n^s s + \theta_{en})}{k_n^s} \left(\frac{n\pi}{a} E_{xn} + j\beta E_{zn}\right) \frac{\varepsilon_r \cosh \theta_{en}}{\cosh k_n^a h} \frac{\cosh k_n^a(y+h+s)}{\cosh(k_n^s s + \theta_{en})}$$

(AIII.7)

in region (2) ; $-s < y < 0$,

$$\psi_n(y) =$$

$$\frac{\coth(k_n^s s + \theta_{en})}{k_n^s} \left(\frac{n\pi}{a} E_{xn} + j\beta E_{zn}\right) \frac{\cosh[k_n^s(y+s) + \theta_{en}]}{\sinh(k_n^s s + \theta_{en})}$$

(AIII.8)

in region (3) ; $0 < y < l$

$$\psi_n(y) = - \frac{\coth k_n^a l}{k_n^a} \left(\frac{n\pi}{a} E_{xn} + j\beta E_{zn} \right) \frac{\cosh k_n^a (l-y)}{\cosh k_n^a l}$$

(AIII.9)

4)For the field H_x in region (1) ; $-(h+s) < y < -s$.

$$\psi_n(y) =$$

$$- \omega\varepsilon\beta \frac{\coth (k_n^s s + \theta_{en})}{k_n^s} \frac{\frac{n\pi}{a} E_{xn} + j\beta E_{zn}}{k_n^2} \frac{\varepsilon_r \cosh \theta_{en}}{\cosh k_n^a h} \frac{\cosh k_n^a (y+h+s)}{\cosh(k_n^s s + \theta_{en})}$$

$$- \frac{n\pi}{a} \frac{j\beta E_{xn} + \frac{n\pi}{a} E_{zn}}{j\omega\mu k_n^2} \frac{\sinh \theta_{hn}}{\sinh k_n^a h} \frac{k_n^a \cosh k_n^a (y+h+s)}{\sinh(k_n^s s + \theta_{hn})}$$

(AIII.10)

in region (2) ; $-s < y < 0$,

$$\psi_n(y) =$$

$$-\omega\varepsilon\beta \frac{\coth (k_n^s s + \theta_{en})}{k_n^s} \frac{\frac{n\pi}{a} E_{xn} + j\beta E_{zn}}{k_n^2} \frac{\cosh [k_n^s (y+s) + \theta_{en}]}{\cosh(k_n^s s + \theta_{en})}$$

$$- j\beta \frac{j\beta E_{xn} + \frac{n\pi}{a} E_{zn}}{j\omega\mu k_n^2} \frac{k_n^a \cosh [k_n^s (y+s) + \theta_{hn}]}{\sinh(k_n^s s + \theta_{hn})}$$

(AIII.11)

in region (3) ; $0 < y < l$

$$\psi_n(y) =$$

$$j\omega\varepsilon \frac{n\pi}{a} \frac{\coth k_n^a l}{k_n^a} \frac{\frac{n\pi}{a} E_{xn} - j\beta E_{zn}}{k_n^2} \frac{-\cosh k_n^a (l-y)}{\cosh k_n^a l}$$

$$- \frac{n\pi}{a} \frac{j\beta E_{xn} + \frac{n\pi}{a} E_{zn}}{j\omega\mu k_n^2} \frac{- k_n^s \cosh k_n^s (l-y)}{\cosh k_n^a l}$$

(AIII.12)

5)For the field H_z in region (1) ; $-(h+s) < y < -s$.

$$\psi_n(y) =$$

$$j\omega\varepsilon \frac{\coth(k_n^s s + \theta_{en})}{k_n^s} \frac{\frac{n\pi}{a} E_{xn} + j\beta E_{zn}}{k_n^2} \frac{\varepsilon_r \cosh\theta_{en}}{\cosh k_n^a h} \frac{\cosh k_n^a (y+h+s)}{\cosh(k_n^s s + \theta_{en})}$$

$$+ j\beta \frac{j\beta E_{xn} + \frac{n\pi}{a} E_{zn}}{j\omega\mu k_n^2} \frac{\sinh\theta_{hn}}{\sinh k_n^a h} \frac{k_n^a \sinh k_n^a (y+h+s)}{\sinh(k_n^s s + \theta_{hn})} \qquad \text{(AIII.13)}$$

in region (2) ; $-s < y < 0$,

$$\psi_n(y) =$$

$$j\omega\varepsilon \frac{\coth(k_n^s s + \theta_{en})}{k_n^s} \frac{\frac{n\pi}{a} E_{xn} - j\beta E_{zn}}{k_n^2} \frac{\sinh[k_n^s (y+s) + \theta_{en}]}{\cosh(k_n^s s + \theta_{en})}$$

$$+ j\beta \frac{j\beta E_{xn} + \frac{n\pi}{a} E_{zn}}{j\omega\mu k_n^2} \frac{k_n^s \sinh[k_n^s (y+s) + \theta_{hn}]}{\sinh(k_n^s s + \theta_{hn})} \qquad \text{(AIII.14)}$$

in region (3) ; $0 < y < l$

$$\psi_n(y) =$$

$$j\omega\varepsilon \frac{n\pi}{a} \frac{\coth k_n^a l}{k_n^a} \frac{\frac{n\pi}{a} E_{xn} - j\beta E_{zn}}{k_n^2} \frac{-\cosh k_n^a (l-y)}{\cosh k_n^a l}$$

$$- \beta \frac{-j\beta E_{xn} + \frac{n\pi}{a} E_{zn}}{j\omega\mu k_n^2} \frac{k_n^a \cosh k_n^s (l-y)}{\sinh k_n^a l} \qquad \text{(AIII.15)}$$

6) For the field H_y in region (1) ; $-(h+s) < y < -s$.

$$\psi_n(y) =$$

$$\frac{1}{j\omega\mu}\left(j\beta E_{xn} + \frac{n\pi}{a} E_{zn}\right) \frac{\sinh \theta_{hn}}{\sinh k_n^a h} \frac{\sinh k_n^a (y+h+s)}{\sinh(k_n^s s + \theta_{hn})} \qquad \text{(AIII.16)}$$

in region (2) ; $-s < y < 0$

$$\psi_n(y) =$$

$$\frac{1}{j\omega\mu}\left(j\beta E_{xn} + \frac{n\pi}{a} E_{zn}\right) \frac{\sinh [k_n^s (y+s) + \theta_{hn}]}{\sinh(k_n^s s + \theta_{hn})} \qquad \text{(AIII.17)}$$

in region (3); $0 < y < l$

$$\psi_n(y) = \frac{1}{j\omega\mu}\left(-j\beta E_{xn} + \frac{n\pi}{a} E_{zn}\right) \frac{\sinh k_n^a (l-y)}{\sinh k_n^a l} \qquad \text{(AIII.18)}$$

Where $k_n^2 = k^2 + \left(\frac{n\pi}{a}\right)^2$

Appendix AIV) Evaluation of Power Flow Components

Here cross-sectional integrals, required for the evaluation of power flow, in chapter (5) are converted into simple analyitic summations.

From the field expansions given by (5.1.8), (5.1.12) the integration in x can be resolved into a summation by virtue of the orthogonality of the functions $\phi_{hn}(x)$. Substitution of the appropriate y variation from appendix AIII gives:

$$P_{1a} = \int \sum_{n=0}^{\infty} \left(\frac{n\pi}{a}\right) \frac{U^L_{en}\, U^L_{hn}\, A_{en}\, A_{hn} k^a_n\, k^2_n \sinh^2 k^a_n(y+h+s)}{\sinh(k^s_n s + \theta_{hn}) \sinh(k^s_n s + \theta_{en})}\, dy$$

$$+ \int \sum_{n=0}^{\infty} \frac{\omega\mu\beta\, (U^L_{hn} A_{hn})^2\, k^2_n \sinh^2 k^a_n(y+h+s)}{\sinh^2 (k^s_n s + \theta_{hn})}\, dy \qquad \text{(AIV.1)}$$

The other component of power flow in this region is obtained from:

$$P_{1b} = - \iint E_y(x,y)\, H_x(x,y)\, dx\, dy \qquad \text{(AIV.2)}$$

Which becomes:

$$P_{1b} = \int \sum_{n=0}^{\infty} \left(\frac{n\pi}{a}\right) \frac{U^L_{en}\, U^L_{hn}\, A_{en}\, A_{hn} k^a_n\, k^2_n \cosh^2 k^a_n(y+h+s)}{\sinh(k^s_n s + \theta_{hn}) \sinh(k^s_n s + \theta_{en})}\, dy$$

$$+ \int \sum_{n=0}^{\infty} \frac{\omega\varepsilon\beta\, (U^L_{hn} A_{hn})^2\, k^2_n \cosh^2 k^a_n(y+h+s)}{\sinh^2 (k^s_n s + \theta_{hn})}\, dy \qquad \text{(AIV.3)}$$

The above are readily evaluated given the integral results:

$$\int_{-(h+s)}^{-s} \sinh^2 k_n^a (h+s+y)\, dy = \frac{\sinh 2k_n^a h}{4k_n^a} - \frac{h}{2} \qquad \text{(AIV.4)}$$

and

$$\int_{-(h+s)}^{-s} \cosh^2 k_n^a (h+s+y)\, dy = \frac{\sinh 2k_n^a h}{4k_n^a} + \frac{h}{2} \qquad \text{(AIV.5)}$$

Within region (2), the dielectric substrate, the two components are given as:

$$P_{2a} = \int \sum_{n=0}^{\infty} \omega\mu\beta\, (U_{hn}^L)\, k_n^2 \frac{\sinh^2 (k_n^s(s+y) + \theta_{hn})}{\sinh^2 (k_n^s s + \theta_{hn})}\, dy$$

$$+ \int \sum_{n=0}^{\infty} \frac{\frac{n\pi}{a} k_n^2 U_{en}^L U_{hn}^L k_n^s \cosh[k_n^s(s+y) + \theta_{en})] \sinh[k_n^s(s+y) + \theta_{hn})]}{\sinh(k_n^s s + \theta_{hn}) \sinh(k_n^s s + \theta_{en})}\, dy \qquad \text{(AIV.5)}$$

and

$$P_{2b} = \int \sum_{n=0}^{\infty} \omega\varepsilon\beta\, (U_{en}^L)\, k_n^2 \frac{\sinh^2 (k_n^s(s+y) + \theta_{en})}{\sinh^2 (k_n^s s + \theta_{hn})}\, dy$$

$$+ \int \sum_{n=0}^{\infty} \frac{\frac{n\pi}{a} k_n^2 U_{en}^L U_{hn}^L k_n^s \sinh[k_n^s(s+y) + \theta_{en})] \cosh[k_n^s(s+y) + \theta_{hn})]}{\sinh(k_n^s s + \theta_{hn}) \sinh(k_n^s s + \theta_{en})}\, dy \qquad \text{(AIV.6)}$$

Integration results required for the evaluation of power flow within region (2) are given as:

$$\int_{-s}^{0} \sinh^2 [k_n^s(s+y) + \theta_1]\, dy = \frac{\cosh(k_n^s s + 2\theta_1)\sinh k_n^s s}{2k_n^s} - \frac{s}{2} \qquad \text{(AVI.7)}$$

$$\int_{-s}^{0} \cosh[k_n^s(s+y) + \theta_1] \sinh[k_n^s(s+y) + \theta_2] \, dy =$$

$$\frac{s}{2} \sinh(\theta_2 - \theta_1) - \frac{\sinh 2k_n^s s \sinh(k_n^s s + \theta_1 + \theta_2)}{2k_n^s} \qquad \text{(AIV.8)}$$

where θ_1 and θ_2 are θ_{hn} and θ_{en} or θ_{en} and θ_{hn} as required.

Finally for the power flowing in region (3):

$$P_{3a} = \int \sum_{n=0}^{\infty} \frac{-n\pi}{a} \frac{k_n^2 U_{en}^R U_{hn}^R k_n^a \sinh^2 k_n^a(l-y)}{\cosh k_n^a l \sinh k_n^a l} \, dy$$

$$+ \int \sum_{n=0}^{\infty} \omega\mu\beta \, k_n^2 (U_{hn}^R)^2 \frac{\sinh^2 k_n^a(l-y)}{\sinh^2 k_n^a l} \, dy \qquad \text{(AIV.9)}$$

and,

$$P_{3b} = \int \sum_{n=0}^{\infty} \frac{n\pi}{a} \frac{k_n^2 U_{en}^R U_{hn}^R k_n^a \cosh^2 k_n^a(l-y)}{\cosh k_n^a l \sinh k_n^a l} \, dy$$

$$- \int \sum_{n=0}^{\infty} \omega\varepsilon\beta \, k_n^2 (U_{hn}^R)^2 \frac{\cosh^2 k_n^a(l-y)}{\cosh^2 k_n^a l} \, dy \qquad \text{(AIV.10)}$$

Analytical evaluation of the above is given by employing modified versions of equations (AIV.4) and (AIV.5).

Orientation(1).

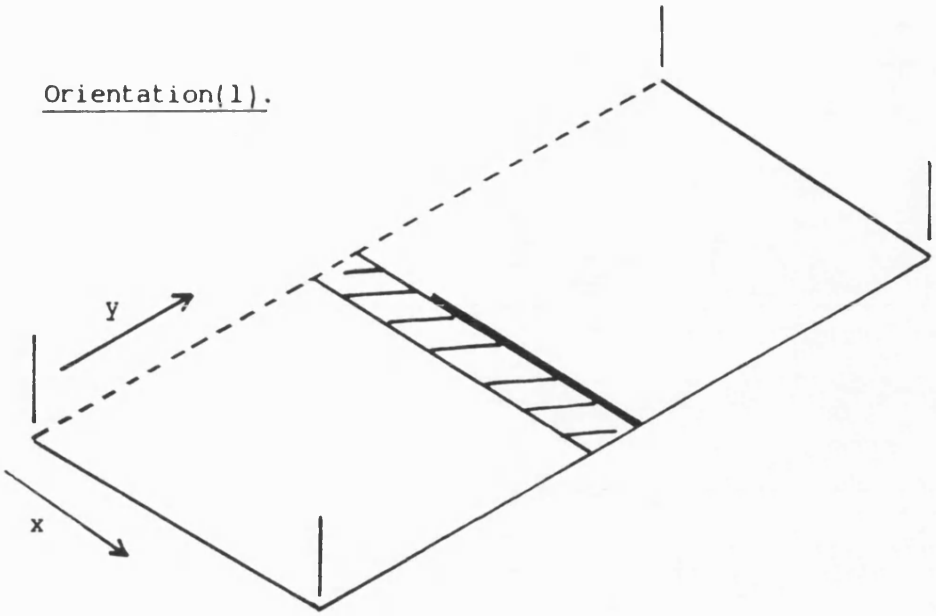

Orientation(2).

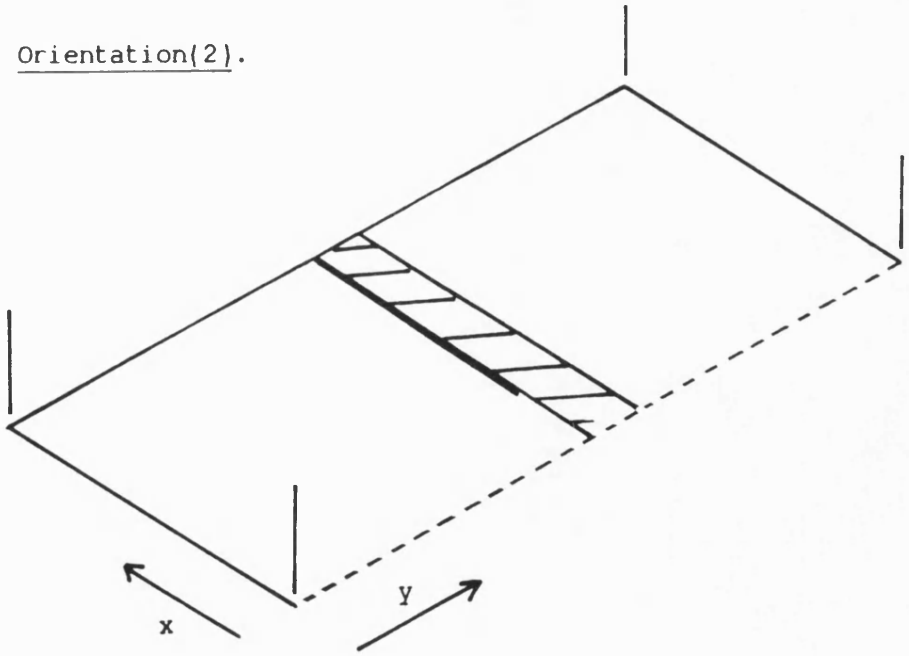

Figure(A1) Key to Isometric Field Displays.